

Porous One-Dimensional Nanomaterials: Design, Fabrication and Applications in Electrochemical Energy Storage

Qiulong Wei, Fangyu Xiong, Shuangshuang Tan, Lei Huang, Esther H. Lan, Bruce Dunn,* and Liqiang Mai*

Electrochemical energy storage technology is of critical importance for portable electronics, transportation and large-scale energy storage systems. There is a growing demand for energy storage devices with high energy and high power densities, long-term stability, safety and low cost. To achieve these requirements, novel design structures and high performance electrode materials are needed. Porous 1D nanomaterials which combine the advantages of 1D nanoarchitectures and porous structures have had a significant impact in the field of electrochemical energy storage. This review presents an overview of porous 1D nanostructure research, from the synthesis by bottom-up and top-down approaches with rational and controllable structures, to several important electrochemical energy storage applications including lithium-ion batteries, sodium-ion batteries, lithium-sulfur batteries, lithium-oxygen batteries and supercapacitors. Highlights of porous 1D nanostructures are described throughout the review and directions for future research in the field are discussed at the end.

1. Introduction

The ever-increasing demand for energy is accompanied by both the rapid growth of the global population and urbanization.^[1–4] Ideally, the increasing demand for energy should be met by using greener and more sustainable resources. However, in order to fully realize the utilization of green and renewable energy sources, such as solar, wind and biomass, there is a critical need for energy storage.^[2,4,5] Among the currently available energy storage technologies, rechargeable electrochemical

energy storage represents one of the most promising approaches as it offers high levels of efficiency for large-scale, smart-grid energy storage systems (ESSs).^[1–8]

Since its successful commercialization by Sony in 1991, rechargeable lithium-ion batteries (LIBs) have become the most widely used energy storage technology for such consumer electronics as cell phones, laptops, tablets and so forth. However, the energy density and power density of LIBs are not sufficient for other applications, particularly various types of electric vehicles (EVs).^[6,9] In addition, ESSs not only require battery systems with high performance but also low cost. In order to meet future requirements for consumer electronics and the electrification of transportation, there not only need to be enhancements in LIB properties but also the development of high-performance

energy storage devices that go beyond LIBs. That is, if energy and power densities are to continue to increase, improvements in the performance of electrode materials and the design of electrode architectures are needed.^[3,5,7–9]

The development of nanotechnology provides an opportunity to develop a new generation of energy storage devices that approach the theoretical limits of electrochemical energy storage.^[3,9–13] Three key features offered by nanoscale materials are their small size, high specific surface area and facile stress relaxation processes. The availability of electrochemical materials with particle sizes ranging from hundreds to tens of nanometers effectively reduces the diffusion length for Li⁺ ions and makes high rate capability possible for LIBs. This advantage also facilitates Na⁺ diffusion and has been instrumental in the recent emergence of sodium-ion batteries (SIBs).^[4,14] Furthermore, the transport of multivalent ions (Mg²⁺ and Al³⁺) is likely to be improved in nanomaterials, enabling the development of Mg-ion batteries^[15] or Al-ion batteries.^[16–18] The benefit of high specific surface area is especially evident in supercapacitors where charge storage occurs by electrical double-layer and surface redox processes; high surface areas lead to correspondingly higher levels of charge storage. Moreover, the large surface area increases electrode-electrolyte contact area and is beneficial for access to the electrochemically active surface. A third

Dr. Q. L. Wei, F. Y. Xiong, S. S. Tan,
L. Huang, Prof. L. Q. Mai
State Key Laboratory of Advanced Technology
for Materials Synthesis and Processing
International School of
Materials Science and Engineering
Wuhan 430070, P. R. China
E-mail: mlq518@whut.edu.cn

Dr. Q. L. Wei, Dr. E. H. Lan, Prof. B. Dunn
Department of Materials Science and Engineering
University of California Los Angeles
Los Angeles, CA 90095–1595, USA
E-mail: bdunn@ucla.edu



DOI: 10.1002/adma.201602300

consideration which occurs with nanoscale materials is the ability to have a significant amount of stress relaxation. Charge storage processes are generally accompanied by volume expansion/contraction upon cycling. It is well known that the large volume expansion, as occurs with alloy formation, will lead to pulverization of bulk materials and cause capacity fading. This stress, however, is able to be accommodated by the use of nanosize materials and for this reason Si, Ge, Sn, SnO₂ and other nanomaterials successfully survive repeated cycling.^[19–35] Other advantages for using nanomaterials in the energy storage field have also been demonstrated.^[3,10,12,36–40]

One-dimensional (1D) nanostructures, which include nanowires, nanofibers, nanoribbons, nanorods and nanotubes among other morphologies, are recognized as one of the most promising materials directions for energy-related applications.^[41–44] Our previous review on this topic emphasized the advantages of nanowires for in situ electrochemical probing, optimization strategies and covered some of the results of using these materials in advanced energy storage devices.^[3] The present paper complements the earlier work by extending to porous 1D nanomaterials which offer a number of advantages through the addition of controlled levels of nanoscale porosity.

Porous materials with large surface area and structural stability have been widely used in various fields such as energy storage, gas storage, adsorption, catalysis, separation, sensing and other areas.^[45–49] Electrochemical energy storage technology, in particular, benefits from porous materials because pores enable higher surface area and faster electrolyte access to active walls. By utilizing the advantages of both 1D architecture and porous properties, there is an opportunity to further enhance the performance of materials for energy storage applications. As shown in **Figure 1**, we define different types of

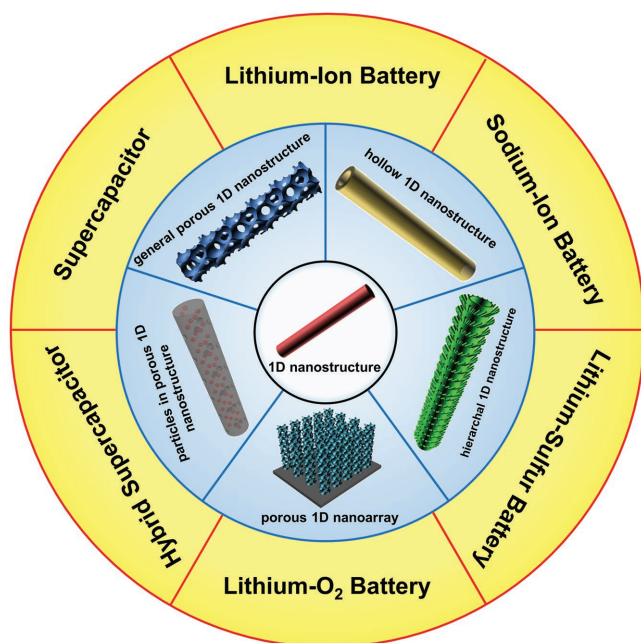


Figure 1. Porous 1D nanostructures and their applications in electrochemical energy storage.



Qiulong Wei received his Ph.D. from the State Key Laboratory of Advanced Technology for Materials Synthesis and Processing, Wuhan University of Technology in 2016, under the supervision of Prof. Qingjie Zhang and Prof. Liqiang Mai. Currently, he is a postdoctoral fellow in Dunn Group at the Materials Science and

Engineering department, UCLA. His current research involves the design and synthesis of nanomaterials for achieving both high energy density and power density, electrochemical energy storage devices, including the lithium-ion battery, sodium-ion battery and the hybrid supercapacitor.



Bruce Dunn is the Nippon Sheet Glass Professor of Materials Science and Engineering at UCLA. Prior to joining UCLA in 1981, he was a staff scientist at the General Electric Research Laboratory. His research interests are in the synthesis of inorganic and organic/inorganic materials, and the design of their electrochemical, optical and

biochemical properties. His current programs in electrochemistry include creating pseudocapacitive materials and the fabrication of three-dimensional batteries. Professor Dunn is a Fellow of the American Ceramic Society and the Materials Research Society.



Liqiang Mai received his Ph.D. from Wuhan University of Technology in 2004. He then carried out postdoctoral research in the laboratory of Professor Zhonglin Wang at Georgia Institute of Technology in 2006–2007 and worked as an advanced research scholar in the laboratory of Professor Charles M. Lieber

at Harvard University in 2008–2011. He is Chair Professor of Materials Science and Engineering at Wuhan University of Technology. He is the recipient of the National Science Fund for Distinguished Young Scholars and the National Ten Thousand of Talent Program of China. His interests include nanowire materials, micro/nanoenergy storage devices, and energy-based nano–bio interface.

porous 1D nanostructures to include general porous 1D nanostructure, hollow 1D geometry (also named a tubular nanostructure), hierarchical porous 1D architecture, nanoparticles in porous 1D configuration, and porous 1D nanoarray. A number of reports clearly demonstrate that creating hollow or porous 1D nanomaterials lead to significant improvements in electrochemical energy storage properties.^[50–68] The intent of this review is to summarize recent advances related to this topic and, more importantly, to provide systematic understanding of porous 1D nanomaterials and their advantages for electrochemical energy storage.

Here, we begin by introducing the various methods for synthesizing porous 1D nanomaterials, including electrospinning, liquid phase, template-assisted approaches, chemical deposition and chemical etching methods. These preparation routes are highly effective and enable the controllable synthesis of porous 1D nanomaterials with different morphology, porosity and inner structure. Representative examples are listed in **Table 1**. Then the structural design of porous 1D nanomaterials as electrodes for applications in electrochemical energy storage devices are discussed. We focus on LIBs because of the significant number of research studies in this field, but also highlight recent results on SIBs, Li-S batteries, Li-O₂ batteries, and supercapacitors. **Table 2** briefly describes the application of porous 1D nanomaterials for batteries and **Table 3** summarizes results for supercapacitors. Finally, we provide a brief discussion regarding future directions for porous 1D nanomaterial applications in electrochemical energy storage devices.

2. Advantages of Porous 1D Nanomaterials for Energy Storage

Porous 1D nanomaterials offer a number of advantages for achieving high capacity, high-rate capability and long-term cycling properties:

- The smaller crystal size increases the utilization of active materials, resulting in the enhanced specific capacity.
- The porous 1D nanostructure provides greater surface area than that of a non-porous system; high surface area ensures effective contact of the electrolyte to the electrode surface, facilitating charge transfer across the electrode-electrolyte interface.
- The ion diffusion length is further shortened, since creating porosity in 1D nanomaterials can effectively decrease the ion transport dimensions.
- The pores in 1D nanostructures are usually continuous, which offers interconnected ion diffusion pathways through the electrolyte to the active materials.
- The empty spaces in porous 1D nanostructures accommodate the volume changes associated with electrochemical reactions, thus limiting structure degradation during cycling.
- The porous 1D nanostructure can assemble into interconnected networks, avoiding the use of binders and lead to free-standing flexible energy storage applications.
- The pores/hollow regions in the porous 1D nanostructure can act as hosts for filling with other materials and enable multi-functional applications.

3. Methodologies for Controllable Synthesis of Porous 1D Nanomaterials

A considerable amount of research has been devoted to investigating nanowire growth mechanisms and controlling 1D nanomaterials in terms of dimensions, composition, surface chemistry and their compounds.^[3,41] Here, we focus on porous 1D nanomaterials, which are likely to be more complex than the solid nanowire/nanorod/nanobelt. The two major strategies for the synthesis of porous 1D nanomaterials are “bottom-up” and “top-down” approaches. However, in most instances, it is a combination of both a “bottom-up” approach to synthesize the 1D nanomaterial backbone and then a “top-down” approach to create a pore or hollow region in/on it. Based on this protocol, various porous 1D structures can be designed and synthesized. Using “bottom-up” synthesis of the 1D nanomaterial backbone, we describe four methods: electrospinning, liquid phase, template-assisted and chemical deposition. The “top-down” approach of chemical etching adapts a bulk synthesis approach to mesoporous nanowires. We consider these methodologies to be the most effective strategies for synthesizing porous 1D nanostructures with controllable morphology, porosity, size, crystal structure and structural/compositional complexity. Table 1 lists examples of synthesis strategies used for different porous 1D nanomaterials.

3.1. Electrospinning

The electrospinning method has been widely used in the fabrication of nanofibers and represents one of the most efficient strategies for the synthesis of complex 1D nanomaterials.^[66,69–71] In the electrospinning process, the precursor is fed through a spinneret by a syringe pump. Under high voltage, precursor droplets are elongated and deformed into a conical structure (Taylor cone) and then a charged jet is ejected from the tip of the Taylor cone and continuously stretched to form nanofibers/nanowires.^[3,13,71] Electrospinning technology can be extended to fabricate porous, tubular and core/shell 1D structures which offer significant void space. To date, a number of porous 1D nanowires/nanotubes/heterogeneous nanowires have been synthesized by electrospinning.^[3,13] In fabricating 1D nanomaterials both electrospinning processing parameters and annealing parameters play important roles in controlling the final nanostructure.^[66,72–77] The former includes the concentration of precursor solution, the type of polymers and the ratio of inorganic component to polymer among other considerations while annealing parameters generally include the heating rate, temperature, time and atmosphere.

Recently, Ma's group developed a novel gradient-electrospinning and controlled-pyrolysis methodology which provides a general approach for synthesizing porous 1D nanomaterials.^[66] A schematic of gradient electrospinning and controlled pyrolysis is shown in **Figure 2a**. In contrast to conventional electrospinning that uses a single polymer, the precursor solution for gradient electrospinning was prepared with mixtures of low-, middle- and high-molecular-weight poly(vinyl alcohol) (PVA). At high voltage, the mixed PVA tends to separate into three layers of low-, medium- and high-molecular-weight,

Table 1. Materials, nanostructures and synthesis methods reported for porous 1D nanomaterials. (E = Electrospinning method, L = liquid phase method, T = template-assisted method, CE = chemical etching method, and CD = and chemical deposit method).

Material	Nanostructure	Synthesis method	Ref.
C	Mesoporous nanowires	T/L	[165,339]
Si	Porous nanowires/porous nanowire arrays	T/CE	[21,189,194–204,340,341]
S/C or S/polymer	Porous nanofibers	T/E	[67,139,253]
Metals (Co, Cu, Pd, Au, Pt)	Porous nanowires/nanotubes/nanorods	T/E/CD	[132,141,145,146,173,342–348]
Ni@Pt	Porous core-shell nanotube arrays	T	[162]
Alloys (Co-Pt, Pd-Ni, Pt-Co, Pt-Ni-P)	Porous nanorods/nanowires/nanotubes	L/T	[131,132,135–137,161,349,350]
SiO ₂	Porous nanowire arrays	T	[145]
TiO ₂	Porous nanowires/nanoneedles/nanotubes	E/L/T	[76,89,97,110,134,154,351]
TiO ₂ /ZnO	Porous nanofibers	E	[82]
V ₂ O ₅	Porous nanotubes	E	[352]
VO ₂	Mesoporous nanowires	L	[94]
MnO ₂	Mesoporous nanotubes/nanowire arrays	E/T	[66,138,353]
Mn ₂ O ₃	Porous nanowires	L	[95]
Fe ₂ O ₃	Porous nanowires	L	[99]
Fe ₃ O ₄	Mesoporous nanowires/bubble-nanorod-structure	L/E	[52,354]
Fe ₃ O ₄ /VO _x	Porous nanowires	L	[64]
Co ₃ O ₄	Porous nanotubes/porous nanorods/porous nanowire arrays	E/L/T	[56,66,85,86,88,91,93,148,355,356]
Co ₃ O ₄ @MnO ₂	Nanowire@nanosheet core/shell arrays	L	[112]
Co ₃ O ₄ @NiO	Porous core/shell nanowire arrays	L	[116]
Co ₃ O ₄ @Co(OH) ₂	Porous core/shell nanowire arrays	L	[117]
CoO	Porous nanowire arrays	L	[91]
NiO	Mesoporous nanowires/nanorods/hierarchical porous nanotube arrays	L/T	[96,130,164]
NiO/ZnO	Porous nanofibers	E	[81]
CuO	Porous nanowires/nanotubes	T	[66,149,343]
CuO/SnO ₂	Porous nanofibers	E	[84]
ZnO	Mesoporous nanowires/nanotubes	T/L/CD	[169,339,342,357]
GeO ₂ /SnO ₂	Porous nanofibers	E	[83]
In ₂ O ₃	Porous nanotubes/nanowires	E/T/L	[97,155,356,358]
SnO ₂	Porous nanotubes/nanofibers/nanobelts/naowires	T/E/L	[58,66,72,73,79,97,98,150,359–362]
W ₁₈ O ₄₉	Porous nanowires	T	[363]
VN	Porous nanowires	L	[100]
GaN	Porous nanowires	CD	[170]
Co(OH) ₂	Mesoporous nanowires/urchin-like ordered arrays of mesoporous nanowires	T/L	[194,364]
Ni(OH) ₂	Porous nanotube arrays	T	[365]
SiGe	Porous nanorod arrays	T	[163]
LiV ₃ O ₈	Mesoporous nanotubes	E	[66]
LiMn ₂ O ₄	Porous nanotubes	E	[66,153]
LiCoO ₂	Porous nanotubes/nanowires/nanowire arrays	E/L	[66,102,127]
AB ₂ O ₄ (A, B = Ni, Co, Zn, Cu, Mn, Fe or Al)	Porous tube-in-tube structures/nanotubes/nanowires/nanowire arrays	E/L/T/CD	[66,74,92,124,125,142,366,367]
NiCo ₂ O ₄ @MnO ₂	Hierarchical core-shell nanowire arrays	L	[114,115]
NiFe ₂ O ₄ @TiO ₂	Porous core-shell nanowires	L	[368]
Ca ₉ Co ₁₂ O ₂₈	Porous nanowires	L	[126]
CaSnO ₃	Porous Nanotubes	E	[75]

Table 1. Continued.

Material	Nanostructure	Synthesis method	Ref.
$A_3V_2(PO_4)_3$ (A = Li or Na)	Mesoporous nanotubes	E	[66]
LiMnPO ₄	Porous nanowires	L	[105]
$Na_{0.7}Fe_{0.7}Mn_{0.3}O_2$	Mesoporous nanotubes	E	[66]
$LiNi_{1/3}Co_{1/3}Mn_{1/3}O_2$	Mesoporous nanotubes	E	[66]
$0.2Li_2MnO_3 \cdot 0.8LiNi_{0.5}Mn_{0.5}O_2$	Porous nanorods	L	[129]
$LiNi_{0.5}Mn_{1.5}O_4$	Porous nanorods	L	[128]
$La_{0.5}Sr_{0.5}Co_{0.8}Fe_{0.2}O_3$	Porous nanorods	E	[369]
$La_{0.5}Sr_{0.5}CoO_{2.91}$	Hierarchical mesoporous nanowires	L	[68]

Table 2. Electrochemical performance of porous 1D nanomaterials in secondary batteries. (The corresponding synthesis methods are the same as in Table 1.)

Material	LIBs					Ref.
	Highest reversible capacity		Cycling performance			
	Capacity/mAh g ⁻¹	Specific current/mA g ⁻¹	Capacity/mAh g ⁻¹	Cycle	Specific current/mA g ⁻¹	
LiCoO ₂ nanotubes (T)	185	10	168	100	10	[206]
LiNi _{0.8} Co _{0.2} O ₂ nanotubes (T)	205	10	145	100	10	[206]
LiMn ₂ O ₄ porous nanotubes (T)	110	495	120	1200	500	[153]
LiNi _{0.5} Mn _{1.5} O ₄ porous nanorods (L)	140	147	113	500	735	[128]
Li ₃ V ₂ (PO ₄) ₃ /C mesoporous nanowires (L)	128	133	96	3000	665	[290]
Li ₃ V ₂ (PO ₄) ₃ mesoporous nanotubes (E)	131	133	86	9500	1330	[66]
N-doped porous carbon nanofibers (E)	632	1000	625	300	1000	[50]
Hierarchical tubular structures constructed from ultrathin TiO ₂ (B) nanosheets (T)	216	335	160	400	1675	[167]
Elongated bending TiO ₂ -based nanotubes (L)	267	33.5	114	10000	8375	[107]
Double-walled Si nanotubes (CD)	1780	200	874	6000	24000	[20]
Porous Si/SiO _x nanowires (CE)	1936	6000	1503	560	600	[204]
Bubble-nanorod-structured Fe ₂ O ₃ /C nanofibers (E)	913	500	812	300	1000	[52]
3D hierarchical tubular CuO/CuO core/shell heterostructure arrays (CD)	1364	100	1140	1000	1000	[215]
Materials	SIBs					Ref.
	Highest reversible capacity		Cycling performance			
	Capacity/mAh g ⁻¹	Specific current/mA g ⁻¹	Capacity/mAh g ⁻¹	Cycle	Specific current/mA g ⁻¹	
Na ₃ V ₂ (PO ₄) ₃ nanoparticles in 1D carbon nanofibers (E)	77	228	–	–	–	[217]
Na ₃ V ₂ (PO ₄) ₃ /nanoparticles in 1D channel mesoporous carbon (T)	115	57	78	5000	228	[219]
Na _{0.7} Fe _{0.7} Mn _{0.3} O ₂ mesoporous nanotubes (E)	109	100	74	5000	500	[66]
Hollow carbon nanowires (L)	251	100	251	400	50	[226]
Nitrogen doped porous carbon fibers (L)	310	50	23	100	50	[222]
Sn-doped TiO ₂ nanotubes (L)	252	50	257	50	50	[370]
Spider web-like Na ₂ Ti ₃ O ₇ nanotubes (L)	425	50	107	500	500	[232]
SnSb nanoparticles in the Porous carbon nanofiber (E)	392	50	110	200	10000	[54]
NiCo ₂ O ₄ hierarchical porous nanowire array on the carbon fiber (L)	761	50	542	50	50	[233]
Porous CuO Arrays (L)	674	20	290	460	200	[371]
MoS ₂ nanoparticles in carbon nanofibers (E)	381.7	100	283.9	600	100	[236]

Table 2. Continued.

Li-S Battery						
Material	Highest reversible capacity		Cycling performance			Ref.
	Capacity/mAh g ⁻¹	Specific current/mA g ⁻¹	Capacity/mAh g ⁻¹	Cycle	Specific current/mA g ⁻¹	
S in hollow carbon nanofiber (T)	≈1000	335	730	150	837.5	[139]
S in hollow carbon nanofibers filled with MnO ₂ nanosheets (T)	1161	83.75	~700	300	837.5	[62]
S in the three-dimensional carbon nanofibers coated with ethylenediamine-functionalized reduced graphene oxide (T)	1314	167.5	950	200	837.5	[67]

Li-O ₂ Battery						
Material	Voltage plateau (vs Li ⁺ /Li)	Achieved capacity		Cycling performance		Ref.
		Capacity/mAh g ⁻¹	Voltage/V	Cycles	Capacity limit	
La _{0.5} Sr _{0.5} CoO _{2.91} hierarchical mesoporous nanowires (L)	2.7 V	11 509	2	–	–	[68]
La _{0.75} Sr _{0.25} MnO ₃ porous nanotubes (E)	2.8 V	9000-11 000	2.4	124	1000	[276]
Co ₃ O ₄ hierarchical porous nanowires (L)	≈2.65V	11 160.8	2.4	73	1000	[271]

Table 3. Electrochemical performance of porous 1D nanomaterials in supercapacitors. (The corresponding synthesis methods are the same as in Table 1.)

Electrode Material	Initial Specific Capacitance	Electrolyte	Potential range	Energy density/ Power density	Test method	Ref.
Mesoporous carbon nanofiber webs (E)	262 F g ⁻¹ at 0.2 A g ⁻¹	1 M H ₂ SO ₄	-0.2-0.5 V	–	Three electrode cell	[283]
Porous carbon fibers (E)	197 F g ⁻¹ at 5 mV s ⁻¹	1 M H ₂ SO ₄	0-1 V	–	Three electrode cell	[285]
Porous carbon nanofiber networks (E)	302 F g ⁻¹ at 0.2 A g ⁻¹	6 M KOH	0-1 V	5.2 Wh kg ⁻¹ / 10 kW kg ⁻¹	Two electrode cell	[286]
Porous carbon nanofibers (E)	–	0.5 M H ₂ SO ₄	0-1.2 V	3.22 Wh kg ⁻¹ / 0.6 kW kg ⁻¹	Two electrode cell	[287]
Bamboo-like porous carbon nanofibers (E)	2.1 F cm ⁻³ at 33 mA cm ⁻³	H ₃ PO ₄ /PVA gel	0-0.9 V	2.37 Wh kg ⁻¹ / 61.3 kW kg ⁻¹	Two electrode cell	[80]
KOH activated CNTs (CD)	53.6 F g ⁻¹ at 50 mA g ⁻¹	7 M KOH	0-1 V	–	Two electrode cell	[281]
N-doped porous carbon Nanofibers (T)	202 F g ⁻¹ at 1 A g ⁻¹	6 M KOH	-1-0 V	–	Three electrode cell	[289]
N, P-co-doped carbon nanofibers (T)	204.9 F g ⁻¹ at 1 A g ⁻¹	2 M H ₂ SO ₄	0-1 V	1.86 Wh kg ⁻¹ / 26.61 kW kg ⁻¹	Two electrode cell	[290]
PEDOT-nanotube (E)	132 F g ⁻¹ at 5 mA cm ⁻²	1 M LiClO ₄	0-1.2 V	–	Two electrode cell	[299]
Hydrous RuO ₂ nanotubes (T)	861 F g ⁻¹ at 0.5 A g ⁻¹	1 M H ₂ SO ₄	0-1 V	–	Three electrode cell	[292]
Hydrous RuO ₂ nanotube arrays (T)	1300 F g ⁻¹ at 0.1 mV s ⁻¹	1 M H ₂ SO ₄	0-1 V	7.5 Wh kg ⁻¹ / 4320 kW kg ⁻¹	Three electrode cell	[293]
MnO ₂ nanotube (E)	320 F g ⁻¹ at 20 mV s ⁻¹	1 M Na ₂ SO ₄	0-1 V	–	Three electrode cell	[294]
Mesoporous MnO ₂ nanotubes (T)	365 F g ⁻¹ at 0.25 A g ⁻¹	1 M Na ₂ SO ₄	-0.2-0.8 V	–	Three electrode cell	[295]
Porous Co ₃ O ₄ nanowires (L)	260 F g ⁻¹ at 2 A g ⁻¹	2 M KOH	0.1-0.6 V	–	Three electrode cell	[372]
Mesoporous Co(OH) ₂ nanowires (T)	993 F g ⁻¹ at 1 A g ⁻¹	1 M KOH	-0.1-0.5 V	–	Three electrode cell	[301]
Mesoporous NiO nanotubes (L)	405 F g ⁻¹ at 0.5 A g ⁻¹	6 M KOH	0-0.5 V	–	Three electrode cell	[302]
H-TiO ₂ nanotube arrays (CE)	3.24 mF cm ⁻² at 100 mV s ⁻¹	0.5 M Na ₂ SO ₄	0-0.8 V	–	Three electrode cell	[373]
Porous NiCo ₂ O ₄ nanowires (L)	743 F g ⁻¹ at 1 A g ⁻¹	1 M KOH	-0.05-0.45 V	–	Three electrode cell	[303]
Mesoporous NiCo ₂ O ₄ nanowire arrays (L)	1283 F g ⁻¹ at 1 A g ⁻¹	6 M KOH	0-0.4 V	–	Three electrode cell	[304]
MnO ₂ /Mn/MnO ₂ sandwich-structured nanotube arrays (T)	955 F g ⁻¹ at 1.5 A g ⁻¹	1 M Na ₂ SO ₄	0-0.8 V	52 Wh kg ⁻¹ / 15 kW kg ⁻¹	Three electrode cell	[65]
MnO ₂ /CNT composites (L)	201 F g ⁻¹ at 1 A g ⁻¹	1 M Na ₂ SO ₄	0-0.9 V	–	Three electrode cell	[374]
Mesoporous Co ₃ O ₄ nanowire arrays (L)	1160 F g ⁻¹ at 2 A g ⁻¹	6 M KOH	0-0.55 V	–	Three electrode cell	[86]

Table 3. Continued.

Electrode Material	Initial Specific Capacitance	Electrolyte	Potential range	Energy density/ Power density	Test method	Ref.
Porous CoO@PPy nanowire arrays (L)	–	3 M NaOH	0–1.8 V	43.5 Wh kg ⁻¹ / 87.5 W kg ⁻¹	Two electrode cell	[307]
Porous VN nanowires-graphene composites (L)	73 F g ⁻¹ at 0.1 A g ⁻¹	1 M LiPF ₆ in EC/DEC (1:1 v/v)	0–4 V	162 Wh kg ⁻¹ / 200 W kg ⁻¹	Two electrode cell	[338]
Porous TiNb ₂ O ₇ nanotubes (T)	–	1 M LiPF ₆ in EC/DMC (1:1 v/v)	0–3 V	≈34.5 Wh kg ⁻¹ / 7.5 kW kg ⁻¹	Two electrode cell	[332]
Intertwined CNT/V ₂ O ₅ nanowires (L)	–	1 M LiClO ₄ in PC	0.1–2.7 V	40 Wh kg ⁻¹ / 210 W kg ⁻¹	Two electrode cell	[319]
Porous CNT/V ₂ O ₅ nanowire composites (L)	≈35 F g ⁻¹ at 0.5 mA	1 M NaClO ₄ in PC	0–2.8 V	38 Wh kg ⁻¹ / 140 W kg ⁻¹	Two electrode cell	[51]

respectively. At the same time, the inorganic materials were distributed homogeneously in the three layers. Porous nanotubes were generated during heat treatment in different atmospheres because the pyrolysis temperatures for three types of molecular weight are different. The pyrolysis and shrinkage of the inner, low-weight PVA layer occurred first with increasing temperature. At the same time, the inner, low-weight PVA and inorganic materials moved to the boundary between the low- and medium-weight PVA. Expansion of the inside diameter of the nanotubes is achieved by pyrolysis of the medium-weight PVA. Finally, mesoporous nanotubes composed of nanoparticles were obtained. Various inorganic mesoporous nanotubes have been synthesized by this gradient electrospinning approach (Figure 2c–g) including metal oxides (CuO, Co₃O₄, SnO₂ and MnO₂), multi-metal oxides (LiMn₂O₄, LiCoO₂, NiCo₂O₄, LiV₃O₈, Na_{0.7}Fe_{0.7}Mn_{0.3}O₂ and LiNi_{1/3}Co_{1/3}Mn_{1/3}O₂), and phosphate systems A₃V₂(PO₄)₃ (A = Li, Na). Furthermore, by changing the heat-treatment conditions, interesting pea-like nanotubes were obtained (Figure 2h). In this process, the

nanowire precursors were placed in a furnace and preheated to 300 °C in air. The three molecular-weight PVAs decomposed and were quickly transported towards the outer layer without carrying any of the inorganic materials. After subsequent annealing at high temperature, the outer PVA was carbonized to form carbon nanotubes while the inner inorganic materials were grown uniformly in the center of the nanotubes. By this approach, other pea-like nanotubes including Co, LiCoO₂, Na_{0.7}Fe_{0.7}Mn_{0.3}O₂ and Li₃V₂(PO₄)₃ have been successfully synthesized as well. The gradient electrospinning method offers a convenient route for expanding the synthesis of various porous 1D nanomaterials with functional properties.

The annealing parameters have a significant influence on the final morphologies of the electrospun nanofibers.^[73] Peng et al.^[74] controlled the nanostructure of ternary transition metal oxides by adjusting heating rates (Figure 3a). Nanowires, nanotubes and tube-in-tube structures of CoMn₂O₄ were obtained by using different heating rates (Figure 3b-d). In addition, various mixed metal oxides such as NiCo₂O₄, CoFe₂O₄,

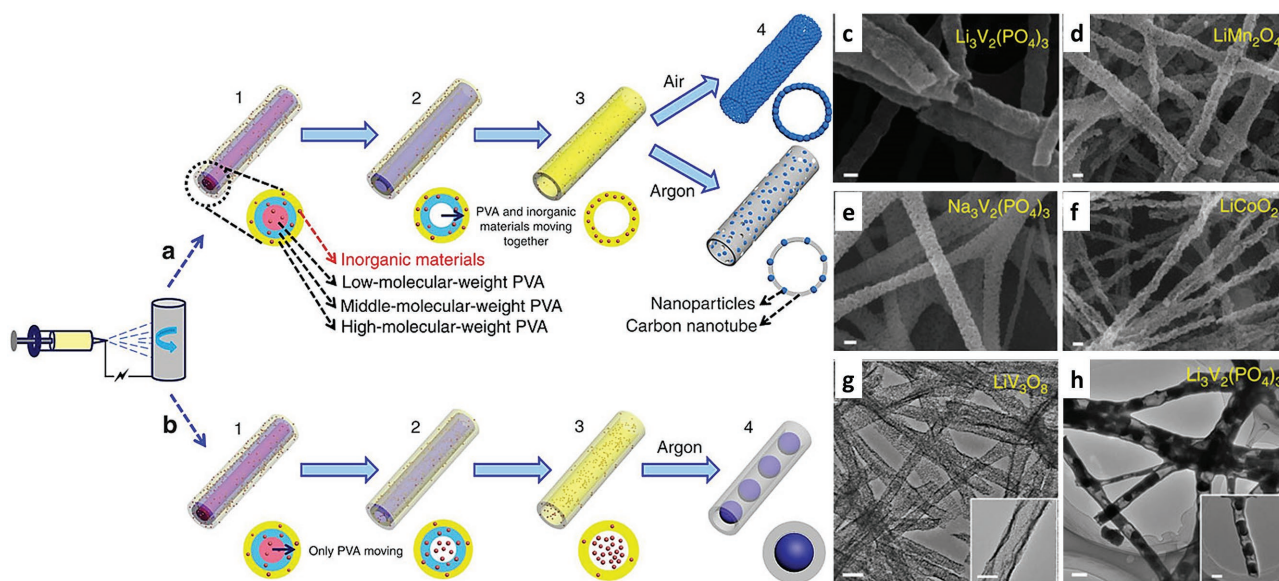


Figure 2. Schematic of gradient-electrospinning and controlled-pyrolysis processes for preparation of (a) mesoporous nanotubes and (b) pea-like nanotubes. c–g) SEM and TEM images of various mesoporous nanotubes, scale bar is 100 nm. h) TEM image of Li₃V₂(PO₄)₃ pea-like nanotubes, scale bar is 200 nm. Scale bars in the inset TEM images of g and h are 100 nm. Reproduced with permission.^[66] Copyright 2015, Nature Publishing Group.

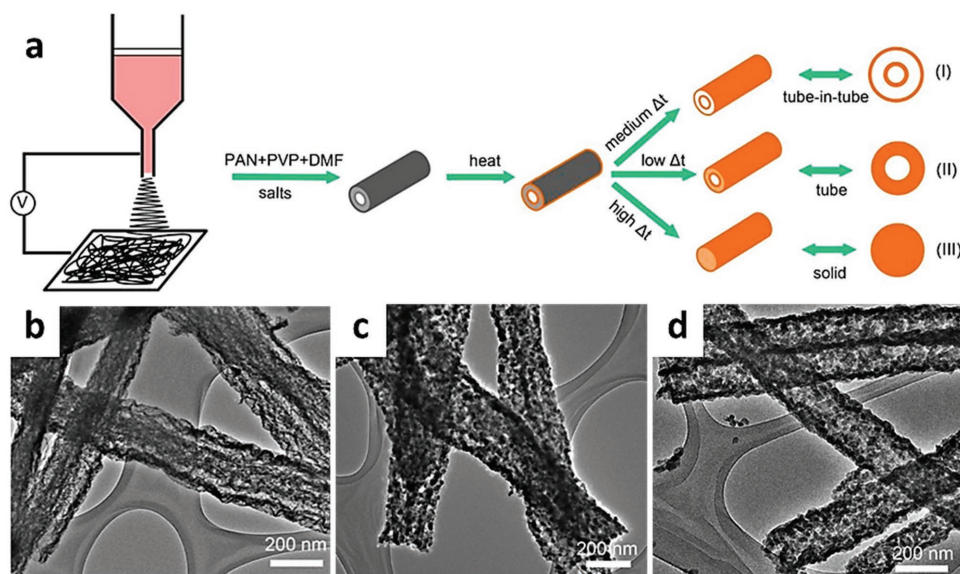


Figure 3. a) Illustration showing nanostructure control using heating rate. SEM images of tube-in-tube nanostructures (b), porous nanotubes (c) and porous nanowires (d). Reproduced with permission.^[74] Copyright 2015, American Chemical Society.

NiMn_2O_4 and ZnMn_2O_4 with porous tube-in-tube structures were successfully obtained. Li et al.^[75] reported processing conditions for obtaining porous CaSnO_3 nanotubes, while CaSnO_3 nanofibers and CaSnO_3 ruptured nanobelts were obtained by changing the annealing temperature. Moreover, the porosity of porous nanowires is also adjustable via the control of annealing temperature. In the case of TiO_2 porous nanowires, the porosity and specific surface area decrease with higher annealing temperature.^[76]

By combining electrospinning with other methods, novel porous 1D nanostructures such as bubble-nanorod-structures^[52,78,79] and bamboo-like structures^[80] have been achieved. The bubble-nanorod-structured Fe_2O_3 -carbon nanofibers involved combining the Kirkendall effect with electrospinning (Figure 4a–d).^[52] First, the precursor nanofibers composed of $\text{Fe}(\text{acac})_3$ (iron acetylacetonate) and polyacrylonitrile (PAN) were synthesized by electrospinning. The FeO_x -carbon nanofibers were obtained by carbonization of PAN and the decomposition of $\text{Fe}(\text{acac})_3$ upon annealing in a reducing atmosphere. In a third step, the FeO_x -carbon nanofibers were annealed in air so that the FeO_x which was reduced to Fe metal in the initial stage was then oxidized to $\text{Fe}@\text{Fe}_2\text{O}_3$ core-shell structure due to the Kirkendall effect (Figure 4b–d). Finally, the bubble-nanorod-structured Fe_2O_3 -carbon nanofibers were generated after the formation of hollow Fe_2O_3 nanospheres, in which the Fe was completely transformed into Fe_2O_3 . The hollow Fe_2O_3 nanospheres were uniformly distributed on/in the carbon nanofibers (Figure 4e). The hollow nanospheres possessed a diameter of ≈ 17 nm and a shell thickness of ≈ 3 nm (Figure 4f). Pure carbon-based materials with a similar morphology also have been synthesized by electrospinning (Figure 4g).^[78,79] A second example of combining methods, a bamboo-like graphitic carbon nanofiber with well-balanced macro-, meso-, and microporosity, was prepared by Cui and co-workers. The material exhibited excellent mechanical flexibility, foldability,

and electrochemical performance.^[80] This novel structure was obtained by pre-synthesizing a uniform distribution of SiO_2 nanoparticles in carbon nanofibers. Upon removing the SiO_2 particles by etching in HF solution, bamboo-like carbon nanofibers were obtained. Similarly, using metal or metal nanocrystals as pre-filled templates is another choice for the synthesis of porous nanofibers.^[50] In this strategy, the porous structure with macro-, meso-, and microporosity can be well controlled.

Electrospinning technology is also efficient for the fabrication of heterogeneous porous 1D nanomaterials. Qiao et al.^[81] used electrospinning to synthesize heterogeneous NiO/ZnO porous nanofibers, while several other heterogeneous porous nanowires, such as TiO_2/ZnO ,^[82] $\text{GeO}_2/\text{SnO}_2$ ^[83] and CuO/SnO_2 ^[84] have also been synthesized by electrospinning.

In summary, electrospinning is a very effective technique for the synthesis of different porous 1D nanomaterials. The control of morphology and porosity can be realized by adjusting the inorganic materials/polymers ratio, the precursor concentration and the annealing temperature. Initial studies suggest that an interesting future direction which can lead to novel porous 1D structures is that of combining electrospinning with other synthesis methods.

3.2. Liquid Phase Method

Liquid phase methods play an essential role in the chemical synthesis of nanomaterials. Based on reaction conditions such as concentration, pH, temperature, time, pressure, additives, etc., various nanostructures have been obtained. In this section, the synthesis of porous 1D nanomaterials by the most common liquid phase approaches including hydrothermal and solvothermal synthesis, the use of microemulsions and various template-assisted methods are reviewed.

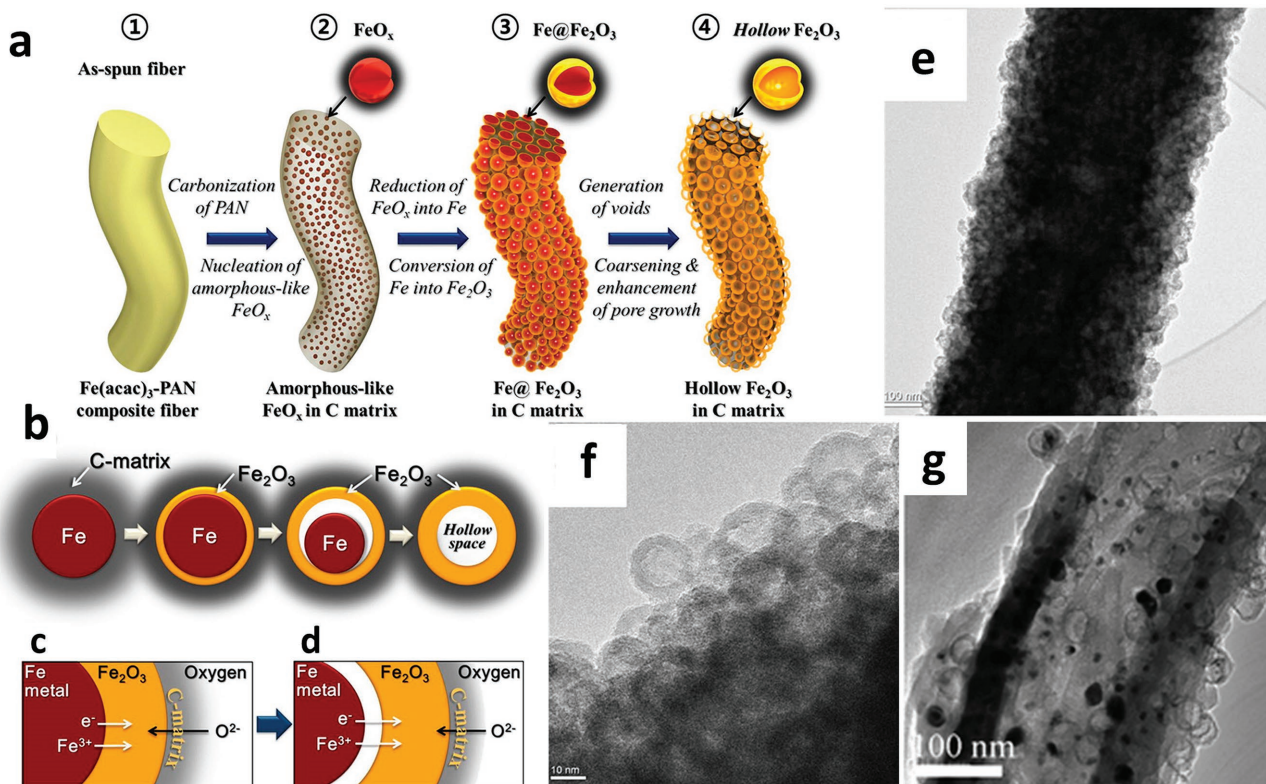


Figure 4. a–d) Schematic of the formation mechanism of $\text{Fe}_2\text{O}_3\text{-C}$ nanofibers with bubble-nanorod-structure. e, f) TEM images of $\text{Fe}_2\text{O}_3\text{-C}$ nanofibers. Figures a–f reproduced with permission.^[52] Copyright 2015, American Chemical Society. g) TEM image of carbon-based materials with bubble-nanorod-structure, reproduced with permission.^[78] Copyright 2012, Royal Society of Chemistry.

3.2.1. Hydrothermal and Solvothermal Method

Hydrothermal and solvothermal methods are very effective routes for synthesizing nanomaterials through the use of aqueous solvents, organic-inorganic hybrid solvents or pure organic solvents. A universal approach for preparing 1D porous nanostructures is to use the hydrothermal or solvothermal process to prepare a 1D nanostructure precursor which is then followed by annealing treatment to create a porous morphology. Depending upon the annealing temperature and atmosphere, the 1D precursor would undergo phase transition, oxidation, reduction or pyrolysis with the escaping gas resulting in the formation of pores. Zheng and co-workers^[56] synthesized a cobalt oxide precursor via a mixed H_2O /ethanol solvothermal treatment at 90°C . The precursor was annealed at 250°C for 2 h in N_2 to obtain mesoporous Co_3O_4 nanowires with high surface area. The mesoporous Co_3O_4 nanowires could also be reduced in NaBH_4 solution, which increased the oxygen vacancy concentration on the nanowire surface and resulted in higher electrical conductivity and greater reactivity. Furthermore, the mesoporous cobalt oxide nanowires could be grown on different substrates (Figure 5a), such as Ni foam,^[85–87] Si,^[88] glass,^[88] steel,^[89] Ti,^[90,91] carbon paper,^[92,93] and polystyrene^[88] to form mesoporous nanowire arrays for additive-free and flexible applications. Other hydrothermal studies of cobalt-based porous nanowires include those of Jiang et al.^[91] for CoO (Figure 5b) and Rakhi et al.^[93] for mesoporous Co_3O_4

nanowire arrays on carbon paper (Figure 5c). After annealing, the mesoporous Co_3O_4 nanowires exhibited a surface area of $76\text{ m}^2\text{ g}^{-1}$ with pore sizes in the range of 2–4 nm. Other porous nanowires which have been reported include VO_2 ,^[94] Mn_2O_3 ,^[95] NiO ,^[96] TiO_2 ,^[97] In_2O_3 ,^[97] PbO ,^[97] SnO_2 ,^[98] and Fe_2O_3 ,^[99] each of which has been synthesized by hydrothermal or solvothermal methods followed by appropriate annealing conditions. Figure 5d shows the results of An et al.^[64] who reported the use of amorphous vanadium oxides as a matrix for supporting hierarchical porous Fe_3O_4 /graphene nanowires. In addition to oxides, porous nitride^[100] and sulfide^[101] nanowires have been obtained. Li and co-workers^[100] prepared porous vanadium nitride nanowires by annealing VO_x nanowires in ammonia at 600°C for 1 h (Figure 5e). During the annealing process, the VO_x nanowires were reduced to porous VN nanowires by the removal of H_2O and O_2 . The loss of oxygen resulted in the formation of porous 1D structure. An interesting process for synthesizing some transition metal oxides for LIBs is to react the precursor oxide hydrothermally with a lithium salt solution.^[102,103] For example, Xia et al.^[102] carried out hydrothermal reaction of Co_3O_4 nanowire arrays in LiOH solution at 240°C for 48 h to achieve lithiation. The low temperature spinel phase (LT- LiCoO_2) transformed to layered LiCoO_2 after annealing at 750°C in air for 2 h.

The use of one-step or two-step liquid-phase reaction without a subsequent annealing treatment also has been developed for the synthesis of porous nanowires. The preparation of porous

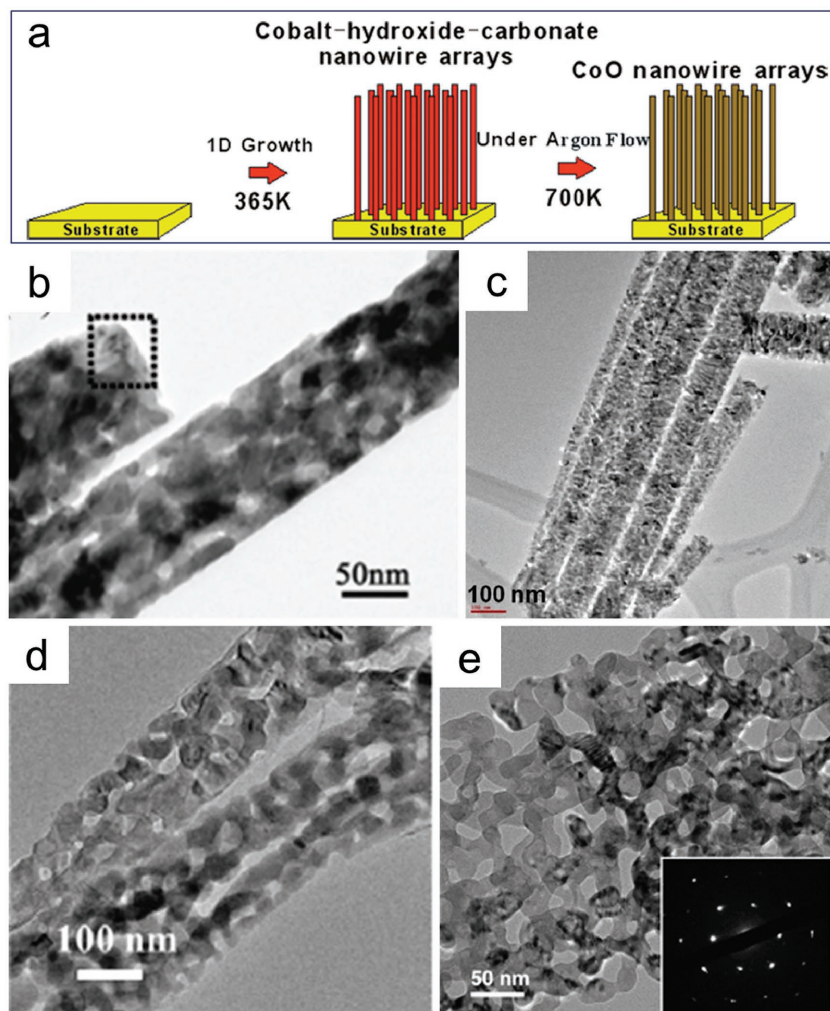


Figure 5. a) Schematic of the porous CoO nanowire growth process on Ti substrates. b) TEM image of porous CoO nanowires. Figures a,b reproduced with permission.^[91] Copyright 2010, American Chemical Society. c) TEM image of porous Co₃O₄ nanowires, reproduced with permission.^[93] Copyright 2012, American Chemical Society. d) TEM image of porous Fe₃O₄/VO_x nanowires, reproduced with permission.^[64] Copyright 2014, American Chemical Society. e) TEM image of a porous VN nanowire with corresponding SAED pattern, reproduced with permission.^[100] Copyright 2012, American Chemical Society.

nanowires through the one-pot hydrothermal or solvothermal method usually needs an ion or organic molecule to serve as a soft template or structure-directing agent. Yuan et al.^[104] successfully synthesized ordered arrays of mesoporous Co(OH)₂ nanowires by a one-step hydrothermal treatment at a low temperature of 100 °C (Figure 6a,b). During the synthesis process, the Co(OH)₂ nanoparticle building blocks aggregated and formed Co(OH)₂ nanowires which contained mesopores to decrease their high surface energy. Growth of the mesoporous nanowires occurred upon continuous hydrothermal treatment by Ostwald ripening. Mixed solvents (glycol and distilled water) developed by Pei et al.^[105] were used to synthesize LiMnPO₄ porous nanowires which formed tubular 1D nanomaterials through the use of controlled growth conditions. Another interesting material, H₂Ti₃O₇ nanotubes, were obtained by a one-step hydrothermal process by treating crystalline TiO₂ in a

concentrated NaOH solution.^[106] TiO₂ reacts with NaOH to form a highly disordered phase which then recrystallizes into thin H₂Ti₃O₇ plates. The deficiency of hydrogen at the surface leads to an asymmetric surface tension, causing the surface layer to bend and the formation of multiwall spiral nanotubes. Tang et al.^[107] added magnetic stirring to this hydrothermal reactive process enabling more elongated nanotubes to be obtained. VO_x nanoscrolls^[108] and H₄Nb₆O₁₇·nH₂O nanoscrolls^[109] have also been obtained by the one-step hydrothermal or solvothermal method.

In the two-step liquid phase method, the 1D nanostructure precursors obtained from the initial hydrothermal or solvothermal treatment develop a porous structure via a second liquid-phase reaction. Kim and co-workers^[110] synthesized hydrogen titanate nanowires (H₂Ti₃O₇·nH₂O) as the precursor which then formed porous TiO₂ nanowires by hydrothermal dehydration at a temperature of 180 °C (Figure 6c). Jin et al.^[111] synthesized porous TiO₂ (anatase) nanowires via an in situ hydrothermal treatment of amorphous TiO₂ nanotubes in a urea aqueous solution at 70 °C (Figure 6d–h). A dissolution–recrystallization process was proposed to explain the morphology transformation from nanotubes to porous nanowires. The authors proposed that hydroxyl ions generated from hydrolysis of the urea at 70 °C reacted with the TiO₂ nanotube surfaces to form TiO₃²⁻, resulting in the gradual dissolution of the TiO₂ nanotube. The TiO₃²⁻ took part in a hydrolytic reaction to transform into aggregated TiO₂ nanocrystallites when the concentration of OH⁻ inside the nanotube decreased to a certain value. Over time, the TiO₂ nanocrystallites gradually occupied the inner space of the nanotube to form the porous nanowires.

Multistep hydrothermal or solvothermal methods can also be used to fabricate hierarchical heterostructured core-shell porous nanowires using nanoparticles, nanowires or nanosheets as building blocks. Fan and co-workers^[112] constructed MO_x (M = Co, Zn, Sn, etc.) nanowire@MnO₂ ultrathin nanosheet core/shell arrays with interconnected porosity through interface reactions between KMnO₄ and graphitic carbon. The MO_x nanowires were impregnated with an aqueous glucose solution and upon annealing in Ar, resulting in a uniform coating of an amorphous carbon layer on the nanowire surface. The MO_x/C nanowires were then placed in a KMnO₄ solution at 160 °C for 1–5 h. The resulting redox process (Equation (1)), enabled the formation of core/shell MO_x nanowire@MnO₂ nanosheet arrays.



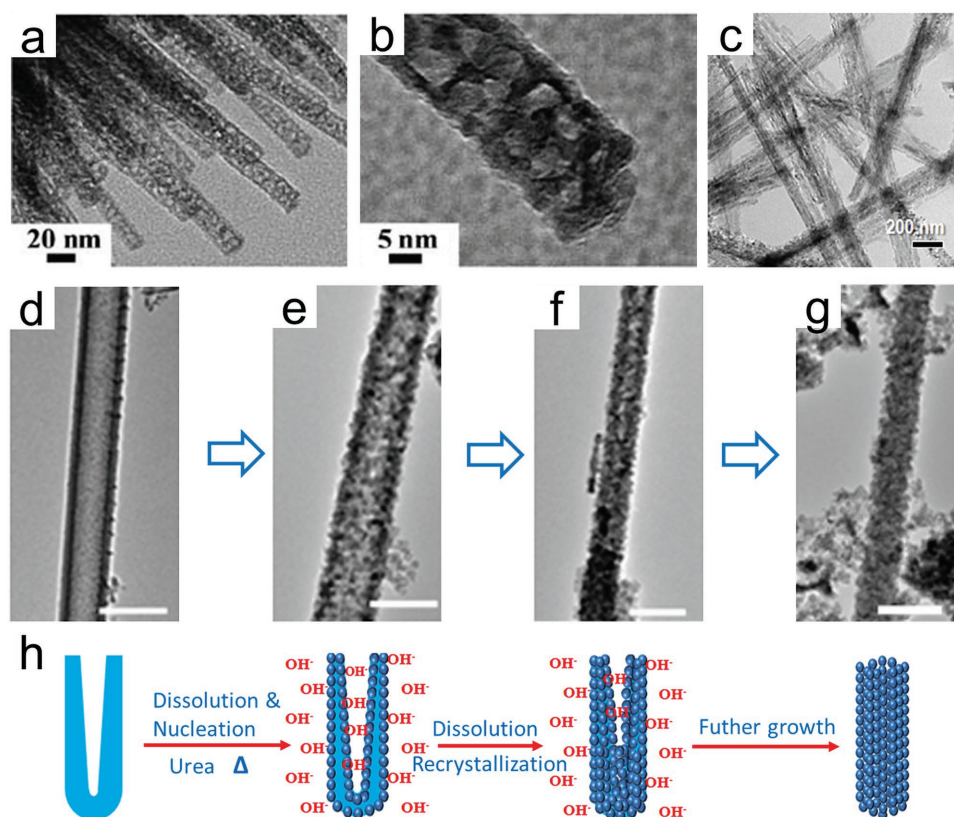


Figure 6. a,b) TEM images of urchin-like mesoporous $\text{Co}(\text{OH})_2$ nanowire arrays, reproduced with permission.^[104] Copyright 2010, Royal Society of Chemistry. c) TEM image of LT- TiO_2 nanowires, reproduced with permission.^[110] Copyright 2010, IOP Publishing. d–g) Morphology transformation from TiO_2 nanotube to porous TiO_2 nanowire at different reaction times: (d) 0 h, (e) 2 h, (f) 4 h, (g) 6 h and (h) corresponding schematic illustration, reproduced with permission.^[111] Copyright 2013, Elsevier.

Moreover, using oriented attachment and self-assembly processes, metal oxide core/shell nanowire arrays can be synthesized by growing NiO nanoflakes on porous Co_3O_4 or ZnO nanowires via simple chemical bath deposition (Figure 7a).^[113] The porous Co_3O_4 (Figure 7b) acted as a backbone to guide preferential deposition of Ni-based hydroxide. With heterogeneous nucleation of many Ni-based hydroxide mesocrystals in supersaturated solution, these mesocrystals attached to the surfaces of Co_3O_4 or ZnO nanowires, lowering their surface energy. The active sites minimize the interfacial energy barrier for the subsequent growth of Ni-based hydroxide. Finally, these Ni-based hydroxide mesocrystals self-assembled into 2D-nanoflake structures (Figure 7c). Similar metal oxide core/shell nanowire arrays, such as $\text{NiCo}_2\text{O}_4@\text{MnO}_2$,^[114,115] $\text{Co}_3\text{O}_4@\text{NiO}$,^[116] $\text{Co}_3\text{O}_4@\text{Co}(\text{OH})_2$ ^[117] can also be obtained by hydrothermal synthesis followed by chemical or electrochemical deposition (Figure 7d). For LIBs, the hierarchical structure effectively reduces the self-aggregation of active materials, increases the electrode–electrolyte contact area and accommodates the volume changes which occur on lithiation and delithiation. The core-shell heterostructure combines the advantages of higher capacity and better stability.

Nanoparticles are beneficial for shortening diffusion length, but they easily self-aggregate, rendering them inactive. Wei et al.^[63] synthesized a hierarchical mesoporous nanowire composite with $\text{Li}_3\text{V}_2(\text{PO}_4)_3$ active nanocrystals embedded in

conductive mesoporous nanowire scaffolds via one-pot hydrothermal synthesis followed by an annealing treatment. During the hydrothermal process, self-assembly of organic surfactants and hydrolysis of colloids resulted in the generation of an inorganic/organic nanowire precursor. The as-prepared nanowire precursor crystallized the $\text{Li}_3\text{V}_2(\text{PO}_4)_3$ nanoparticles, and the organic compounds pyrolyzed in situ into mesoporous carbon scaffolds during the annealing process. The final hierarchical nanostructure consisted of $\text{Li}_3\text{V}_2(\text{PO}_4)_3$ nanoparticles uniformly embedded in conductive mesoporous carbon nanowires. This kind of novel porous 1D nanocomposite enabled both continuous electron transport and ion transport (Figure 7e). In addition, the stable mesoporous nanostructure effectively confined the expansion of nanocrystals and restrained the structural damage arising from repeated Li^+ ion insertion. In this way, nanocrystals embedded in porous carbon scaffolds were very effective in enhancing overall electrochemical performance. Jiang et al.^[118] constructed core-shell hybrid nanowires with a core of manganese oxide and a shell of mesoporous carbon (Figure 7f,g). The mesoporous carbon layer was coated on the MnO_2 nanowire via carbonization of self-polymerized dopamine. In their method, poly (ethylene oxide)-poly (propylene oxide)-poly (ethylene oxide) (PEO-PPO-PEO, P123) was used as a structure-directing agent to generate the mesoporous structures. After annealing under flowing argon, highly graphitic carbon-tipped MnO_x /mesoporous carbon hybrid nanowires

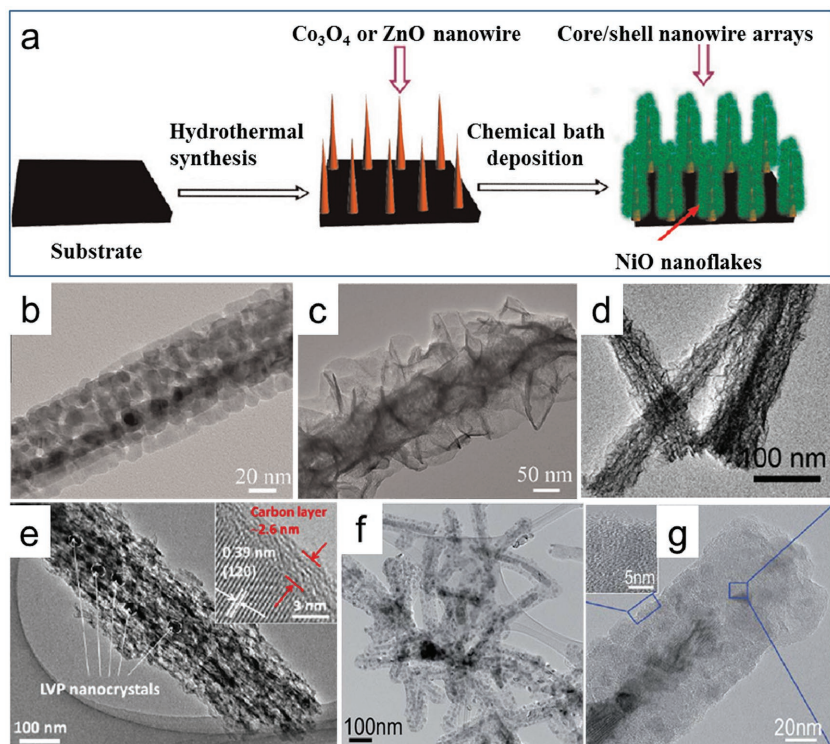


Figure 7. a) Schematic of the two-step synthesis of metal oxide core/shell nanowire arrays. b,c) TEM images of Co_3O_4 nanowire and $\text{Co}_3\text{O}_4/\text{NiO}$ core/shell nanowire. Figures a–c reproduced with permission.^[113] Copyright 2012, American Chemical Society. d) TEM image of $\text{NiCo}_2\text{O}_4@\text{MnO}_2$ core-shell heterostructured nanowires on Ni foam, reproduced with permission.^[114] Copyright 2013, Royal Society of Chemistry. e) TEM image of $\text{Li}_3\text{V}_2(\text{PO}_4)_3/\text{C}$ mesoporous nanowires, reproduced with permission.^[63] Copyright 2014, American Chemical Society. f,g) Low and high magnification TEM images of highly graphitic carbon-tipped manganese oxide/mesoporous carbon/manganese oxide hybrid nanowires, reproduced with permission.^[118] Copyright 2011, Royal Society of Chemistry.

were obtained. Other core/shell nanostructures which have been prepared via a multistep hydrothermal process followed by annealing include mesoporous $\text{TiO}_2\text{-Sn}/\text{C}$ core-shell nanowires,^[119] MnO_x/C yolk-shell nanorods,^[120] and MnO/C nanopeapods.^[121]

3.2.2. Microemulsion Method

The microemulsion method is an efficient approach for synthesizing nanomaterials. Its energy-saving nature and facile processing make this method attractive.^[122] During the reaction, collisions among reverse micelles containing the reactants lead to nucleation. A major advantage of the microemulsion method is the ability to control the morphology and pore size, which can be tailored by controlling reactant concentrations, temperature, water to surfactant ratios, and aging time.^[3]

In forming microemulsions, cetyltrimethyl ammonium bromide (CTAB) is the most common surfactant used to form reverse micelles. Xu et al.^[123] prepared nanoparticle-assembled porous Co_3O_4 nanorods with a diameter of ≈ 200 nm and length of 3–5 μm obtained via microemulsion and subsequent

annealing (Figure 8a). Reverse micelles containing Co^{2+} coming in contact with $\text{C}_2\text{O}_4^{2-}$ resulted in the formation of precursor CoC_2O_4 nuclei. After CTAB surfactant molecules adsorbed onto the surface of the CoC_2O_4 nuclei, nanorods formed by direct growth. During subsequent annealing, the CoC_2O_4 nanorods transformed to porous Co_3O_4 nanorods from the release of CO_2 . Similar strategies can be used to synthesize cobalt-based binary-metal oxides. Du et al.^[124] reported porous ZnCo_2O_4 nanowires via a microemulsion-based nanostructuring approach. The lengths of nanowires were several micrometers with diameters of 100–300 nm, with many pores well distributed in the nanowires (Figure 8b–e). NiCo_2O_4 ,^[125] $\text{Ca}_9\text{Co}_{12}\text{O}_{28}$,^[126] and LiCoO_2 ^[127] porous nanowires were also obtained using the same synthesis approach but replacing/adjusting the reaction sources.

Li-rich layered cathode materials with porous 1D nanostructures have been obtained through the microemulsion method. Zhang et al.^[128] prepared porous $\text{LiNi}_{0.5}\text{M}_{1.5}\text{O}_4$ nanorods using MnCo_2O_4 nanowires as precursors, which transformed to porous Mn_2O_3 nanowires during subsequent annealing. Afterwards, Li and Ni were incorporated into porous Mn_2O_3 nanowires via solid state heat treatment to obtain porous $\text{LiNi}_{0.5}\text{Mn}_{1.5}\text{O}_4$ nanorods. Porous nanorods with the composition $0.2\text{Li}_2\text{MnO}_3 \cdot 0.8\text{LiNi}_{0.5}\text{Mn}_{0.5}\text{O}_2$ have also been synthesized using a similar strategy with porous Mn_2O_3 nanowires as a precursor.^[129]

Control of morphology and pore size distribution in the microemulsion synthesis method has also been investigated. Bai et al.^[130] reported that porous NiO nanorods were obtained with CTAB as the surfactant, and that pore size distribution can be tuned by varying the $\text{Ni}^{2+}/\text{CTAB}$ molar ratios. In addition, the microemulsion method is also suitable for synthesizing complex nanostructures, such as hierarchical mesoporous nanowires. Zhao et al.^[68] reported hierarchical mesoporous $\text{La}_{0.5}\text{Sr}_{0.5}\text{CoO}_{2.91}$ nanowires consisting of nanorods that were 40 nm in diameter, with a specific surface area of $97 \text{ m}^2 \text{ g}^{-1}$ and average pore width of ≈ 10 nm.

Liquid phase synthesis methods feature simplicity, mild chemical conditions, scalability and possess the potential for controlling size and structure on the nanoscale. However, exact growth and formation mechanisms for many 1D nanomaterials synthesized via liquid phase methods remain unknown and require more research to elucidate. More precise control of the reaction processes occurring in liquid phase synthesis is needed in order to make these methods more attractive. Moreover, for large-scale manufacture in industry, efficient and cost-effective recycling of the solvents involved in the solvothermal or microemulsion-based systems need to be developed.

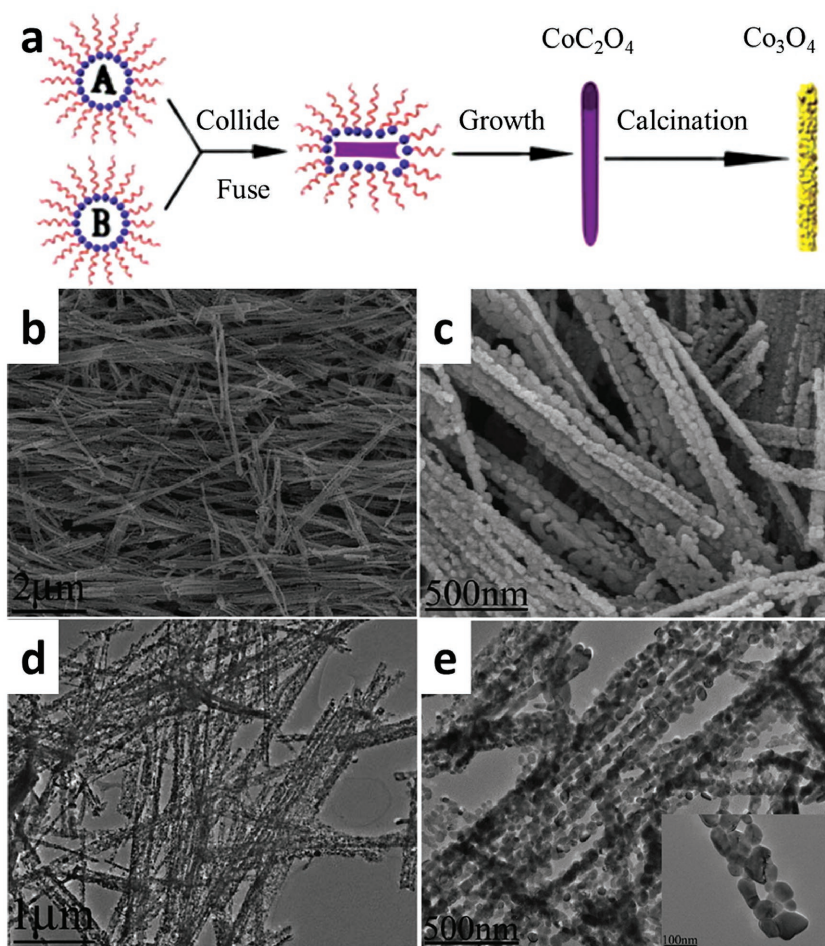


Figure 8. a) Schematic of the growth mechanism in porous Co_3O_4 nanorods, reproduced with permission.^[123] Copyright 2009, Elsevier. b,c) SEM and (d,e) TEM images of ZnCo_2O_4 nanowires reproduced with permission.^[124] Copyright 2009, American Chemical Society.

3.3. Template-Assisted Method

The template-assisted approach is one of the most widely used strategies for synthesizing nanomaterials, especially 1D nanomaterials. Different types of templates have been developed in the synthesis of porous 1D nanomaterials depending on the desired growth mechanism. There are two general categories of templates used in synthesizing porous nanowires: one is the nanoconfined template and the other is the oriented template. Nanoconfined templates include anodic alumina oxide (AAO) membranes, polycarbonate (PC) membranes and mesoporous templates (e.g., SBA-15, CMK-3), among others. In the case of oriented templates, they usually contain carbon nanofibers (CNFs), carbon nanotubes (CNTs), inorganic metal oxide nanowires, metal nanowires and so forth.

3.3.1. Nanoconfined Template Method

AAO is one of the most common nanoconfined templates and many porous nanowires have been obtained using this approach.^[131–139] In one instance, nanoporous Pt-Co

alloy nanowires were formed in a porous AAO membrane via electrodeposition (Figure 9a–f).^[131] After a subsequent de-alloying treatment, cobalt atoms were selectively dissolved leading to porous nanowires. During the de-alloying treatment, the AAO membrane was removed partly or completely resulting in porous Pt-Co nanowires with a Pt-enriched outer surface. The width of the nanowires ranged from 2 to 8 nm with the pore size less than 5 nm. Several other porous 1D nanomaterials (Au,^[132,133] Pt,^[132,134] Pt-Ni alloy,^[135–137] MnO_2 ,^[138] among others) have been obtained using similar procedures with the AAO membrane as a template.

Other nanoconfined templates have been successfully used in the synthesis of porous nanowires. Gu et al.^[61] used SBA-15 as a template to prepare mesoporous peapod-like Co_3O_4 @carbon nanotube arrays. The as-synthesized nanotube arrays possess high surface areas (up to $750 \text{ m}^2 \text{ g}^{-1}$) and large pore sizes. Many other porous nanowires, such as mesoporous CoN,^[140] porous Ni,^[141] mesoporous CuCo_2O_4 ^[142] and mesoporous Si@carbon core-shell,^[143] have been synthesized with SBA-15 as the template.

Interestingly, biological templates have also been used in the synthesis of porous nanowires. Liu et al.^[144] used a crab shell biological template to synthesize porous nanowires. Crab shells were annealed in air to remove organics on the surface and ground into powders. Precursor solution was then impregnated into the crab shell powders, and after heating, the precursor was carbonized. After removing the biological template, the resulting mesoporous carbon nanofiber arrays had a mean diameter of 70 nm and pore size of 11 nm.

Diameter and the pore size distribution are two significant parameters for porous nanowires, so that the control of these parameters is very important. Li et al.^[145] reported a dual template approach, wherein both porous membranes and small spheres were used as templates and the diameter and pore size were well controlled by adjusting the channel size of the membrane and the diameter of spheres (Figure 9g). Two pieces of porous membranes (e.g., AAO membranes) with different channel sizes were first stacked parallel to each other, and then polymer (e.g., polystyrene, PS) spheres were filled into the top membrane by filtration. Afterwards, the bottom membrane was removed and the top membrane with spheres was used as an electrode for electrodeposition. Precursors were infiltrated into the membrane-sphere composite during the electrodeposition process and novel porous nanowires were obtained after dissolving the membrane and spheres. Bechelany et al.^[146] used PC membranes and PS spheres as templates to synthesize porous Co nanowires with different diameters and pore sizes. Combining the nanoconfined template-assisted method with

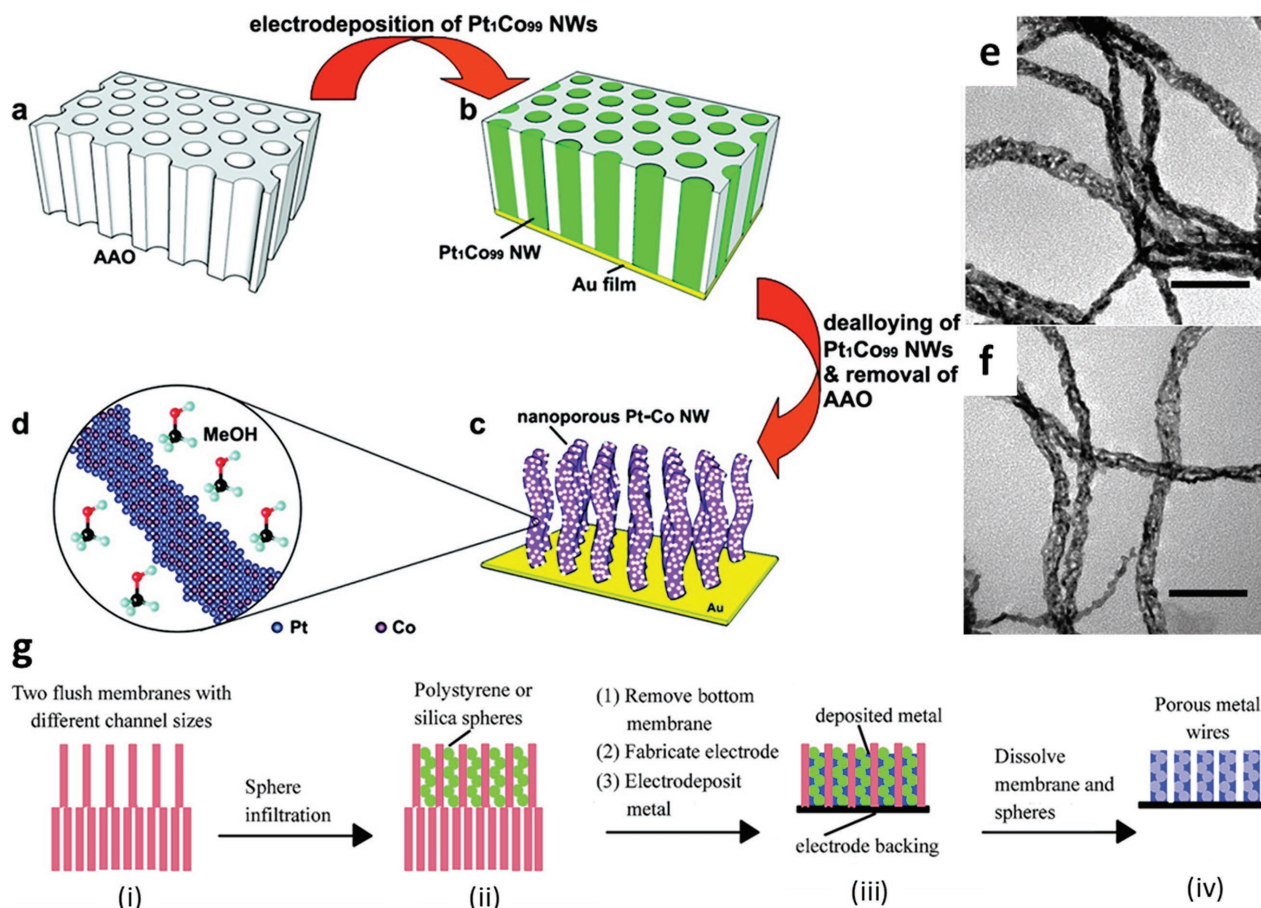


Figure 9. a–d) Schematic of the process for fabricating porous Pt-Co alloy nanowires. (e,f) TEM images of porous Pt-Co alloy nanowires, scale bar is 50 nm. Figures a–f reproduced with permission.^[131] Copyright 2009, American Chemical Society. g) Fabrication process of porous nanowires via a dual template technique, reproduced with permission.^[145] Copyright 2003, American Chemical Society.

electrodeposition is a very effective means of preparing porous nanowires and is described in a later section 3.4.2.

3.3.2. Oriented Template Method

CNTs are one of the most popular oriented templates because of their adjustable diameter, large-scale yield and easy removal. CNTs are an efficient template for the synthesis of porous 1D nanomaterials because of their original 1D nanostructure. Zhu et al.^[147] fabricated CNT@Ni₃S₂ 1D hybrid nanostructures via a multi-step conversion route with CNT as template (Figure 10a). A silica coating was grown on CNT by hydrolyzing tetraethyl orthosilicate. Nickel silicate nanosheets were then grown in situ on the silica layer to form a CNT@SiO₂@Ni₃Si₂O₅(OH)₄ precursor. The final CNT@Ni₃S₂ product was obtained by the transformation of Ni₃Si₂O₅(OH)₄ to Ni₃S₂ and elimination of the silica layer (Figure 10b). Other porous metal oxide/CNT 1D hybrid nanostructures, including Co₃O₄/CNT,^[148] CuO/CNT,^[149] SnO₂/CNT,^[58,150,151] and mesoporous carbon/CNT^[152] have been synthesized using CNT as the template. Metal oxide nanotubes such as LiMn₂O₄,^[153] TiO₂,^[154] and In₂O₃,^[155] can also be obtained after removing CNT templates from the initial composites.

Another carbon-based one dimensional material, CNF, has been widely used as a template in the synthesis of porous nanowires.^[156] Zhang et al.^[157] synthesized hierarchical 1D NiO/CNF nanomaterials where Ni-precursors were grown on the surface of CNFs via a mild solution-phase method. During subsequent heat treatment, Ni-precursors transformed to NiO and hierarchical NiO/CNF nanocomposites were obtained. The as-synthesized 1D nanomaterial had a yolk-shell structure with CNFs inside hierarchical NiO nanotubes (composed of interconnected nanosheets) with void space between the inner CNFs and outer NiO (Figure 10c). Several other materials, including MnO/CNF,^[158] CoMn₂O₄/CNF,^[158] MoS₂/CNF^[159] and V₂O₅/CNF^[160] with porous 1D nanostructures have been synthesized with CNFs as a template.

Inorganic oriented templates may also be used in the synthesis of porous nanowires. Ding et al.^[161] reported porous Pt-Ni-P nanotube arrays prepared by using ZnO nanorod arrays as template. The Pt-Ni-P nanoparticles were electrodeposited on the surface of ZnO to form ZnO@Pt-Ni-P core-shell nanorod arrays. Porous Pt-Ni-P nanotube arrays were obtained after removing the ZnO nanorod template by acid etching. In addition, porous Ni@Pt core-shell nanotube arrays,^[162] porous SiGe nanorod arrays^[163] and hierarchical porous NiO nanotube arrays^[164] have also been synthesized with the assistance

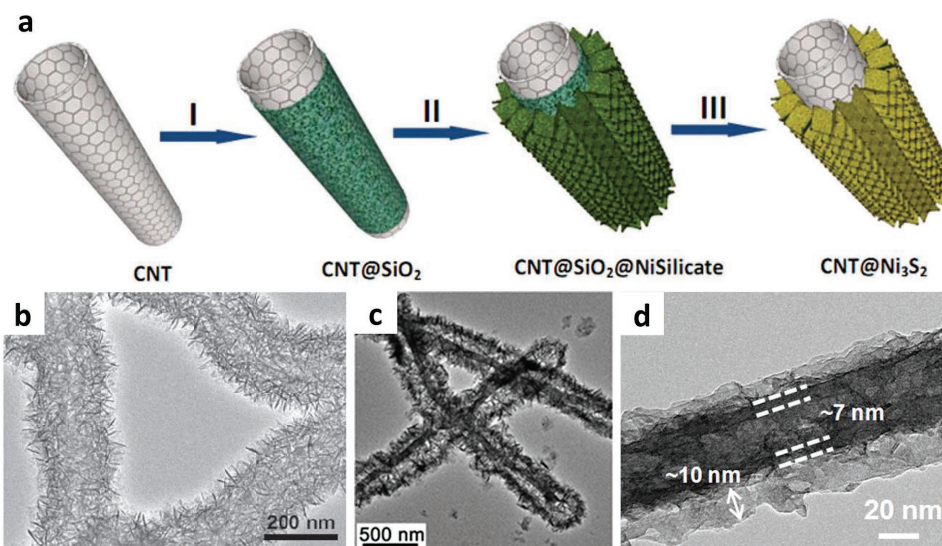


Figure 10. a) Schematic of the formation and (b) TEM images of CNT@Ni₃S₂ 1D nanostructures, reproduced with permission.^[147] Copyright 2012, WILEY-VCH. c) TEM image of hierarchical CNF/NiO nanotubes, reproduced with permission.^[157] Copyright 2013, Royal Society of Chemistry. d) TEM image of porous V₂O₅@MnO₂ nanotubes, reproduced with permission.^[166] Copyright 2014, American Chemical Society.

of ZnO nanorod arrays as a template. Liu et al.^[165] reported mesoporous carbon nanotubes synthesized using MnO₂ nanorods as template. Tan et al.^[166] used V₂O₅ nanowires as a template to synthesize porous V₂O₅@MnO₂ nanotubes and V₂O₅@MnO₂/M nanotubes (M = Fe₂O₃, Co₂O₃/Co(OH)₂, Ni(OH)₂) (Figure 10d). In addition to metal oxide templates, metal nanowires are also viable templates for the synthesis of novel nanostructures.^[156,167] Hu et al.^[167] used Cu nanowires as a template to synthesize hierarchical TiO₂ tubular nanostructures. Recently, Yu and co-workers summarized their work on ultrathin Te nanowires as a versatile template to construct a series of 1D nanostructures, including CNFs.^[156]

The template-assisted approach, due to its reliability and controllability, is a very effective approach for the synthesis of porous 1D nanomaterials. Moreover, the ability to combine a wide range of novel templates provides a creative feature in this process. As the introduction of new materials and approaches to the template-assisted method will extend the development of nanomaterial design and synthesis.

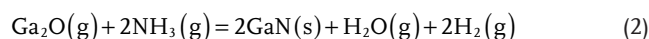
3.4. Chemical Deposition Method

3.4.1. Chemical Vapor Deposition

Chemical vapor deposition (CVD) is a common way to synthesize semiconductor nanowires for energy storage, electronics, photonics and other fields. In the synthesis of porous nanowires, a two-step process consisting of CVD for the growth of well-defined nanowires followed by a heat treatment for the formation of porous structure, is an effective way to prepare designed nanowires. For instance, Shan et al.^[168] synthesized CdSe and ZnCdSe precursor nanowires by metal-organic chemical vapor phase deposition (MOCVD) on Si (100) substrates using Au as a catalyst. Porous ZnO and ZnCdO nanowires were subsequently obtained by subsequent oxidation

of ZnSe and ZnCdSe nanowires in air at 700 °C for 1 h (Figure 11a,b).^[169] Porous ZnO and ZnCdO nanowires composed of nanoparticles and nanopores were formed due to the rapid oxidation process occurring at boundaries or defects.

It is also possible to achieve direct synthesis of porous single-crystalline nanowires via CVD. Bae et al.^[170] reported porous GaN nanowires, synthesized by CVD of a Ga/Ga₂O₃/B₂O₃/C mixture under NH₃. The low magnification TEM image (Figure 11c) revealed straight, porous, high-density, pure GaN nanowires without any other nanostructures. The diameter of the GaN nanowires was in the range of 30–70 nm with a pore size of 5–20 nm as shown in Figure 11d. The corresponding SAED pattern further proved that the wurtzite GaN nanowire was single crystal with a [011] growth direction. During the reaction, Ga₂O vapor was first generated by the Ga and Ga₂O₃ mixture, followed by a vapor-liquid-solid (VLS) growth process. The Ga₂O vapor deposited on catalytic nanoparticles and formed a miscible liquid alloy. Subsequently, Ga and NH₃ dissolved, leading to the precipitation of GaN as follows (Equation (2)):



The escape of H₂ and H₂O leads to the formation of a porous structure during the growth of GaN nanowires.

3.4.2. Electrodeposition

Electrodeposition has been developed extensively over the past several decades for the preparation of metal,^[171] semiconductor^[172] and polymer nanomaterials, as it offers a low-energy, facile process, with good uniformity that can be well controlled. For the synthesis of porous nanowires, a template-assisted electrodeposition method is effective. Laocharoensuk et al.^[173] constructed shape-tailored porous Au

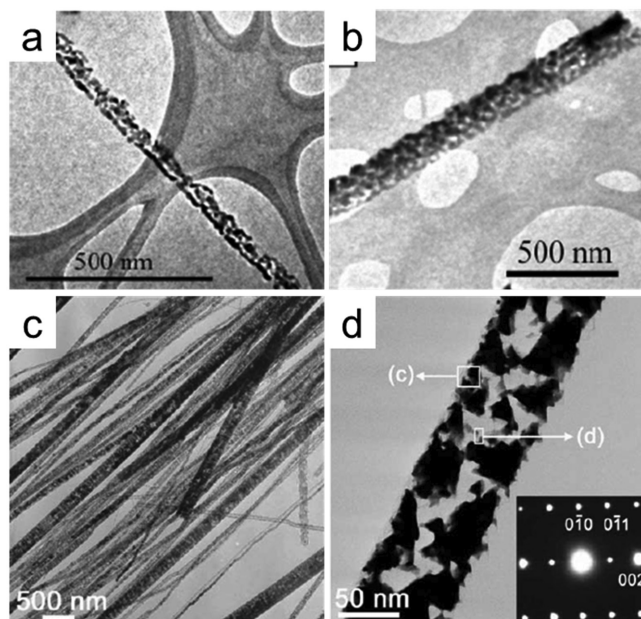


Figure 11. a,b) TEM images of porous ZnO and ZnCdO nanowires, respectively, reproduced with permission.^[169] Copyright 2006, American Chemical Society. c,d) TEM images of porous GaN nanowires (inset in d is corresponding SAED pattern), reproduced with permission.^[170] Copyright 2003, Elsevier.

nano-barbells or nano-step-cone nanowires via Ag dissolution from Au-Ag alloy nanowires which had segments of different compositions (Figure 12a). These segments of different compositions could be obtained controllably by changing Au/Ag composition ratios in the plating solution during the electro-deposition process. This is a simple and controllable way to prepare porous nanowires with different sizes and porosities, i.e., by deliberately adjusting the composition of the plating solution in the electro-deposition process. Similarly, porous Pd and Cu nanowires were synthesized by Yang et al.^[174,175] using electro-deposition followed by etching (Figure 12d).

Core/shell nanowire arrays can be prepared using porous nanowires as the core backbone and electrodepositing the shell materials. Some examples are hierarchical core/shell $\text{NiCo}_2\text{O}_4@\text{MnO}_2$,^[114,115] $\text{Co}_3\text{O}_4@\text{NiO}$,^[116] and $\text{Co}_3\text{O}_4@\text{Co}(\text{OH})_2$ ^[117] nanowire arrays. Xia et al.^[117] synthesized Co_3O_4 nanowire arrays by hydrothermal growth on nickel foam. $\text{Co}(\text{OH})_2$ was then electrodeposited on Co_3O_4 nanowires to form the core/shell structure (Figure 12e,f). Duay et al.^[172] synthesized hierarchical $\text{MnO}_2@\text{MnO}_2$ nanowire/nanofibrils by combining AAO template-assisted and electro-deposition methods. The MnO_2 core nanowires were obtained by electro-deposition into the AAO template using a manganese acetate solution. The MnO_2 nanofibrils were then deposited on the MnO_2 cores by multistep electro-deposition-oxidation, $\text{Mn}(\text{OH})_2$ to MnO_2 , using different potentials and plating solutions. As

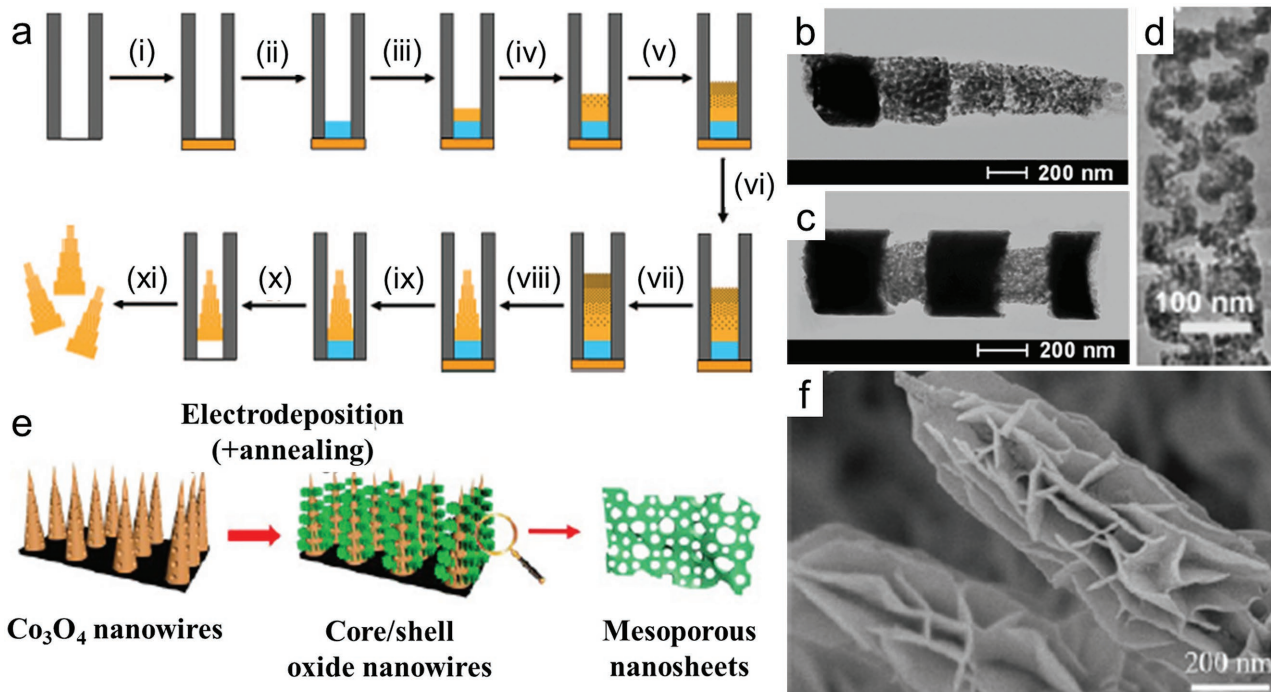


Figure 12. a) Illustration of the template-assisted electrochemical preparation of asymmetric porous gold nanowires. b) TEM image of porous step-cone nanostructures prepared by varying Au/Ag ratios in plating solutions. c) TEM image of porous nano-barbell nanostructures. Figures a–c reproduced with permission.^[173] Copyright 2007, American Chemical Society. d) SEM image of a porous and spiral PdCu nanowire bundle, reproduced with permission.^[174] Copyright 2013, American Chemical Society. e) Schematic of the hydrothermal-electrodeposition of hierarchical porous core/shell nanowire arrays. f) SEM image of core/shell $\text{Co}_3\text{O}_4@\text{Co}(\text{OH})_2$ nanowire. Figures e,f reproduced with permission.^[117] Copyright 2012, American Chemical Society.

a cathode material, hierarchical porous core/shell nanowire arrays offer high surface area with good electrolyte penetration and fast ion/electron transfer, leading to improved electrochemical performance.

3.4.3. Atomic Layer Deposition

Atomic layer deposition (ALD) is an emerging technology that is rapidly gaining acceptance for use in surface modification and fabrication of complex nanostructured materials because of its simplicity, reproducibility and conformality.^[176] This method enables the deposit of a uniform coating of complex compounds on nanoparticles, nanowires, nanotubes, soft materials or AAO templates. Moreover, the thickness of the deposited film can be precisely controlled from angstroms to nanometers.^[177]

Chen et al.^[178] reported TiO₂-coated porous Si nanowires using evaporation-induced self-assembly followed by ALD. Qin et al.^[179] synthesized various helical oxide nanotubes (Al₂O₃, SiO₂, TiO₂, HfO₂, and ZnAl₂O₄) by ALD using carbon nanocoils as templates followed by annealing in air (Figure 13a). These authors^[180] also prepared porous Cu/Al₂O₃ nanopeapods consisting of Cu nanoparticle chains by reducing CuO nanowires in H₂ and growing an Al₂O₃ shell by ALD (Figure 13b). Fan

and co-workers^[181] synthesized coaxial SnO₂-ZnO-TiO₂ nanowires on carbon cloth by ALD and etched the ZnO to obtain a novel hollow architecture of SnO₂-in-TiO₂ wire-in-tube structures (Figure 13c). The hollow wire-in-tube structure can confine the volume expansion of SnO₂ upon lithiation, resulting in good cycling stability for LIBs.

Uniform, multiple-walled nanostructures^[182] can be designed and synthesized by multi-step ALD with subsequent etching. The thickness of different layers are precisely controlled by adjusting the ALD growth cycles. Gu et al.^[183] prepared multiwall Pt-Pt/TiO₂-TiO₂ nanotubes with uniform shape and size using a porous Si template (Figure 13d). These multiwall hollow nanostructures of different materials have the potential to be used in biosensors, broadband detectors, photovoltaic devices and energy storage devices. The ALD technique, combined with liquid phase methods, was used to construct hierarchical porous 1D nanostructures, such as hierarchical ZnO nano-architectures (Figure 13e).^[184]

These examples highlight the versatility, conformality and uniqueness of ALD for the fabrication of complex nanomaterials. In the fabrication of porous 1D nanomaterials, ALD enables the design and synthesis of materials with different shapes and structures.

3.5. Chemical Etching

Etching technology, such as etching the Ag component in Ag/Au alloy nanowires, removing sacrificial layers during synthesis process, etc., is an effective method for creating porous 1D nanomaterials through a “top-down” approach. The etching method is usually accompanied by the other methods discussed above. In this section, we focus primarily on direct etching of bulk Si to form porous Si nanowires.^[185]

In general, etching of Si is performed in two ways: anodic etching in HF-containing aqueous or organic solutions,^[186] or chemical etching in HNO₃/HF solution.^[187] Simple metal-assisted chemical etching has attracted considerable attention because it offers better controllability of shape, diameter, length, orientation, doping type, and doping level of Si nanostructures.^[185] In general, metal-assisted chemical etching reactions are classified as being either one-step reactions in an etchant solution containing HF and metal salts, such as AgNO₃,^[188–191] KAuCl₄,^[192] K₂PtCl₆,^[193] or two-step reactions that involve pre-deposition of metal nanoparticles or patterned metal thin films followed by chemical etching in the presence of HF and H₂O₂.^[194]

The classic one-step reaction consists of immersing clean *p*-type Si substrates in an etchant solution containing AgNO₃ and HF, as reported by Yang and co-workers.^[189] It has been demonstrated that the porous morphology of as-synthesized Si nanowires depends on the electrical resistivity of the original Si wafers. With decreasing wafer resistivity, Si nanowires become rougher and finally evolve into nanowires containing micro- or mesopores (Figure 14a–c). Duan and co-workers^[194] reported a two-step metal assisted electroless chemical etching method, which was adopted to obtain Si nanowire arrays from heavily doped *n*-type Si wafers. The main etching process involves pre-deposition of Ag metal on the Si substrate followed

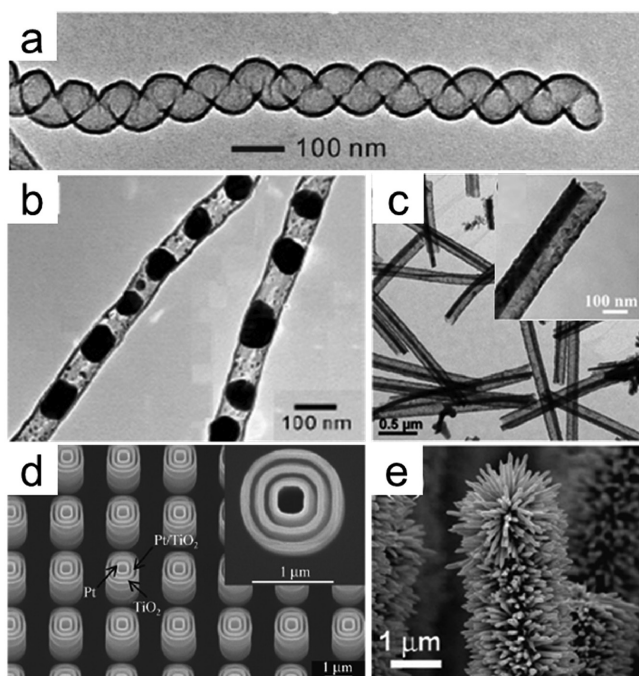


Figure 13. a) TEM image of helical Al₂O₃ nanotube obtained by applying 50 cycles of Al₂O₃ deposition, reproduced with permission.^[179] Copyright 2010, Wiley-VCH. b) TEM image of Cu nanoparticle chains embedded in Al₂O₃ shell, reproduced with permission.^[180] Copyright 2008, American Chemical Society. c) TEM image of hollow SnO₂-in-TiO₂ wire-in-tube nanostructure, reproduced with permission.^[181] Copyright 2014, American Chemical Society. d) SEM image of nested multiple-walled Pt-Pt/TiO₂-TiO₂ nanotubes with uniform shape and size of lumen, reproduced with permission.^[183] Copyright 2011, Springer. e) SEM image of hierarchical ZnO nanoarchitectures produced by ALD and hydrothermal methods, reproduced with permission.^[184] Copyright 2009, American Chemical Society.

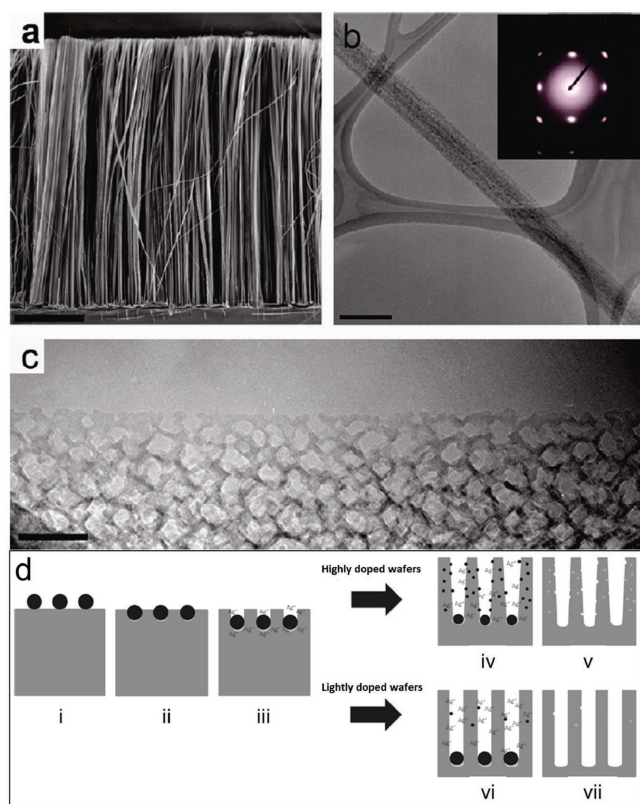


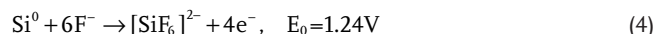
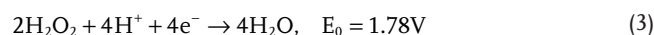
Figure 14. a) SEM and b,c) TEM images of porous silicon nanowires synthesized from highly doped *p*-type Si wafers (inset in b is corresponding SAED pattern), the scale bar is 10 mm, 200 nm, and 50 nm in a–c, respectively, reproduced with permission.^[189] Copyright 2009, American Chemical Society. d) Schematic of the formation of porous and nanoporous Si nanowire arrays from highly or lightly doped wafers through a two-step silver assisted etching method, reproduced with permission.^[198] Copyright 2011, American Chemical Society.

by electroless etching in an etchant solution containing varying concentrations of H_2O_2 and HF. These authors found that the concentration of H_2O_2 and the doping level of the Si wafer were key factors affecting the porous structures of Si nanowires. Beginning with highly doped *n*-type Si (100) wafers with increasing H_2O_2 concentration, the Si nanowires evolved from smooth-to-rough surfaces, and that the solid/porous core/shell nanowires transformed to porous nanowires. The porous nature of nanowires gradually increased with increasing H_2O_2 concentration and reaction time. Interestingly, with this etching method, the as-obtained porous Si nanowire was still single-crystal. Using a lightly doped *n*-type Si(100) wafer and *p*-type Si(100) wafer, Chen et al.^[195] and Wang et al.^[196] synthesized porous Si nanowires by controlling the etching temperature, duration, concentration of H_2O_2 and AgNO_3 , and amount of etching solution. Once again, the reaction conditions and resistivity of starting Si wafers were key factors in controlling the porosity and specific surface area of as-synthesized Si porous nanowires. To further explore the factors that affect the formation and porosity of silicon nanowires, more detailed studies of the metal-assisted chemical etching mechanism are needed.

In the one-step chemical etching process for the synthesis of porous Si nanowires, there is an Ag cathode where Ag^+

ions reduce, while at the Si nanowire anode, Si dissolves into aqueous HF solution.^[185] These two simultaneous electrochemical reactions are responsible for etching the nanowire surface leading to varying degrees of surface roughness and porosity.^[189,197]

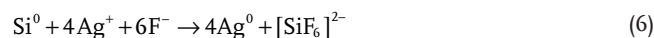
In the two-step chemical etching process, Ag nanoparticles serve as cathode and are pre-deposited on a clean Si surface to ensure uniformity in vertical etching (Figure 14d).^[198] The reactions are described in Equations (3) and (4) listed below:^[194,198]



The Si anode is continuously dissolved as electrons transfer to the upper surfaces of the Ag nanoparticles, while H_2O_2 is reduced to H_2O . Ag nanoparticles are oxidized to Ag^+ ions by H_2O_2 according to the following reaction (Equation (5)).^[190]



At the same time, Ag^+ ions quickly react with Si and are reduced to Ag particles again (Equation (6)).



In this way, etching is localized around the Ag nanoparticles trapped in self-created nanopits, leading to continued etching in the vertical direction and the formation of vertical silicon nanowire arrays. The concentration of H_2O_2 and the etching duration greatly affect the porosity of silicon nanowires. Ag^+ ions are not completely recovered into the original Ag nanoparticles and some of them may diffuse out. Out-diffused Ag^+ ions will nucleate on side walls near defect sites and extract electrons from the Si nanowires, forming new Ag nanoparticles which serve as a new etching pathway along the lateral direction of the nanowires. As a result, porous nanostructures are formed.

The porosity of as-prepared nanowires have been controlled using one-step chemical etching, two-step metal-assisted chemical etching, and Au-assisted (or Au/Ag co-assisted) etching.^[199–202] Li et al.^[203] prepared mesoporous Si nanowires with adjustable porosity from metallurgical Si by a two-step metal-assisted chemical etching process. Porosity of the Si nanowires was adjusted by controlling the concentration of impurities within the metallurgical Si. Upon annealing the porous Si nanowires in air, a thin silicon oxide layer (≈ 3 nm) was formed on the surface of the porous Si nanowires, which is beneficial for maintaining structural stability.^[204]

4. Application of Porous 1D Nanomaterials for Electrochemical Energy Storage

As mentioned in section 2, porous 1D nanomaterials have multiple advantages which make them attractive in electrochemical energy storage and other applications.^[3,48,135,146,149,204] In this section, we will present several examples where these nanomaterials have been investigated for use in LIBs, SIBs,

Li-S batteries, Li-O₂ batteries and supercapacitors. The advantages of porous 1D nanomaterials and their electrochemical performance will be discussed.

4.1. Lithium-Ion Batteries

LIBs have become the ubiquitous power sources for portable devices used in a wide range of consumer, health, and military applications.^[1,5,6] Numerous applications are now demanding improved electrical energy storage with higher specific capacities and faster charging, a feature particularly important for EVs.^[39] In addition, higher energy densities, longer cycle life and low cost are also required in electrical energy storage from renewable energy sources.^[1,5]

In order to achieve improved LIBs with high capacity, high rate and long cycle life, both cathode and anode need to have the following characteristics: thermodynamic stability at the potentials of usage, electron and ion diffusion pathways which enable rapid ion and electron transport, chemical stability in appropriate electrolytes and a robust structure for repeated lithiation and delithiation processes.^[1,8,39] In the paragraphs below, advances in porous 1D nanomaterials for LIBs focus on intercalation, alloying and conversion reactions.

4.1.1. Intercalation Reaction

The kinetics of intercalation involves solid-state diffusion of Li⁺ ions from the electrode-electrolyte interface to the interior of the material.^[205] This process is influenced by a number of factors including the dimensionality of the material, whether phase transformations occur upon lithiation/delithiation associated with different magnitudes of volume changes. In order to operate at high rates and achieve long cycle life, there needs to be careful consideration of transport kinetics as well as structural stability.

The well-known, commercial cathode material, LiCoO₂, delivers a capacity of about 140 mAh g⁻¹ but its capacity fades rapidly at higher cycling rates.^[206] Chen and co-workers^[206] reported that LiCoO₂ nanotubes reached a capacity of 185 mAh g⁻¹, much higher than that of nanoparticles or solid nanowires. LiNi_{0.8}Co_{0.2}O₂ nanotubes synthesized by a similar route delivered a higher capacity of 205 mAh g⁻¹.^[206] Because of its abundance, low cost, and environmental friendliness, LiMn₂O₄ in its spinel form is an alternative candidate as a high-power cathode for LIBs, but it is limited by sluggish Li⁺ ion diffusion kinetics.^[153,207] Ding et al.^[207] reported the synthesis of single-crystal LiMn₂O₄ nanotubes with a diameter of about 600 nm and a wall thickness of about 200 nm produced using β-MnO₂ nanotubes as a sacrificial template. These LiMn₂O₄ nanotubes exhibited better rate capabilities and cycling stability compared to LiMn₂O₄ powders. Wu and co-workers reported the fabrication of LiMn₂O₄ nanotubes with preferred orientation that used multiwall CNTs as the sacrificial template.^[153] The as-synthesized LiMn₂O₄ nanotubes displayed extremely fast charging (54% capacity at 600 C) and excellent cycling performance in aqueous LIBs. The improved capacity was attributed to the hollow tubular structure so that: (i) there are more

active sites for Li⁺ ion intercalation/de-intercalation; (ii) the very small thickness of the nanotubes reduced the ion diffusion pathway, resulting in significantly faster electrochemical kinetics; (iii) the relative flexibility of hollow tubular 1D structure provided excellent stability during charge/discharge cycles.

Spinel LiNi_{0.5}Mn_{1.5}O₄, which possesses three dimensional Li⁺ ion diffusion channels and high operational voltage (≈4.7 V vs Li⁺/Li), is a promising high-power cathode material. However, simultaneously delivering good capacity at high rate and retaining cyclability are challenging due to several factors that affect performance, particularly electrolyte and structural instability under high potentials. Zhang et al.^[128] showed that novel porous LiNi_{0.5}Mn_{1.5}O₄ nanorods exhibited much better rate capability and cycling stability compared to the bulk oxide (Figure 15a,b). The porous LiNi_{0.5}Mn_{1.5}O₄ nanorods displayed specific capacities of 140 and 109 mAh g⁻¹ at 1 and 20 C rates, respectively (Figure 15c). In addition, a capacity retention of 91% after 500 cycles at a rate of 5 C was obtained (Figure 15d). It was noted that instability of the electrode and electrolyte under high operating voltage led to fast capacity fade. However, the porous 1D LiNi_{0.5}Mn_{1.5}O₄ nanorods which formed a stable solid electrolyte interphase (SEI) layer under high voltage had excellent stability. Facile strain relaxation in 1D porous structures is able to maintain the structural integrity of the SEI, which leads to enhanced electrochemical performance. These results demonstrate that porous 1D nanomaterials can be structurally and interfacially stable, and offer significant advantages for high-voltage cathodes.

Polyanionic compounds, such as LiFePO₄, LiMnPO₄, and Li₃V₂(PO₄)₃, have been widely investigated due to their operating voltage, high theoretical specific capacity and thermodynamic stability.^[6,63,66,208,209] But, their poor electronic conductivity results in relatively low electrochemical utilization, even at slow rates, restricting the use of these materials in practical applications. Carbon-coated single crystalline LiFePO₄ nanowires displayed improved rate capacity,^[208] and there is an indication that combining active electrode materials within conductive mesoporous 1D matrices/scaffolds can significantly enhance the electrochemical performance (Figure 15e). The electrically conductive matrix facilitates good electron transport while the interconnected porosity of the scaffold provides numerous ion diffusion tunnels. In addition, by incorporating small nanocrystals embedded in the scaffold uniformly, ion diffusion distances can be further decreased. The empty voids within the scaffold provide enough space to accommodate volume changes associated with lithiation and delithiation during repeated cycling. Wei et al. reported the fabrication of hierarchical Li₃V₂(PO₄)₃/C mesoporous nanowires (Figure 7e), in which Li₃V₂(PO₄)₃ nanocrystals were uniformly embedded in mesoporous nanowires while staying in tight contact with conductive carbon scaffolds.^[63] These Li₃V₂(PO₄)₃/C mesoporous nanowires displayed improved rate and cycling performance compared to standard carbon coated LVP particles. 88% of theoretical capacity was delivered at rates up to 10 C and 80% capacity was retained after 3000 cycles at 5 C (Figure 15f,g). Afterwards, Mai group developed a gradient electrospinning method to synthesize Li₃V₂(PO₄)₃ mesoporous nanotubes, with Li₃V₂(PO₄)₃ nanoparticles uniformly dispersed in/on thin mesoporous carbon nanotubes (Figure 2c).^[66] At a rate of 10 C,

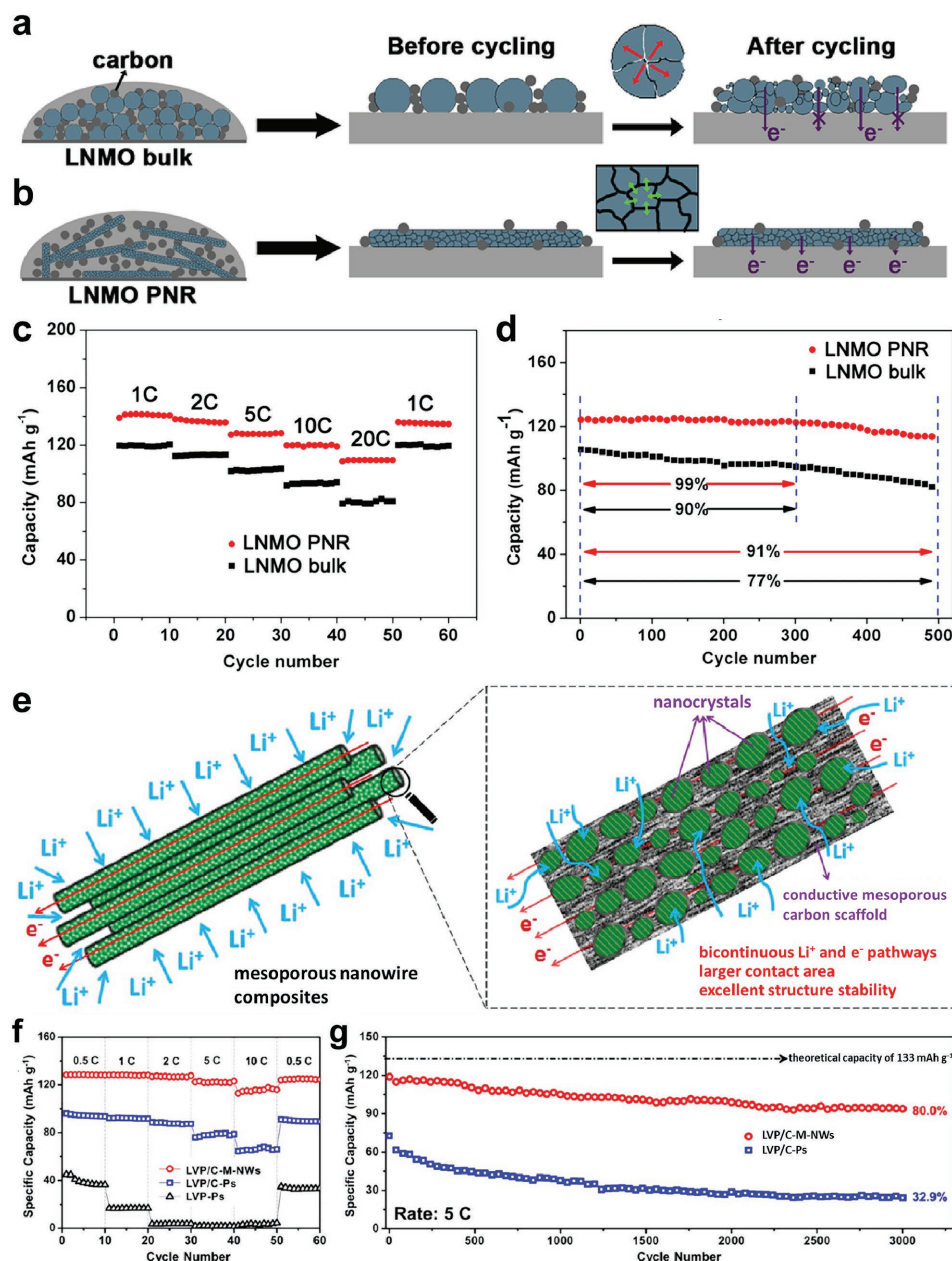


Figure 15. Schematic of the morphology changes and electron transport in bulk (a) and 1D nanoporous LNMO (b) electrodes upon electrochemical cycling. c) Rate capability and (d) cycling performance of LNMO porous nanorods compared to bulk. Figures a–d reproduced with permission.^[128] Copyright 2013, American Chemical Society. e) Schematic of mesoporous LVP nanowire composites having bicontinuous electron/ion transport pathways and facile strain relaxation during Li^+ insertion/extraction. f) Rate capability and (g) cycling performance of LVP at rate of 5 C. Figures e–f reproduced with permission.^[63] Copyright 2013, American Chemical Society.

the $\text{Li}_3\text{V}_2(\text{PO}_4)_3$ mesoporous nanotubes operated with excellent stability for nearly 9500 cycles, much longer than that of normal $\text{Li}_3\text{V}_2(\text{PO}_4)_3/\text{C}$ nanowires. In addition, an assembled $\text{Li}_3\text{V}_2(\text{PO}_4)_3/\text{Li}_4\text{Ti}_5\text{O}_{12}$ full cell retained 73 and 75% of the initial capacity after 1000 cycles at the rate of 2 C and 3 C, respectively. The outstanding performance of $\text{Li}_3\text{V}_2(\text{PO}_4)_3$ is attributed to the hierarchical architecture where mesoporous 1D nanocomposites have bicontinuous electron/ion pathways, large electrode-electrolyte contact area, low charge transfer resistance, and robust structural stability upon prolonged cycling.

These results demonstrate that the novel mesoporous 1D nanostructure is an outstanding morphology for improving both the rate capability and long-term cycling performance of LIBs.

Graphite is the most common intercalation-type anode for LIBs. For the most part, however, graphite is unable to achieve high power capability due to sluggish ion diffusion kinetics. Recently, porous carbon nanofibers (PCNFs) reported by Li et al. displayed very good rate capability properties.^[50] By doping with nitrogen, N-doped PCNFs (N-PCNFs) exhibited a reversible capacity of $\approx 500 \text{ mAh g}^{-1}$ at a specific current of

1 A g⁻¹. At a much higher rate of 20 A g⁻¹, a very respectable capacity of 172 mAh g⁻¹ was achieved. The porous 1D structure and graphitization in the PCNFs provide fast electron transport pathways. Large mesopores formed by the elimination of metal nanocrystals and small-sized mesopores formed through pyrolysis in N-PCNFs can effectively store electrolyte and enlarge the interface between the active material and electrolyte. As a result, the capacity at high rates is improved considerably as compared to commercial graphite anodes.

4.1.2. Alloying Reaction

Silicon has a high theoretical capacity of 4200 mAh g⁻¹ based on the Li-Si alloying reaction.^[210] The main challenges for the practical use of Si anodes are its very large volume variation during lithiation/delithiation processes (>300%), unstable SEI layers and fast capacity fading.^[210] In addition, as a semiconductor, Si displays relatively low electronic conductivity which seriously hinders the ability to operate at high rates.

Recently, different research groups demonstrated that mesoporous Si nanofibers or Si nanoparticles embedded in conductive mesoporous carbon nanofibers exhibited enhanced cycling and rate performance compared to bulk Si, particles and nanowires.^[21,72,204,211] Hollow Si nanotubes also delivered high performance.^[210] Park et al.^[212] synthesized Si nanotubes with

stabilized SEI layers, resulting in superior capacity retention. The hollow tubular structure can be further developed into a multi-shell structure with designed properties. Wu et al.^[20] synthesized a double-walled Si-SiO_x nanotube structure (DWSiNT) with an inner wall of Si which was active and an outer wall of SiO_x which confined the tube. In the lithiation process, the expansion of the inner Si moved toward the hollow space with the formation of a stable outer SEI layer (**Figure 16a**). This SEI layer was thin and stable during cycling, leading to improved cycling performance compared to that of Si nanowires and nanotubes (**Figure 16b**). Even at a high rate of 12 C, there was no obvious capacity fading after 6000 cycles (**Figure 16c**). Well-designed porous Si nanowires synthesized through a low-cost metal-assisted chemical etching method displayed excellent electrochemical performance.^[203] Similar to the DWSiNT with a durable SiO_x outer layer,^[20] porous Si nanowires with a thin oxide coating (≈3 nm) on the surface show structural stability during cycling along with good cycling performance.^[204] A highly reversible capacity of 1503 mAh g⁻¹ after 560 cycles was obtained, corresponding to an average of only 0.04% capacity drop per cycle compared with its initial capacity. This field of research continues to grow, with a focus on the design and synthesis of composite electrode materials, especially electrospinning composite materials. Through appropriate surface modifications and synergetic effects between different components, improved physical and/or chemical properties are achievable.^[20]

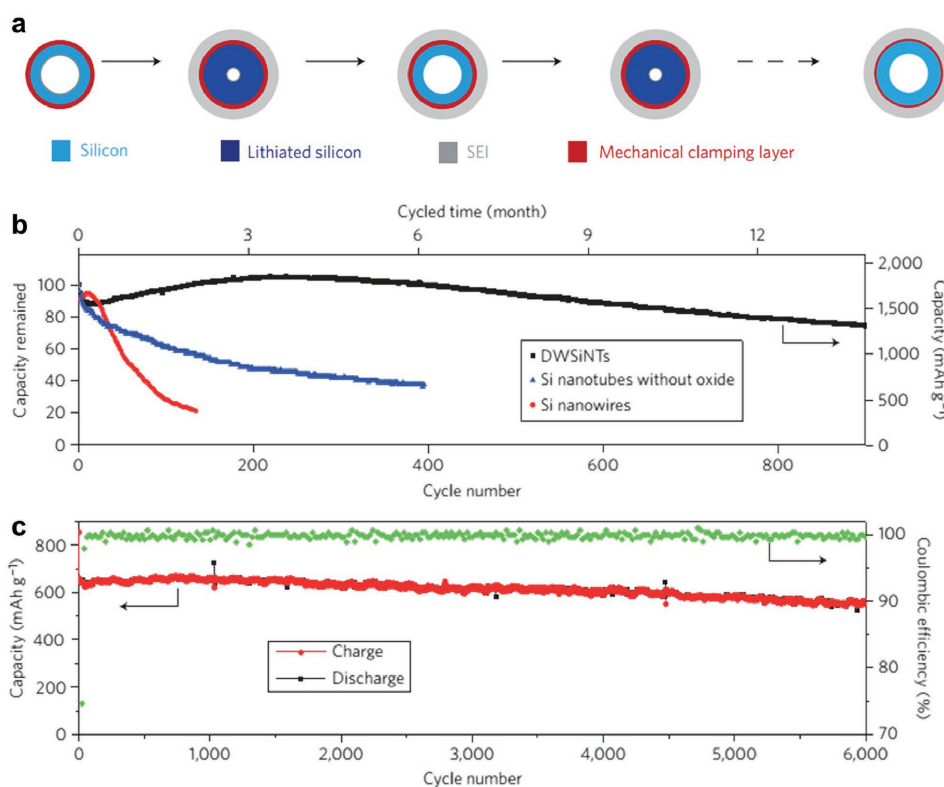


Figure 16. a) Schematic of SEI formation on surfaces of SiO_x. The SiO_x mechanical constraining layer can prevent Si from expanding outward (towards electrolyte) during lithiation, thereby building a stable SEI. b) Capacity retention of different Si nanostructures cycled at the same charge/discharge rate of C/5. c) Charge/discharge capacity and coulombic efficiency of DWSiNTs cycled at 12 C for 6000 cycles. Reproduced with permission.^[20] Copyright 2012, Nature Publishing Group.

4.1.3. Conversion Reaction

Conversion reaction type materials, such as transition metal oxides, sulfides, nitrides, phosphides or other related compounds, have exhibited much higher capacity for lithium than graphite materials. These materials are actually composites as they typically consist of metallic nanoparticles (2–8 nm) dispersed in amorphous matrices.^[10] The lithiation/delithiation processes are frequently accompanied by large volume changes and the loss of electronic connection, resulting in rapid capacity fading.^[12,55,213,214] In addition, complex reaction processes within the composite can exhibit slow reaction kinetics and lead to poor rate performance. To overcome these drawbacks, hierarchical tubular structures were successfully designed.^[213] Lou and co-workers showed that various metal oxide and sulfide tubular structures can serve as high-performance anodes for

LIBs.^[57,59,213] Hierarchical tubular structures based on carbon-coated ultrathin SnO₂ nanoplates have also been prepared. This nanostructure integrates the advantages inherent in ultrathin nanoplates, hollow tubular structures, and carbon nanocoating, resulting in high specific capacity and excellent cycling performance (Figure 17a–d).^[59] Tubular structures grown directly on conductive metals that contained no binder nor conductive agent exhibited excellent performance.^[213] Recently, Wang et al.^[215] reported tubular CuO/metal oxide core/shell heterostructure arrays directly grown on Cu foam (Figure 17e–f). The highly ordered tubular CuO backbone was electrically connected to the current collector, enabling short, direct electron pathways, and at the same time reducing any interface resistance occurring between the current collector and the active material. The hierarchical tubular structure facilitated electrolyte penetration into the inner regions, decreasing the path

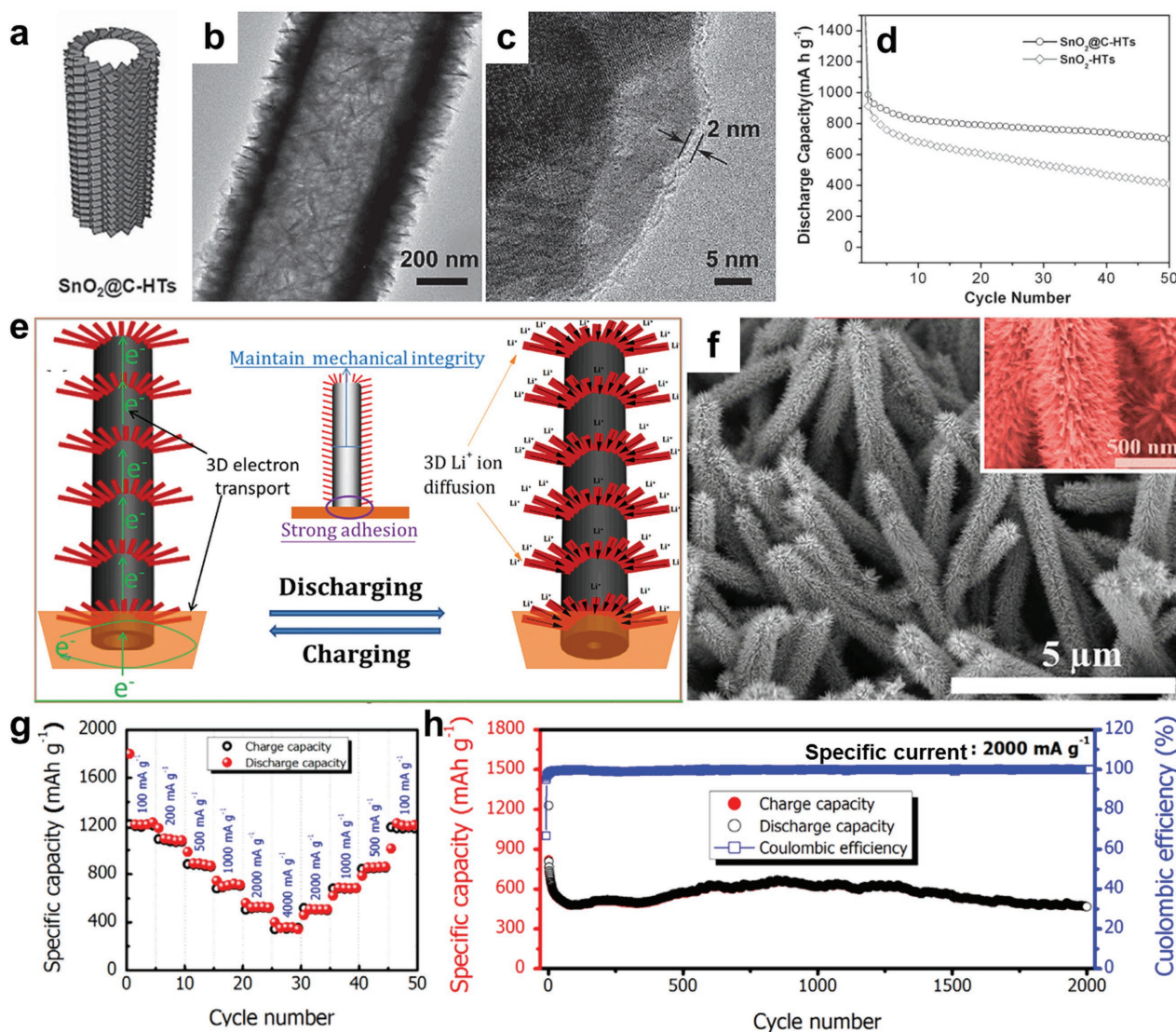


Figure 17. a) Schematic, (b) TEM and (c) HRTEM images of SnO₂@C-HTs. d) Cycling performance of SnO₂@C-HTs and SnO₂-HTs at 200 mA g⁻¹ for LIBs. Figures a–d reproduced with permission.^[59] Copyright 2013, WILEY-VCH. e) Schematic of hierarchical tubular transition metal oxide core/shell heterostructures with 3D Li⁺/electron transport pathways. f) SEM image, (g) rate performance, and (h) cycling performance of hierarchical tubular CuO/CoO core/shell heterostructures. Figures e–h reproduced with permission.^[215] Copyright 2015, Elsevier.

length for both electron and Li⁺ ion transport. The inner hollow CuO cores were strongly connected to the Cu foam to maintain mechanical integrity. Meanwhile, the hollow void spaces were able to act as a buffer against volume change, allowing the nanotubes to expand in diameter without breaking in length, thereby ensuring stable cycling. The as-prepared tubular CuO/CoO core/shell arrays delivered a capacity of 1364 mAh g⁻¹ at 100 mA g⁻¹ after 50 cycles and maintained 1140 mAh g⁻¹ after 1000 cycles at 1.0 A g⁻¹ (Figure 17g,h).

Hierarchical porous Fe₃O₄/VO_x/rGO nanowires (Figure 5d) reported by An et al.^[64] showed an excellent reversible capacity of 1146 mAh g⁻¹ at 0.1 A g⁻¹ and ≈500 mAh g⁻¹ at 5 A g⁻¹. Transition metal oxide spinels (AB₂O₄) with porous 1D nanostructures were also shown to exhibit good electrochemical performance.^[158,213,214] Recently, an interesting porous nanofiber model (Figure 4) was developed by Kang and co-workers,^[52] that is bubble-nanorod-structured Fe₂O₃-C nanofibers composed of nanosized hollow Fe₂O₃ spheres uniformly dispersed in amorphous carbon nanofiber matrices. The hollow nanospheres accommodate the volume change that occurs during cycling, while the inner carbon matrix provides continuous electron transport, resulting in better rate and cycling performance. The bubble-nanorod-structured Fe₂O₃-C nanofibers displayed a highly reversible capacity of 812 mAh g⁻¹ at 1.0 A g⁻¹ for 300 cycles, much better than that of hollow Fe₂O₃. The synergistic effect of porosity, the 1D structure and carbon matrix resulted in superior cycling and rate performance for conversion reactions. We believe that further development of binary metal oxides in porous 1D nanostructures, for example Sn-based and Zn-based derivatives which offer a combination of conversion and alloying reactions, will lead to an improvement in reversible capacity and stability.^[124]

4.2. Sodium-Ion Batteries

Although LIBs have been widely applied in portable electronics, when it comes to EVs and ESSs, the cost and resource reserves of lithium may be a limiting factor because of these large-scale applications.^[1] For this reason, SIBs are being studied as an alternative class of energy storage devices because of the natural abundance and low cost of sodium sources.^[4,14,216] Since the Na⁺ ion is larger (1.5 times) and heavier (3.3 times) than the Li⁺ ion, the diffusion of Na⁺ ion is inherently slower than that of Li⁺ ion during charge/discharge processes, making reversible and rapid ion intercalation and extraction more difficult.^[14] In order to develop suitable host materials with sufficiently large interstitial space to accommodate Na⁺ ions, rational material design that allows fast diffusion kinetics is necessary. It is, moreover, even more challenging to design suitable nanoarchitectures for SIBs. The advantages of a short ionic diffusion length, good electrolyte access to the redox active material and the ability to accommodate volume changes associated with electrochemical reactions, makes porous 1D nanostructures a viable candidate for SIBs electrodes.^[3]

For most parts, research on SIB cathodes is focused on polyanionic compounds and layered sodium transition-metal oxides among other host materials.^[216] For polyanionic compounds, Na₃V₂(PO₄)₃ is regarded as a promising cathode for advanced

SIBs due to its high theoretical capacity and stable structure based on the NASICON (sodium super ion conductor) structure.^[217,218] The main limitation is the poor electronic conductivity of phosphates, making it difficult to achieve theoretical capacity. Liu et al.^[217] adopted a simple electrospinning method to construct a novel 1D nanostructure with Na₃V₂(PO₄)₃ nanoparticles encapsulated in interconnecting 1D porous carbon nanofibers (Figure 18a). The porous 1D nanocomposites offered several advantages: short diffusion length of Na⁺ ions into the carbon nanofibers and Na₃V₂(PO₄)₃ nanoparticles, easy access of the organic electrolyte and fast electron transport through the fibers. With improvement in both ion diffusion and electron transport, the as-prepared electrode showed high capacity and good rate performance (Figure 18b,c). Recently, Jiang et al.^[219] introduced carbon-coated Na₃V₂(PO₄)₃ nanoparticles into a highly ordered 1D channel mesoporous carbon (CMK-3 matrix) to form Na₃V₂(PO₄)₃@C@CMK-3. The material exhibited a superior rate capability (78 mAh g⁻¹ at 30 C) and long cycle life (2000 cycles at 5 C). These results demonstrate that porous 1D nanostructures with conductive scaffolds are beneficial for realizing fast charge/discharge of SIBs.

Among the layered transition metal oxides, the P2-type layered Na-Fe-Mn system is a very promising candidate for high-capacity SIB cathodes.^[220,221] However, the material suffers from volume changes during electrochemical operation which leads to poor cycle stability.^[216] Mesoporous nanotubes of Na_{0.7}Fe_{0.7}Mn_{0.3}O₂ were prepared using gradient electrospinning as highlighted in Figure 2.^[66] The mesoporous nanotubes are composed of ultrathin carbon nanotubes (≈200 nm in diameter) and Na_{0.7}Fe_{0.7}Mn_{0.3}O₂ nanoparticles (≈10 nm) on the tubes (Figure 18d). The Na_{0.7}Fe_{0.7}Mn_{0.3}O₂ mesoporous nanotubes showed outstanding rate capability and cyclability in comparison to Na_{0.7}Fe_{0.7}Mn_{0.3}O₂ nanoparticles. The nanotubes delivered a capacity of 108 and 82 mAh g⁻¹ at specific currents of 100 and 500 mA g⁻¹, respectively (Figure 18e). At 100 mA g⁻¹, its capacity retention was 90% after 1000 cycles (Figure 18f). Moreover, 90% of initial capacity was retained after 5000 cycles at 500 mA g⁻¹ (Figure 18g). The superior performance is attributed to the mesoporous nanotube morphology, which ensures fast Na⁺ ion diffusion. In addition, the ultrathin continuous carbon nanotubes improve the electronic conductivity while the abundant mesopores on the tube walls effectively accommodate the volume changes during charge/discharge processes.

Similar to LIBs, anode materials for SIBs are based on carbonaceous materials, metal compounds and polyanionic compounds.^[216] Graphite cannot be utilized as an intercalation host for Na⁺ ions,^[222] thus the discovery/development of suitable anode materials for SIBs is of primary importance. Various types of carbonaceous materials with disordered structures and larger interlayer distance have been investigated for Na⁺ storage including hard carbon,^[223] black carbon,^[224] hollow carbon nanospheres,^[225] nitrogen doped porous carbon fibers^[222] and hollow carbon nanowires.^[226] Porous 1D carbon nanostructures show good electrochemical performance. Fu et al.^[222] fabricated N-doped activated porous carbon fibers derived from polypyrrole. The reversible capacity of the as-prepared electrode ranged from 153 to 72 mAh g⁻¹ at relatively large specific currents of 1 and 10 A g⁻¹, respectively (Figure 19a). The good electrochemical performance was due to the porous 1D morphology with a

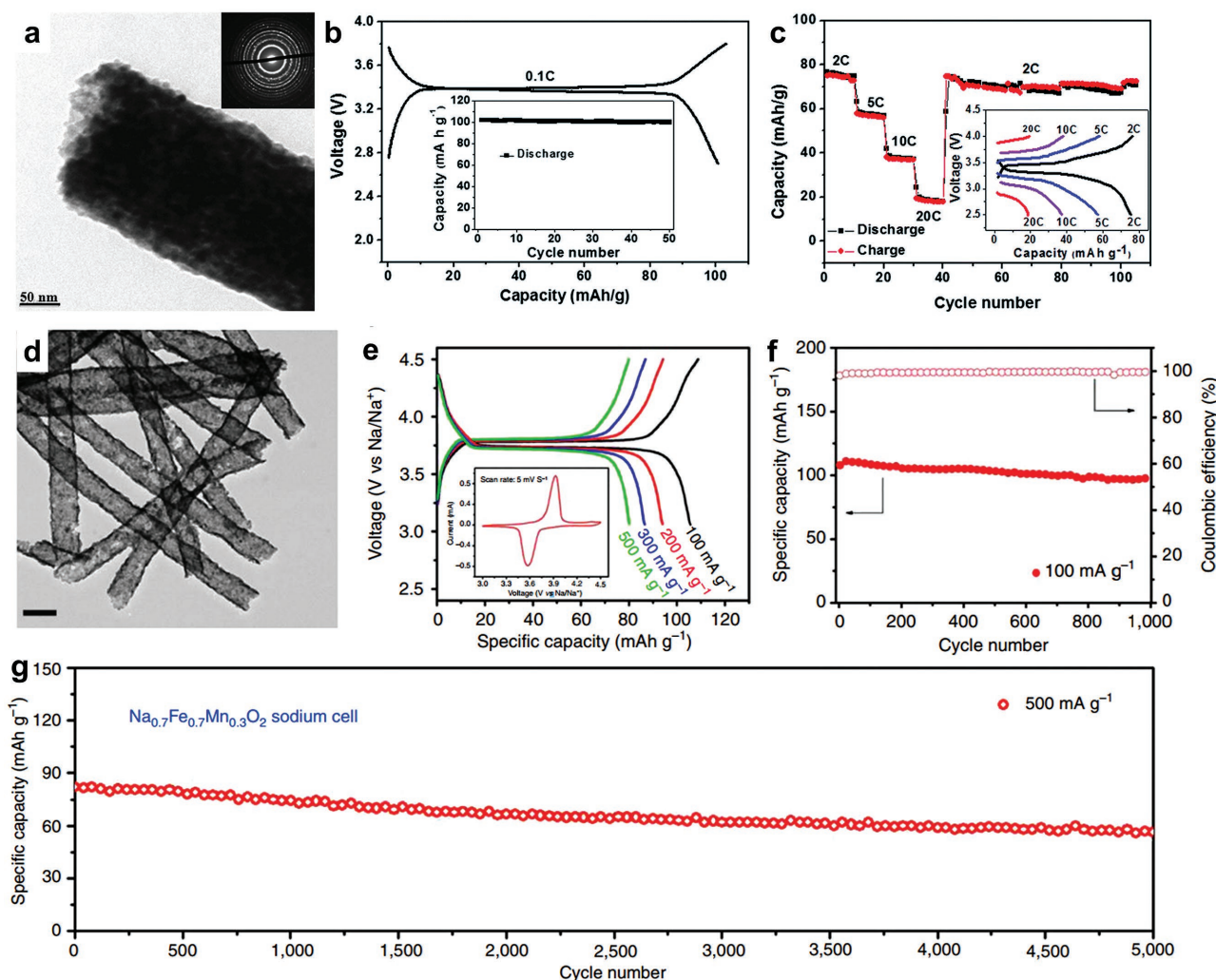


Figure 18. a) TEM image, (b) first charge-discharge curves and cycling performance at 0.1C and (c) rate performance of $\text{Na}_3\text{V}_2(\text{PO}_4)_3/\text{C}$ porous nanofibers, reproduced with permission.^[217] Copyright 2014, Royal Society of Chemistry. d) TEM image (scale bar is 200 nm), (e) charge-discharge curves (inset showing CV curve at 5 mV s^{-1}) and (f,g) cycling performance of $\text{Na}_{0.7}\text{Fe}_{0.7}\text{Mn}_{0.3}\text{O}_2$ mesoporous nanotubes, reproduced with permission.^[66] Copyright 2015, Nature Publishing Group.

large interlayer distance, while charge transfer was improved because of N-doping to increase electronic conduction.

Various titanates have been considered as potential anodes for SIBs because of their low price, low potential, and absence of safety risks. Several Ti-based porous 1D nanostructures have been investigated for SIBs, including TiO_2 nanotubes,^[227] $\text{Na}_2\text{Ti}_3\text{O}_7$ nanotubes,^[228] $\text{Na}_2\text{Ti}_7\text{O}_{15}$ nanotubes,^[229] $\text{MgTi}_2\text{O}_5/\text{C}$ nanorods,^[230] and $\text{Na}_2\text{Ti}_2\text{O}_5/\text{VS}_2$ heterostructures^[231] among others. In work reported by Zhang et al.,^[232] spider web-like $\text{Na}_2\text{Ti}_3\text{O}_7$ nanotubes displayed a capacity of 107 mAh g^{-1} after 500 cycles at a specific current of 0.5 A g^{-1} (Figure 19b). The charge capacity was maintained at 100 mAh g^{-1} for specific currents as high as 3 A g^{-1} , indicating excellent rate performance (Figure 19c). The advantages of $\text{Na}_2\text{Ti}_3\text{O}_7$ nanotubes are the easy access of electrolyte to active materials and adaptative volume variations.

Large volume changes occur in SIB anode materials, such as metal alloys, oxides and sulfides during the repeated charge/discharge cycling.^[216] However, the porous 1D

nanostructure are able to accommodate expansion and remain stable capacity during long-term cycling. Ji et al.^[54] embedded SnSb into porous carbon nanofibers (CNF-SnSb) which provided a conductive scaffold and as well as space for the effective release of mechanical stress (Figure 19d). As a result, the CNF-SnSb showed a high reversible capacity of 350 mAh g^{-1} (Figure 19e), excellent cycling stability and good rate performance (113 mAh g^{-1} at 20C, Figure 19f). With the addition of fluoroethylenecarbonate (FEC), stable and thin SEI layers formed on the porous CNF-SnSb interface, suppressing further decomposition of the electrode and facilitating transport of Na^+ ions through the SEI layer. Mo et al.^[233] synthesized 3D hierarchical porous NiCo_2O_4 nanowire arrays on carbon fiber cloth (NCO@CFC). The nanowires were composed of numerous nanoparticles with many mesopores, forming a 3D cross-linked reticular structure on the CFC (Figure 19g). As an anode in SIBs, NCO@CFC exhibited a significant improvement in cycling ability and rate performance compared to NCO powers

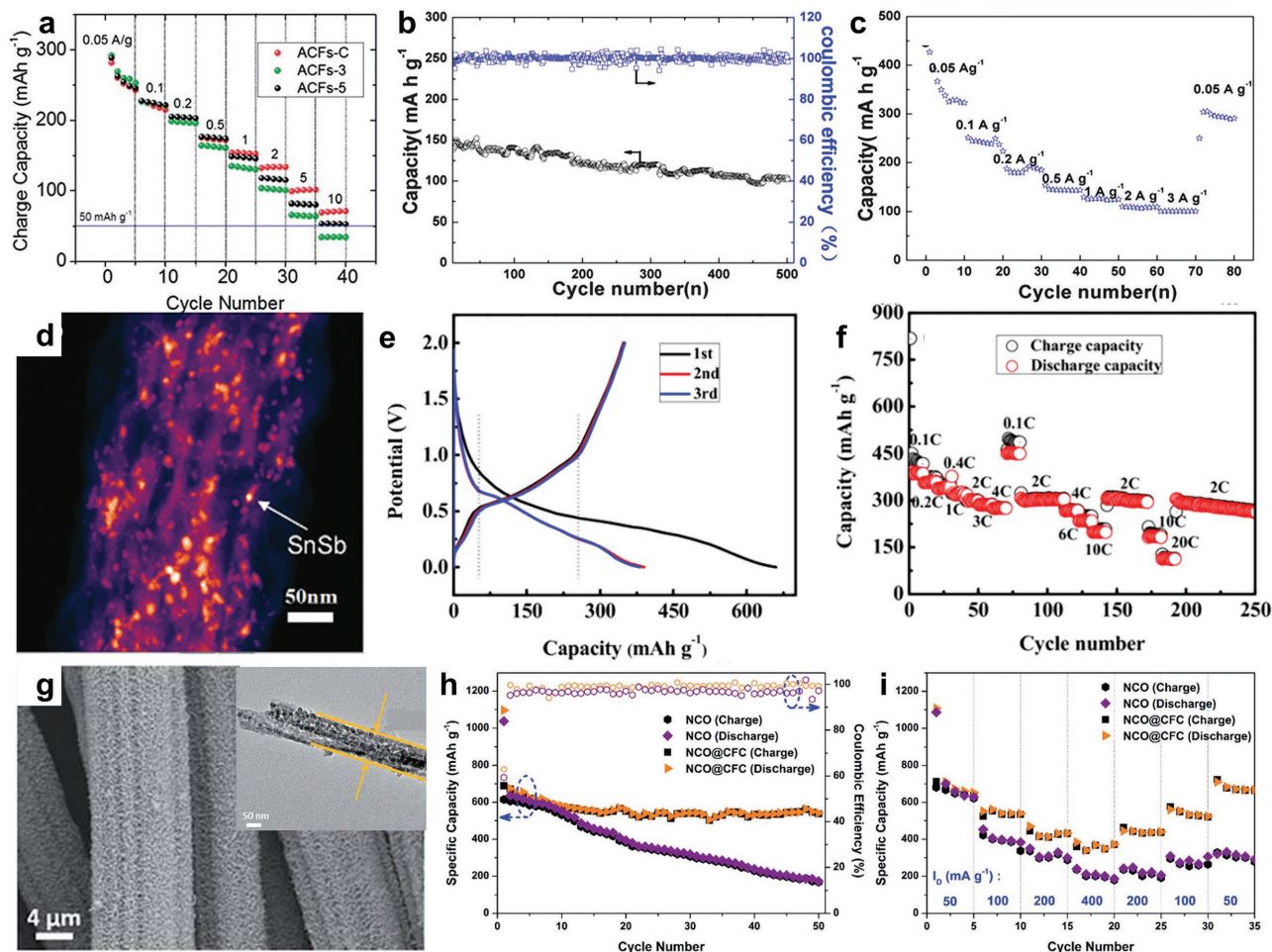


Figure 19. a) Rate performance of N-doped porous carbon fibers in 0–3 V vs. Na^+/Na , reproduced with permission.^[222] Copyright 2014, Royal Society of Chemistry. b) Cycling curves at 500 mA g^{-1} and (d) rate performance of $\text{Na}_2\text{Ti}_3\text{O}_7$ nanotubes, reproduced with permission.^[232] Copyright 2014, Royal Society of Chemistry. d) High resolution 3D TEM image (d), charge-discharge curves at 0.2 C (e) and rate capability of porous CNF-SnSb, reproduced with permission.^[54] Copyright 2014, Wiley-VCH. g) SEM image of NCO nanowire arrays on CFC substrates, inset is TEM image of NCO nanowire. h) Long-term cycling performance at 500 mA g^{-1} and (g) rate performance of NCO powder and NCO@CFC nanowires. Figures g–i reproduced with permission.^[233] Copyright 2015, Royal Society of Chemistry.

(Figure 19h,i). Forming 3D nanowire arrays by introducing CFC not only retained the advantage of the porous nanowires, but also provided a 3D electron transfer networks. Other porous 1D nanostructures, such as Sb,^[234] CuO^[235] and MoS₂^[236,237] have also been utilized as alloying or conversion type anodes for SIBs.

At the present time, the electrochemical performance of SIBs still lags behind that of LIBs in terms of capacity, high rate operation and cycling performance. Innovations in novel porous 1D nanostructures with fast Na^+ kinetics should lead to improvements in SIB performance. Significant advances reported recently, such as the layered P2-system and the NASICON structure, suggest that with further development, SIBs will continue to improve both in energy density and power density.

4.3. Lithium-Sulfur Batteries

The Li-S battery delivers a high theoretical capacity of 1672 mAh g^{-1} with the lithiation of sulfur: $\text{S} + 2\text{Li}^+ \rightarrow$

$\text{Li}_2\text{S} + 2\text{e}^-$. This high capacity is an order of magnitude larger than commercialized LIB cathodes. Thus, Li-S batteries are regarded as one of the most promising candidates for next-generation energy storage systems.^[163,238–240] However, for commercial use, sulfur cathodes face some serious limitations:^[36,38,239,241–243] (1) During the discharge process, the S_8 breaks into short S-S chains and reacts with Li^+ ions to form soluble lithium polysulfide (Li_2S_x , $2 < x < 8$) intermediates. The Li_2S_x intermediates dissolve easily in the electrolyte, causing a “shuttle effect”, which leads to rapid capacity loss. (2) The sulfur and Li_2S_x intermediates are both insulating, reducing the conductivity of electrode and leading to sluggish electrochemical kinetics. (3) The large volume expansion and shrinkage of sulfur during the discharge and charge processes will cause collapse of the electrode structure.

In order to solve these problems, the ideal cathode material for Li-S batteries should possess the following features:^[38,139,244]

- (1) limit the dissolution of polysulfides out of the cathode;
- (2) facilitate the transport of electrons and Li^+ ions;
- (3) contain

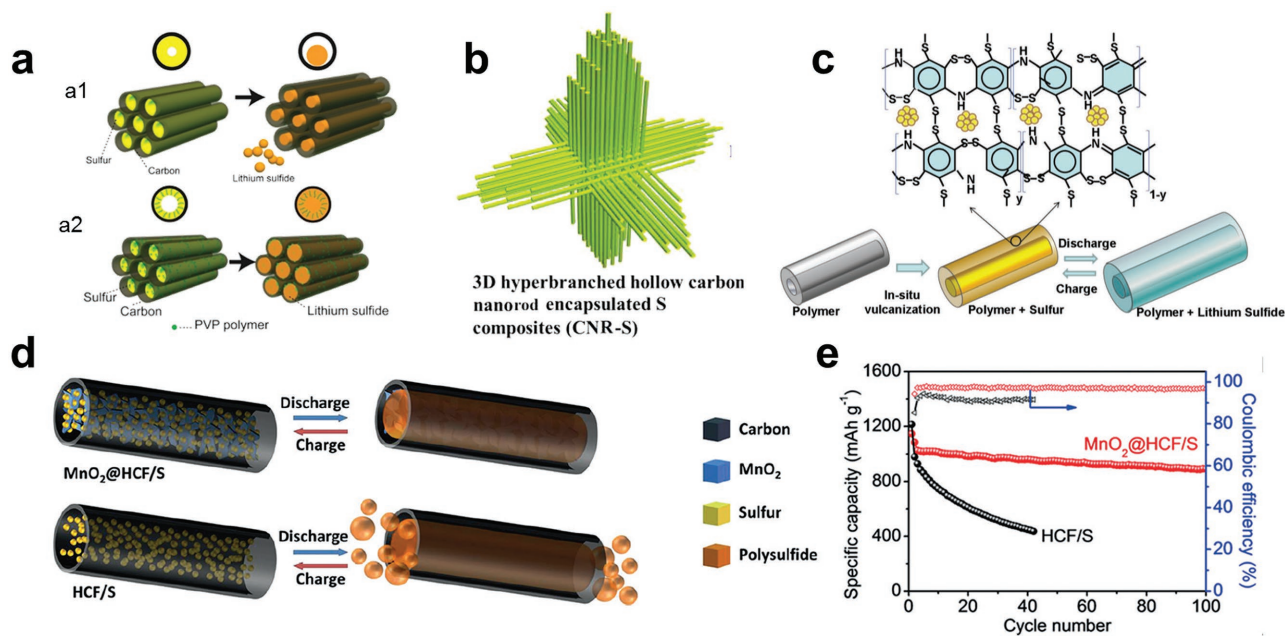


Figure 20. a) Schematic of structural changes in hollow carbon nanofiber with encapsulated sulfur (a1) without PVP and (a2) with PVP, reproduced with permission.^[250] Copyright 2013, American Chemical Society. b) Schematic of 3D hyperbranched hollow carbon nanorod-sulfur (CNR-S) nanocomposites, reproduced with permission.^[251] Copyright 2014, Wiley-VCH. c) Drawing of SPANI-NT/S composite structure, reproduced with permission.^[253] Copyright 2012, Wiley-VCH. d) Schematic and (e) electrochemical performance of MnO₂@HCFs/S and HCF/S, reproduced with permission.^[62] Copyright 2015, Wiley-VCH.

sufficient space and elasticity in the structure to accommodate volume changes. Porous nanowires/nanofibers with high specific surface area are a plausible solution because they have strong adsorption capability, which facilitates the transport of electrons and Li⁺ ions, and accommodates volume changes.^[244,245] In addition, the porous structure keeps the sulfur in short chains and prevents the transformation between S₈ and S₂^{•-}, inhibiting the shuttle effect.^[246–248] Porous 1D nanostructures, such as hollow/porous carbon nanofibers,^[139,249–251] and porous conductive polymers,^[252,253] have been utilized as a host for sulfur in Li-S batteries.

Another alternative is CNTs, which are highly conductive and good for electron transport.^[244,254] Recently, a tube-in-tube carbon nanomaterial (TTCN) was constructed as the sulfur host, in which MWCNTs were encapsulated inside porous carbon nanotubes.^[60] Due to the good electrical conductivity, large pore volume and prevention of polysulfide diffusion outside the carbon walls, the sulfur filled TTCN (S-TTCN) cathode exhibited very promising Li-S battery performance: a good reversible capacity of 918 mAh g⁻¹ at 500 mA g⁻¹ after 50 cycles and a high rate capacity of 550 mAh g⁻¹ at 6 A g⁻¹.

Hollow 1D carbon structures possess the high conductivity needed for fast electron transport, open channels for rapid Li⁺ ions diffusion, and sufficient void space for accommodating the volume changes associated with the lithium polysulfide reactions. At the same time, the carbon walls restrain the diffusion of Li₂S_x. Compared to CNTs, hollow carbon structures with larger inner volume accommodate much more sulfur impregnation while maintaining excellent electrochemical performance.^[38,139,251] These features were utilized in the sulfur-impregnated disordered carbon nanotubes (SDCNTs) fabricated

by Guo et al.^[249] The disordered carbon nanotubes had a diameter of ≈200 nm, which provided a large space for sulfur impregnation. The hollow 1D tubular nanostructure facilitated the access of Li⁺ ions through the axial direction while minimizing the out-diffusion of polysulfides. Moreover, through the sulfur vapor infusion process, the long-chain S₈ could be broken into short-chain S₆ or S₂ and incorporated into smaller voids (meso/micropores). Another consideration is the sufficiently high sulfur content, which is critical for commercial applications. Highly reversible capacity of ≈730 mAh g⁻¹ after 150 cycles at C/5 and high Coulombic efficiency of 99% was reported with a sulfur content up to 75 wt%.^[139] The electrochemical performance of hollow carbon nanofibers/sulfur was further improved by interfacial modification through addition of amphiphilic polymers (polyvinylpyrrolidone, PVP).^[250] The amphiphilic polymers on the carbon surface function as anchoring points to strengthen the interaction between the polar Li_xS clusters and the nonpolar carbon (Figure 20a). A capacity retention of 80% was achieved over 300 cycles at C/2, while the pure hollow carbon nanofibers (without amphiphilic polymers) retained only 48.5% of its initial capacity after 150 cycles. To further inhibit the shuttle effect, Chen et al. synthesized 3D hyperbranched hollow carbon nanorods which encapsulated sulfur (CNR-S) for Li-S batteries (Figure 20b).^[251] The complex 3D hyperbranched structure formed by high aspect ratio (length/radius) hollow nanorods inhibited the shuttle effect and increased polysulfide diffusion pathways. The CNR-S nanocomposites demonstrated a high capacity of 990 mAh g⁻¹ at 1 C with a capacity retention of 94.4% after 500 cycles.

Porous carbon nanofibers have been applied as sulfur hosts for improving electrochemical performance.^[67,245,255] Porous

carbon nanofibers with good conductivity establish intimate electronic contact with sulfur while the porous structure can provide strong adsorption to restrain the diffusion of polysulfides. Porous carbon nanofibers fabricated by Ji et al.^[238] demonstrated a high initial discharge capacity 1400 mAh g⁻¹ at 0.05 C. Li et al.^[67] designed an interesting lotus root-like multi-channel carbon (LRC) that was prepared through electrospinning followed by carbonization. Sulfur was then introduced into the hollow channels of carbon nanofibers by heating the sulfur to 300 °C. Compared to hollow carbon nanofibers, the LRC provided a more conductive framework and higher void volume to achieve high sulfur loading (85.1 wt% and 3.6 mg cm⁻²), thus demonstrating that this design enables high mass loading. At 0.2 C, the initial capacity of the LRC/S electrode was 1214 mAh g⁻¹ (≈72% of theoretical capacity). Furthermore, by decorating the surfaces of LRC/S with ethylenediamine-functionalized reduced graphene oxide (EFG), the stability of the LRC/S electrode was further improved by inhibiting the shuttle effect. Finally, by embedding Cu particles in the porous carbon nanofibers, cycling performance was improved, presumably because of the enhanced conductivity and chemical bonding between Cu and sulfur.^[256]

Conductive porous 1D polymers with high electron mobility possess the potential to achieve high capacity and long cycle life in Li-S batteries. Polymers with tailored functional groups may bond to sulfur and further chemically confine polysulfides.^[38,253] Polyaniline nanotubes (PANI-NTs) filled with sulfur (PANI-NT/S) have been synthesized through an in situ vulcanization process.^[253] The PANI-NT/S formed chemical bonds with sulfur so as to encapsulate the polysulfides, while the soft polymer matrix of PANI-NTs reduced the volume change through self-breathing (Figure 20c). At a rate of 0.1 C, the discharge capacity increased from an initial value of 755 to 837 mAh g⁻¹ after 100 cycles. The increase in capacity was attributed to the full penetration of the electrolyte during cycling.

Besides trapping soluble polysulfides inside conductive porous carbon matrices, one can improve capacity and stability through increased adsorption or chemical bonds between sulfur and carbon. Carbonaceous materials exhibit nonpolar C-C bonding, and their nonpolar surfaces possess poor affinity to polar polysulfides. When polysulfides diffuse into the electrolyte, they detach from the carbon surface leading to irreversible capacity loss.^[250,257,258] Recently, polar transition metal oxides/sulfides have exhibited a significant improved performance in Li-S batteries.^[62,258,259] Lou and co-workers reported that MnO₂ nanosheet-filled hollow carbon nanofibers (MnO₂@HCFs) serve as a sulfur host.^[62] The interior MnO₂ nanosheets were capable of binding with polysulfides, promoting redox activity and inhibiting the shuttle effect (Figure 20d). At 0.2 C, the MnO₂@HCFs delivered an initial discharge capacity of 1147 mAh g⁻¹ and maintained a stable capacity of ≈1000 mAh g⁻¹ after 100 cycles, while pure HCFs showed an initial discharge capacity of 1216 mAh g⁻¹ and with rapid capacity decay to ≈400 mAh g⁻¹ after 40 cycles (Figure 20e).

Research in porous 1D nanostructures has led to a number of advancements in Li-S battery performance. These previous studies also show that the electrochemical behavior can be further enhanced through (1) developing hierarchical

macro/meso/micro-porous gradient structures which increase sulfur loading, facilitate Li⁺ ion diffusion and inhibit polysulfide dissolution, (2) achieving the proper balance between Li⁺ ions diffusion and the sulfur-electrolyte contact area, and (3) maintaining the conductivity of cathodes during cycling.

4.4. Lithium-Oxygen Batteries

The Li-O₂ battery has generated strong interest world-wide due to its energy density which is substantially greater than that of traditional LIBs.^[260,261] The superior electrochemical performance is attributed to the open cell configuration (O₂ is absorbed from the external environment) and the use of lithium metal, which possesses a high specific capacity.^[262,263] The electrochemical reactions in a Li-O₂ battery take place in a three phase zone of gas(O₂)-solid(electrode)-liquid(electrolyte).^[262,264] During discharge, O₂ diffuses into the electrolyte and reacts with Li⁺ ions on the surface of cathode material to form superoxides, peroxides or oxides, while the process is reversed during charging. To guarantee continuous discharge and charge reactions, the cathode should meet several requirements:^[265–267] (1) sufficient porosity to facilitate the transport of O₂ and Li⁺ ions; (2) high catalytic activities for both the oxygen reduction reaction (ORR) and the oxygen evolution reaction (OER) to ensure the fast reduction of O₂ during discharge and fast decomposition of discharge products during charge; (3) high conductivity to ensure adequate electron transport; (4) stable interfaces to suppress the formation of byproducts as well as prevent coverage of active sites. Porous nanowires can meet these criteria because they provide high surface area, continuous O₂ diffusion channels and enough sites for the deposition/decomposition of discharge products. Thus, porous 1D nanostructured materials offer the prospect of improving Li-O₂ battery performance.

Noble metals are excellent catalysts for the ORR and OER processes and deliver high performance for Li-O₂ batteries. Porous AgPd-Pd composite nanotubes were synthesized as electrocatalysts and cathodes for Li-O₂ batteries by Luo et al.^[268] These tubular metal nanotubes acted as bifunctional electrocatalysts and enabled continuous diffusion of O₂ and electrolyte, as well as high conductivity for electrons. The AgPd-Pd composite nanotubes showed good ORR and OER performance in rotating disk electrode (RDE) experiments with a low charging potential, even after 100 cycles at 0.2 mA cm⁻² and a fixed capacity of 1000 mAh g⁻¹.

Even though noble metals demonstrate high electrocatalytic performance and good stability in Li-O₂ batteries, they come with high cost. To meet commercial demands while maintaining high capacity and excellent cycling performance, non-noble metal oxides, such as MnO₂,^[269,270] Co₃O₄,^[271] CoO,^[272] NiCo₂O₄,^[273] with high ORR and OER electrocatalysis have been investigated for Li-O₂ batteries. Ultrathin δ-MnO₂ nanosheet-assembled nanotubes have been developed through template-assisted hydrothermal methods.^[270] The hollow and porous 1D structures provide numerous catalytic sites and the intrinsically high catalytic activity of the material induced formation of Li₂O₂, which enhanced the reversible capacity, rate capability, and cycling stability. Another electrocatalyst, Co₃O₄

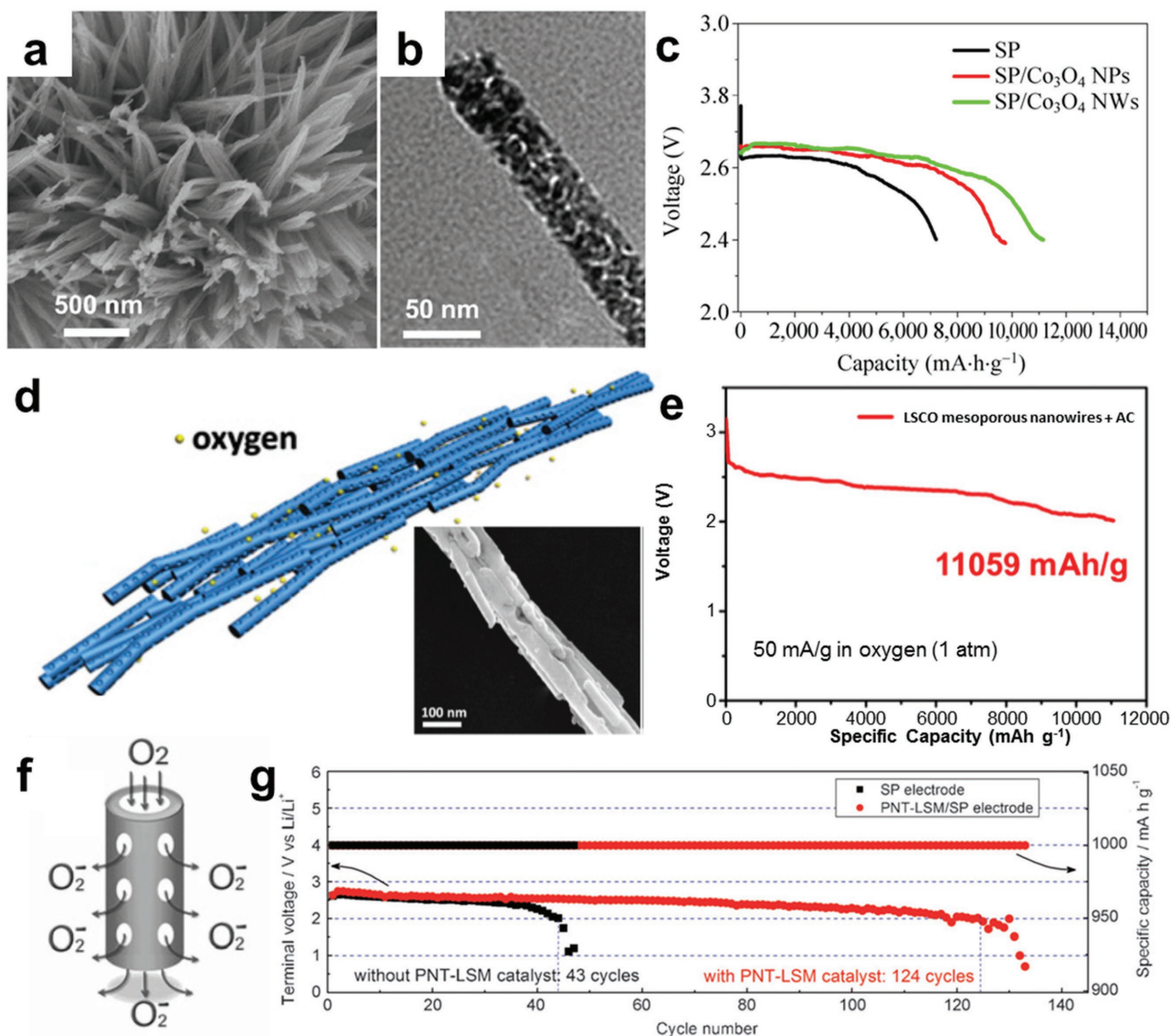


Figure 21. a) SEM and (b) TEM images of porous Co_3O_4 nanowires. c) The first discharge curves of $\text{Li}-\text{O}_2$ batteries at 0.1 A g^{-1} . Figures a–c reproduced with permission.^[271] Copyright 2015, Springer. d) Schematic of $\text{La}_{0.5}\text{Sr}_{0.5}\text{CoO}_{2.91}$ porous nanowires and SEM image (inset). e) The first discharge curve of $\text{Li}-\text{O}_2$ batteries with $\text{La}_{0.5}\text{Sr}_{0.5}\text{CoO}_{2.91}$ porous nanowires at 50 mA g^{-1} . Figures d,e reproduced with permission.^[68] Copyright 2012, the National Academy of Sciences. f) Schematic of oxygen diffusion in porous $\text{La}_{0.75}\text{Sr}_{0.25}\text{MnO}_3$ nanotubes. g) Terminal discharge voltage vs. cycle number of $\text{Li}-\text{O}_2$ batteries with and without porous $\text{La}_{0.75}\text{Sr}_{0.25}\text{MnO}_3$ nanotubes at 0.15 mA cm^{-2} . Figures f,g reproduced with permission.^[276] Copyright 2013, Wiley-VCH.

porous nanowires, fabricated through hydrothermal method followed by annealing (Figure 21a,b),^[271] exhibited a specific surface area of $87 \text{ m}^2 \text{ g}^{-1}$ with the majority of pore diameters between 5 and 10 nm. $\text{Li}-\text{O}_2$ batteries fabricated with Co_3O_4 porous nanowires as cathode showed an initial capacity in excess of $11\,000 \text{ mAh g}^{-1}$ with a cut-off voltage of 2.4 V at 0.1 A g^{-1} . These values are higher than that of Super-P carbon black (7206 mAh g^{-1}) and Co_3O_4 nanoparticles (9765 mAh g^{-1}) (Figure 21c). CoO mesoporous nanowire arrays have also been reported for high performance $\text{Li}-\text{O}_2$ battery.^[272]

Perovskites are another promising candidate for electrode materials in $\text{Li}-\text{O}_2$ batteries as they have high ORR/OER catalytic activities and are capable of reducing

the overpotential between discharge and charge plateaus.^[274,275] Zhao et al.^[68] synthesized hierarchical perovskite $\text{La}_{0.5}\text{Sr}_{0.5}\text{CoO}_{2.91}$ mesoporous nanowires through a facile multistep microemulsion and annealing method (Figure 21d), while the obtained mesoporous nanowires with a surface area of $\approx 97 \text{ m}^2 \text{ g}^{-1}$. The porous structure and high surface area provided continuous diffusion paths and numerous reactive sites for O_2 , resulting in high ORR and OER activities. A fabricated $\text{Li}-\text{O}_2$ battery with $\text{La}_{0.5}\text{Sr}_{0.5}\text{CoO}_{2.91}$ mesoporous nanowires as cathode delivered a high capacity of over $11\,000 \text{ mAh g}^{-1}$ (Figure 21e), which was much higher than that of nanoparticles (5302 mAh g^{-1}). Another perovskite, porous $\text{La}_{0.75}\text{Sr}_{0.25}\text{MnO}_3$ nanotubes (PNT-LSM) was prepared through electrospinning

method (Figure 21f).^[276] The PNT-LSM nanowires reduced the overpotential between the ORR and OER processes, leading to improved capacity, rate capability, cycling stability and efficiency. A Li-O₂ battery with PNT-LSM operated for 124 cycles with a fixed capacity of 1000 mAh g⁻¹ (Figure 21g). The ensemble of these results clearly establishes that transition metal oxides with porous 1D nanostructures can significantly enhance Li-O₂ battery performance.

Porous nanowires with high surface area, continuous O₂ and electrolyte diffusion channels, and sufficient sites for reversible product deposition/decomposition show great promise for high performance Li-O₂ batteries. To further improve capacity and the cycle life, some research strategies could be undertaken: (1) constructing electrodes that have high catalytic activity, conductivity and free of by-products; (2) modifying the surface of nanowires to tailor the Li₂O₂ into smaller sizes; (3) designing hierarchical macro/meso/microporous structures for both the diffusion of O₂ and deposition of discharged products.

4.5. Supercapacitors

Supercapacitors or electrochemical capacitors represent a class of energy storage devices that possess high power density and fast charge/discharge kinetics.^[277–279] The energy storage mechanisms for electrochemical capacitors can be divided into two basic types: electrical double-layer capacitance and pseudocapacitance.^[37] Electrical double-layer capacitance is generated from the electrostatic adsorption of ions on the surface of active materials. The surface non-faradaic electrostatic adsorption process is fast, resulting in high power density but low energy density owing to limited charge storage numbers. To improve upon energy density, researchers have begun to introduce faradaic redox mechanism, that is pseudocapacitance, where charge storage occurs via Faradaic charge transfer at or near the surface of materials. In recent years, the advanced intercalation pseudocapacitance has been demonstrated. The advantage of intercalation pseudocapacitance is the utilization of bulk ion intercalation, not just the surface, thus allowing higher energy density still with high power density. Based on the different energy storage mechanisms, electrochemical capacitor (or supercapacitor) devices can be placed into three main categories: (1) electric double-layer capacitors (EDLCs) which consist of two double-layer capacitor electrodes characterized by non-Faradaic processes; (2) pseudocapacitors which consist of two pseudocapacitive electrodes that exhibit Faradaic processes; (3) hybrid devices where different charge storage mechanisms are involved for the cathode and anode.

Because energy storage in double-layer capacitor materials occurs on the surface of the electrode, the specific surface area greatly affects their electrochemical performance. Similar to LIBs and SIBs, pseudocapacitive materials store charge via the redox reactions which accompany the intercalation of ions (mostly Li⁺ or Na⁺). In this case, reducing ion and electron diffusion pathways will play an important role in improving electrochemical performance. In this section, we will focus on porous 1D nanomaterials for supercapacitors.

4.5.1. Electric Double-Layer Capacitance

EDLCs can exhibit fast charge–discharge responses which results in high power density and long-term cycling stability.^[40] However, the energy density is relatively low. Since double-layer capacitance is mainly derived from the surface adsorption of ions. Thus the key is to increase the specific surface area available for ionic adsorption. 1D carbonaceous materials have been widely applied as electrodes or conductive matrices in EDLC materials due to their high conductivity, high stability and low cost.^[280] To further improve their energy storage performance, several methods have been proposed for increasing their surface area, while the creating of pores in nanowires/nanofibers is the most effective one.

CNTs with high conductivity, open channels and flexible structures are regarded as promising supercapacitor materials. However, the specific surface area of CNTs is usually below 200 m² g⁻¹, far lower than other carbonaceous materials. To increase the surface area of the CNTs, chemical activation method is applied to create defects and porosity. CNTs treated by KOH activation inhibited an increased specific surface area from 166 to 644 m² g⁻¹.^[281] This enabled the specific capacitance to increase significantly from 18.5 F g⁻¹ (pristine CNTs) to 54 F g⁻¹ (activated porous CNTs), which showed a linear relationship between the specific capacitance and specific surface area.

The porous structure has a significant influence on the electrochemical performance of the carbon nanofibers. Porous carbon nanofibers synthesized by CVD using an alkali-doped copper catalyst exhibited a specific capacitance of 297 F g⁻¹ when tested in a 6 M KOH electrolyte.^[282] By adjusting the surface area and porous structure of the designed 1D nanomaterials, the electrochemical performance could be further optimized.^[283] The effect of porous structure and the pore size distribution on the electrochemical performance of carbon nanofibers is further investigated. Lu et al.^[284] synthesized porous carbon nanofibers through a novel centrifugal spinning approach. The specific surface area and the total pore volume were controlled by adjusting the weight ratio between PAN and poly(methyl methacrylate) (PMMA) and the carbonization temperature. Porous carbon nanofibers yielded a specific surface area from ≈405 to ≈444 m² g⁻¹ and total pore volume from 0.171 to 0.31 cm³ g⁻¹. The materials with the highest specific surface area and largest pore volume delivered the highest capacitance of 144 F g⁻¹ at 0.1 A g⁻¹. The porosity of the nanofibers can be easily controlled using SiO₂ nanoparticle templates.^[285] Specific surface areas ranged from 1625 to 1796 m² g⁻¹ while pore volumes varied from 0.81 to 1.54 cm³ g⁻¹. The high content of macro-, meso-, and micropores in nanofibers increased the capacitance to 197 F g⁻¹ at 5 mV s⁻¹. The improvement is attributed to the high volume ratio of mesopores to micropores and high micropore volume. These results show that the hierarchical pore size design is beneficial for enlarge charge storage.

The addition of insulating binders will block the pathways for ion transport, which generates more impedance at the electrode-electrolyte interface and causes lower capacitance values at high charge/discharge rates. To avoid the drawback of binders, porous nanofibers can be assembled into binder-free and self-standing films, which is promising in flexible energy storage applications.^[53,80,286,287] Recently, Huang et al.^[80] produced bamboo-like

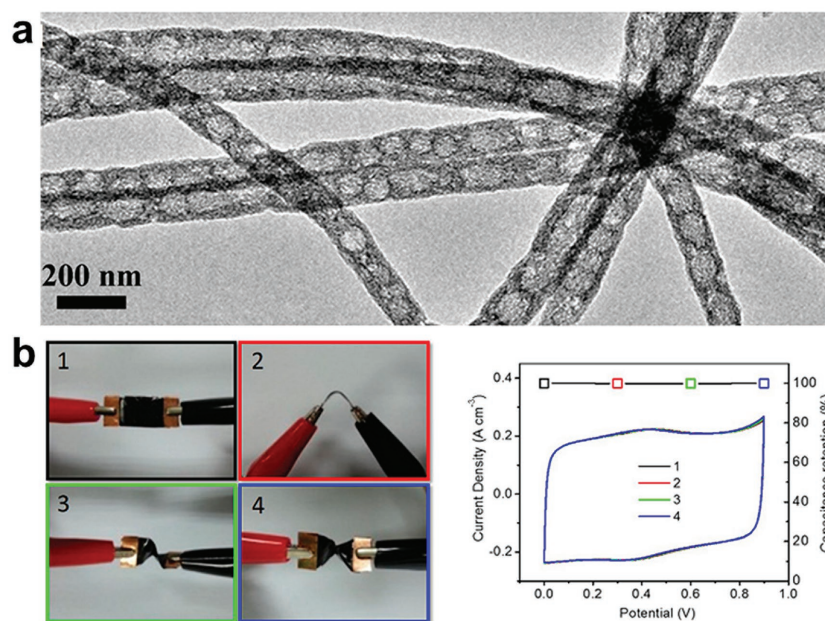


Figure 22. a) TEM image of free-standing porous carbon nanofibers. b) Electrochemical behavior of all-solid-state supercapacitor under different degrees of mechanical deformation with the flexible device (1) bent 0° and (2) bent 90° , (3) twisted 90° and (4) twisted 180° . On the right panel, the corresponding CV curves and capacitance retention at 100 mV s^{-1} for (1) to (4). Reproduced with permission.^[80] Copyright 2015, American Chemical Society.

porous carbon fiber films via electrospinning (Figure 22a). The robust structure of bamboo-like fibers led to a nanofiber network electrode that was highly flexible, foldable, and pliable. The all solid-state symmetric supercapacitor exhibited excellent performance even under bending and twisting (Figure 22b). The specific power and energy densities for these bamboo-like carbon nanofibers could reach values as high as 61.3 kW kg^{-1} and 2.37 Wh kg^{-1} . Another approach demonstrated by Liu et al.^[287] is free-standing porous carbon nanofibers synthesized by electrospinning $\text{Co}(\text{NO}_3)_2/\text{PVP}/\text{DMF}$ with a further acid treatment to generate high porosity. Symmetric supercapacitors which incorporated the porous nanofibers demonstrated excellent flexibility as 90% of its initial capacitance after 500 bending cycles. Similarly, Qin et al. fabricated micrometer-thin flexible solid-state supercapacitors with free-standing porous carbon nanofibers as the electrode, ultrathin graphite as the current collector and PVA/ H_2SO_4 gel as the electrolyte.^[53] This flexible supercapacitor device exhibited high volumetric energy density (2.4 mWh cm^{-3}) and power density (23 W cm^{-3}).

In summary, porous 1D nanostructures have exhibited excellent electrochemical performance when utilized as EDLC materials. One important direction for the future will be to design carbon-based materials with appropriate pore size and/or hierarchical porous architectures to optimize the diffusion and storage of ions.

4.5.2. Redox Pseudocapacitance

Pseudocapacitance store charge through reversible redox faradaic reactions occurring on/near the surface of electrode

materials. The charge transfer process enables these materials to attain higher energy density than EDLC.^[278,288] The most studied pseudocapacitance materials are heteroatom-doped carbonaceous materials,^[289–291] RuO_2 ^[292,293] and MnO_2 .^[294,295]

Conductive carbonaceous materials are usually considered for EDLC. However, with heteroatom-doping, they are able to deliver pseudocapacitive owing to the redox reactions between the doped heteroatoms, increasing the total capacitance accordingly. N-doped porous carbonaceous are the successful examples. N-doped porous carbon nanofibers have been synthesized by Yu and co-workers^[289] through facile carbonization of carbon nanofibers@Ppy (Figure 23a). The peaks observed in the cyclic voltammetry (CV) indicate a combination of both double-layer capacitance and pseudocapacitance (Figure 23b). The N-doped carbon nanofibers exhibited a reversible specific capacitance of 202 and 165 F g^{-1} at 1.0 and 30 A g^{-1} , respectively, and the capacitance was maintained at 196 F g^{-1} after 3000 cycles at 1.0 A g^{-1} (Figure 23c). These authors also synthesized co-doped N- and P- carbon nanofibers (N,P-CNF) via pyrolysis of bacterial cellulose in

$\text{NH}_4\text{H}_2\text{PO}_4$.^[290] When evaluated in a symmetric supercapacitor, the N,P-CNF exhibited a specific capacitance of 205 F g^{-1} at 1.0 A g^{-1} , significantly higher than that of the pure CNF. In addition, the symmetric supercapacitor based on N,P-CNF electrodes displayed an high energy density of 7.76 Wh kg^{-1} .

Besides carbonaceous materials, conductive polymers with high electronic conductivity also exhibit pseudocapacitive.^[296–298] Poly(3,4-ethylenedioxythiophene) (PEDOT) nanotubes were fabricated with the assistance of porous alumina templates.^[299] When tested in 1 M LiClO_4 electrolytes, PEDOT reacted with the ClO_4^- in the electrolyte to give a specific capacitance of 132 F g^{-1} at the current density of 5 mA cm^{-2} . Similarly, PANI-porous carbon nanofiber electrodes showed a specific capacitance of 296 F g^{-1} at 1 A g^{-1} and a capacitance retention of 98% after 1000 cycles in 1 M H_2SO_4 electrolyte.^[300] This enhancement is attributed to the short diffusion path and low ionic resistance, so that the reactive sites of the polymer remain active during charge/discharge.

Many transition metal oxides are pseudocapacitive materials. Zhang et al. synthesized porous tubular hydrous RuO_2 with manganite as a sacrificial template.^[292] At a specific current of 0.5 A g^{-1} , the capacitance of tubular hydrous RuO_2 could reach 861 F g^{-1} . To further facilitate proton transport, tubular hydrous RuO_2 arrays were fabricated on AAO-coated graphite substrates through electrodeposition.^[293] Specific capacitances as high as 1300 F g^{-1} were delivered in this novel nanoarchitecture. Although RuO_2 exhibits superior performance, its high cost restricts the applications, especially for large scale applications. Thus, low-cost transition metal oxides alternatives were developed.^[294,295,301,302] Xia et al. synthesized MnO_2 nanotube arrays with wall thicknesses of 40–50 nm by electrochemical

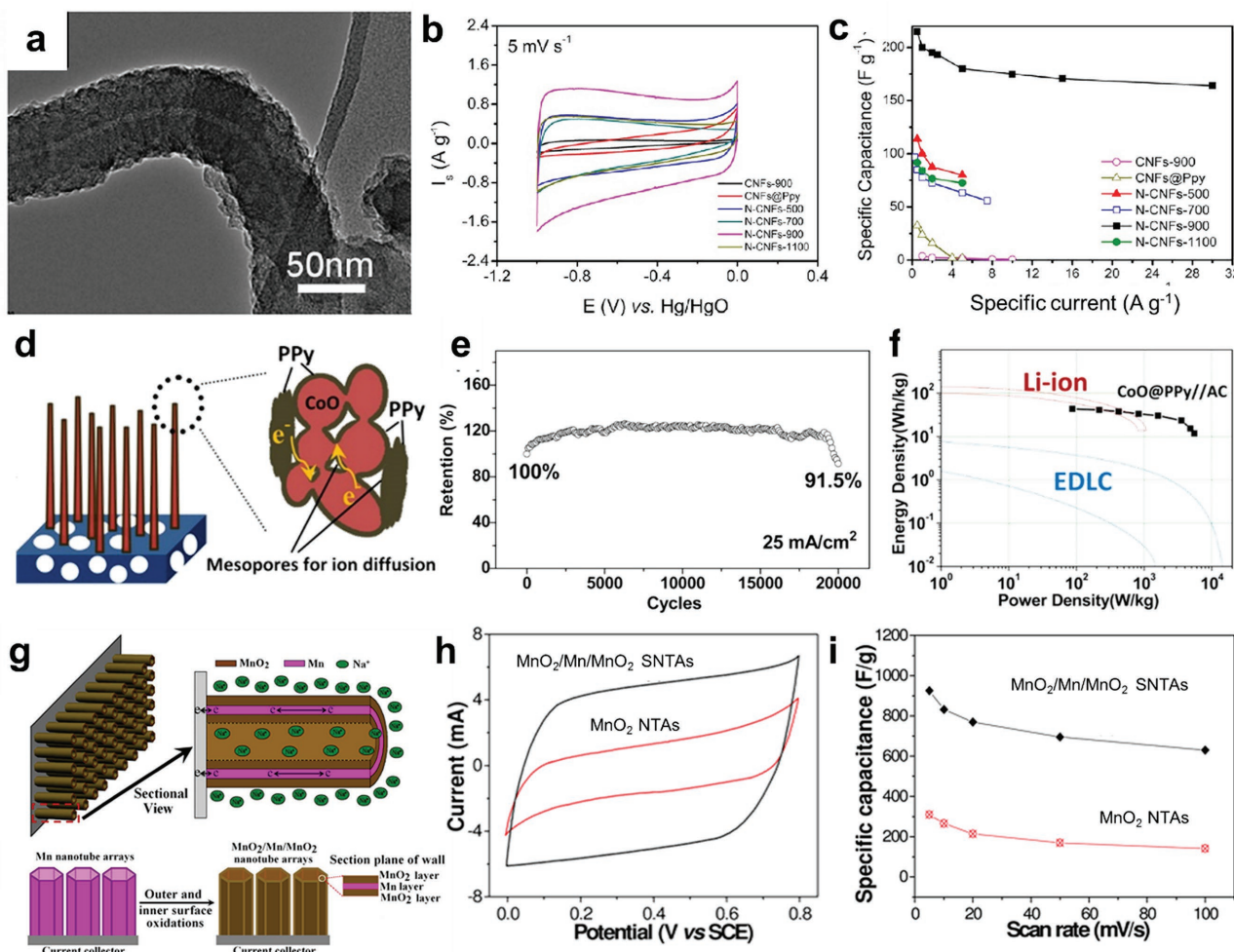


Figure 23. a) HRTEM image (b) CV curves, and (c) specific capacitances of N-doped CNFs, reproduced with permission.^[289] Copyright 2012, American Chemical Society. (d) Illustration, (e) cycling performance and (f) Ragone plots of mesoporous CoO@PPy nanowire arrays, reproduced with permission.^[307] Copyright 2013, American Chemical Society. g) Illustration, (h) CV curves and (i) rate performance of MnO₂/Mn/MnO₂ SNTAs and MnO₂ NTAs, reproduced with permission.^[65] Copyright 2012, American Chemical Society.

deposition with the assistance of an alumina template.^[294] When tested in 1 M Na₂SO₄ electrolyte, the MnO₂ nanotubes exhibited 320 F g⁻¹ at the scan rate of 20 mV s⁻¹, while solid MnO₂ nanowires only delivered a specific capacitance of 101 F g⁻¹. Furthermore, nanosheet-assembled mesoporous MnO₂ nanotubes, with a specific area of 85 m² g⁻¹ and an average pore size of ≈18 nm, exhibited a specific capacitance of 365 F g⁻¹ with a capacitance retention of 90% after 3000 cycles.^[295] These results demonstrate that tubular and hierarchical porous structures offer excellent electrochemical performance.

Porous oxides or hydroxides in the form of nanowires showed pseudocapacitive behavior and provided a high specific capacitance. However, their rate performance needs to be improved because of their low electronic conductivity. Mixed transition-metal oxides (AB₂O₄) possess high electronic conductivity and reversible redox properties.^[214] The porous NiCo₂O₄ nanowires showed a high specific capacitance of 743 F g⁻¹ at 1 A g⁻¹ and good cycling stability with 94% capacitance retention after 3000 cycles.^[303] In addition, mesoporous NiCo₂O₄ nanowire arrays were grown on carbon textiles by a hydrothermal method

followed by heat treatment.^[304] A capacitance of 1010 F g⁻¹ was achieved at 20 A g⁻¹, corresponding to nearly 80% of the capacitance at 1 A g⁻¹.

Incorporating active electrochemical materials into conductive matrices or directly attaching active materials onto conductive substrates can effectively circumvent the use of binders, and enable bi-continuous electron and ion transport for faster charge storage.^[305,306] Liu and co-workers reported that CoO@PPy porous nanowires on nickel foam (Figure 23d)^[307] exhibited higher capacitance than pure CoO nanowires and retained ≈99.8% of its initial capacitance after 2000 cycles. When assembled in an asymmetric supercapacitor with aqueous electrolyte, over 90% of the capacitance was retained after 20,000 cycles (Figure 23e). The asymmetric supercapacitor displayed energy densities of 43.5 Wh kg⁻¹ and 11.8 Wh kg⁻¹ at power densities of 87.5 W kg⁻¹ and 5.5 kW kg⁻¹, respectively (Figure 23f). An advantage of using nickel foams is that they serve as flexible substrates which can be assembled into flexible devices.^[307] Recently, novel MnO₂/Mn/MnO₂ sandwich-structured nanotube arrays (MnO₂/Mn/MnO₂ SNTAs) were constructed

using electrodeposition and a template assisted process (Figure 23g).^[65] The middle Mn layer provided fast electron conduction pathways while the tubular structure maintained ion access. At a specific capacitance of 955 F g^{-1} at 1.5 A g^{-1} , the amount of charge storage for $\text{MnO}_2/\text{Mn}/\text{MnO}_2$ SNTAs was over 75% greater than the MnO_2 NTAs (Figure 23h,i). The better rate capability for the $\text{MnO}_2/\text{Mn}/\text{MnO}_2$ SNTAs is attributed to its higher conductivity and the nanotubular arrays.

The porous 1D nanostructures described above have successfully demonstrated the ability to exhibit high redox pseudocapacitance. Since this type of pseudocapacitance includes surface redox reactions and charge transfer, the design of nanoarchitectures can take into following considerations: (1) appropriate porous structure with high surface to volume ratio for enhancing the pseudocapacitive contribution; (2) facilitating fast electron transport to achieve better rate performance; (3) stabilizing the electrode-electrolyte interface to obtain long-term cycling.

4.5.3. Intercalation Pseudocapacitance

Intercalation pseudocapacitance is based on the intercalation of ions and thus involves charge storage in the bulk of material rather than the surface.^[37] Compared to electrode materials in LIBs and SIBs, intercalation pseudocapacitance represents a similar energy storage mechanism in terms of storing ions in the host, but the kinetics are different. The kinetics of LIBs and SIBs are controlled by solid-state diffusion, while capacitors, whether electric double-layer capacitive or pseudocapacitive (including intercalation pseudocapacitive), are surface-controlled.^[308,309] In a cyclic voltammetry (CV) curves, the current response (i) to the applied scan rate (ν) depends on which processes are involved. For a redox reaction limited by semi-infinite linear diffusion, as occurs in a battery material, the current response varies with $\nu^{1/2}$ while for a capacitive process, the current varies directly with ν . Thus, the current from both diffusion-controlled and capacitive-controlled processes at any given potential can be expressed as (Equation (7)).

$$i(\text{V}) = k_1\nu + k_2\nu^{1/2} \quad (7)$$

The capacitive and diffusion contributions can be determined individually by solving for values of k_1 and k_2 . Capacitive contribution is the result of surface processes which is independent of scan rate, so that the collected CV curves from energy storage mechanism does not show obvious shifts.^[310]

It should be noted that whether a material shows battery-like or capacitor-like behavior is largely dependent on intrinsic material properties and their morphology. Up to now, the materials which demonstrated as intrinsic pseudocapacitive include $T\text{-Nb}_2\text{O}_5$,^[311–314] $\text{TiO}_2(\text{B})$ ^[315] and hydrogen titanate.^[316–318] These materials exhibit capacitive behavior as large particles as they tend to possess rapid diffusion tunnels that have lower energy barriers. Dunn and co-workers reported that $T\text{-Nb}_2\text{O}_5$ exhibited intrinsic pseudocapacitance for Li^+ ions even at a high mass loading.^[309,312–314] The CV curves for $T\text{-Nb}_2\text{O}_5$ showed a pair of broad redox peaks (Figure 24a) with peak currents varying linearly with scan rate (Figure 24b). The crystalline $T\text{-Nb}_2\text{O}_5$

structure also shows better energy storage performance than the corresponding amorphous material,^[311] since the pseudocapacitive behavior of $T\text{-Nb}_2\text{O}_5$ is arisen from the fast diffusion of Li^+ ions in specific tunnels with lower energy barrier.^[37,312,313] In contrast, for extrinsic pseudocapacitor materials such as V_2O_5 ,^[51,319,320] LiCoO_2 ,^[321] TiS_2 ,^[310] and $\text{TiO}_2(\text{anatase})$,^[322–324] their capacitive behavior is largely affected by particle size and the amount of surface exposed to electrolytes. LiCoO_2 has been widely used as a cathode material for LIBs.^[321] The material exhibits a voltage plateau during galvanostatic charge/discharge which is associated with the bulk-intercalation behavior (Figure 24c). However, when the size of LiCoO_2 particles was reduced to 6.0 nm, the plateau was replaced by a continuously sloping voltage profile, which indicates a capacitive response. In this case, the change of charge/discharge curves is attributed to increased contribution of surface Li^+ ion storage in the small nanoparticles.^[321] This phenomenon represents an example of extrinsic pseudocapacitive behavior activated by constructing nanostructures. V_2O_5 is another example that exhibits pseudocapacitive behavior when the sizes below 10 nm.^[320]

Several approaches can be used to enhance intercalation pseudocapacitance: (1) utilize nanomaterials to achieve short diffusion distance; (2) introduce porosity to increase the access of electrolyte to intercalation sites; (3) increase the electronic conductivity of the active materials. Therefore, the porous nanowires are helpful as they offer fast electron transport, short ion diffusion distance and increased surface area and reaction sites.

$\text{TiO}_2(\text{B})$ has been identified as an intrinsic pseudocapacitive material. To improve the electrochemical performance of $\text{TiO}_2(\text{B})$, tubular structures were synthesized to increase the number of intercalation sites and thus further enhance pseudocapacitive performance.^[325–327] Nanoparticle-deposited double-walled $\text{TiO}_2(\text{B})$ nanotubes^[326] showed good electrochemical performance at high rate (130 mAh g^{-1} at 20 C), attributing to the decreased Li^+ ion diffusion distance arising from the thin walls of nanotubes. Layered hydrogen titanates also deliver pseudocapacitive behavior in both nanotube and nanowire forms,^[316,317,328] which have an open layered structure with large interlayer spacing (0.8 nm) and enable fast Li^+ ion intercalation. Layered $\text{H}_2\text{Ti}_3\text{O}_7$ nanotubes synthesized through hydrothermal exhibited 82% of the initial capacity remaining after 1000 cycles and showed pseudocapacitive features in CV curves. Similar results have been observed with sodium titanate in non-aqueous electrolytes.^[329] Comparing the performance of sodium titanate nanotubes to nanorods, pseudocapacitive behavior is more obvious in the former, owing to more active sites in the nanotubular structure.^[329]

Hybrid capacitors based on incorporating materials that store charge by intercalation pseudocapacitance are just beginning to be reported in the literature.^[330–338] Nitrogen-rich CNT/C composites were tested as electrodes in lithium ion capacitors (LICs), and demonstrated a capacity of $>200 \text{ mAh g}^{-1}$ for 600 cycles.^[330] To improve the capacitance of the anode, porous VN nanowire-reduced graphene oxide composites (VN-RGO) were developed by Wang et al. (Figure 24d,e).^[338] The porous VN-RGO composite showed higher capacitance and better cycling stability than pure VN nanowires, probably due to higher electrical conductivity from the RGO. The pseudocapacitance contribution to

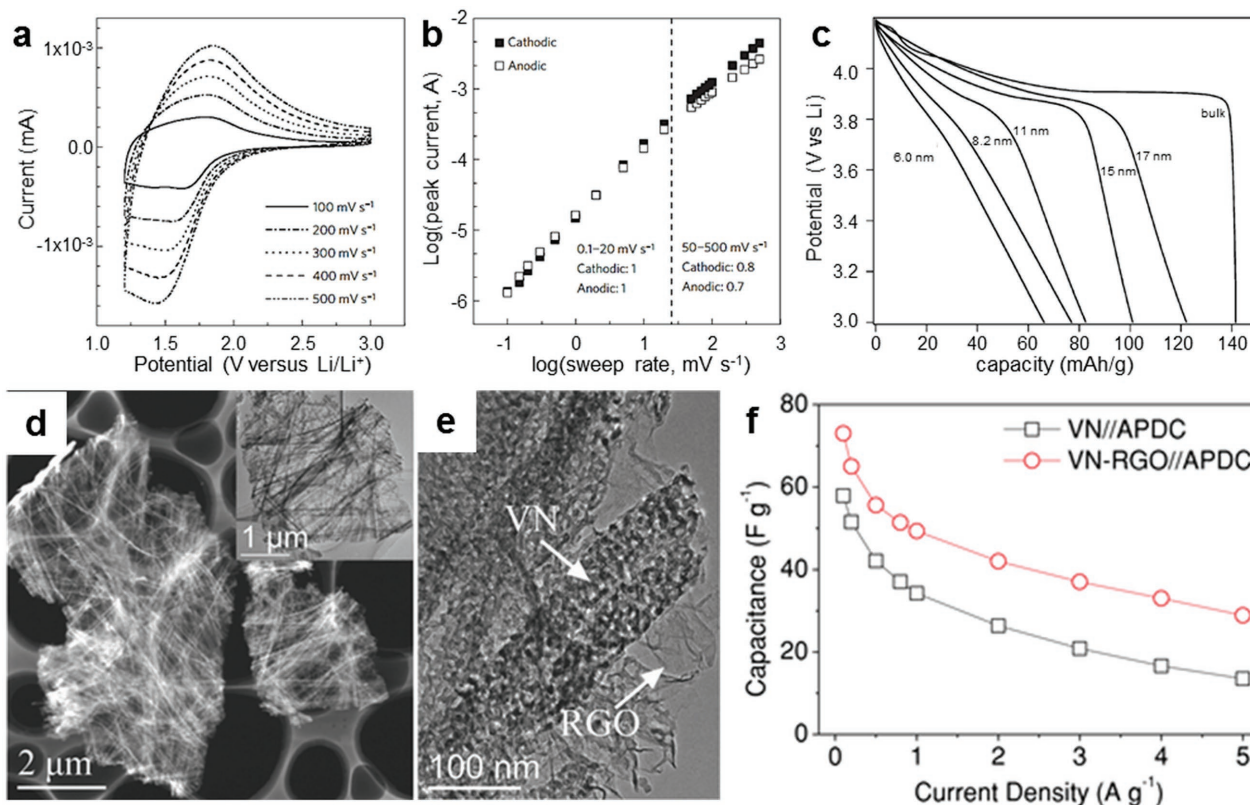


Figure 24. a) CV curves and (b) relationship between peak current and scan rate in a $T\text{-Nb}_2\text{O}_5$ film at different scan rates, reproduced with permission.^[309] Copyright 2013 Nature Publishing Group. c) Discharge curves for LiCoO_2 bulk and nanoparticles, reproduced with permission.^[321] Copyright 2007 American Chemical Society. d) Dark-field TEM image of porous VN-RGO composite, with bright-field TEM image in inset. e) TEM image of VN-RGO composite. (f) The capacitance of VN-RGO//APDC and VN//APDC. Figures d–f reproduced with permission.^[338] Copyright 2015, Wiley-VCH.

the total energy storage was $\approx 80\%$ in the VN-RGO composite. Using activated polyaniline-derived porous carbon (ADPC) nanorods as a cathode, hybrid VN-RGO//APDC capacitors were found to produce 1.5 to 2 times higher capacitance than VN//APDC (based on the total mass of two electrodes, Figure 24f) with energy densities of 162 and 64 Wh kg^{-1} at power densities of 200 and 10000 W kg^{-1} , respectively. TiNb_2O_7 has also been investigated as anode material with intercalation pseudocapacitive.^[331,332] Ordered 3D porous TiNb_2O_7 nanotubes were fabricated using AAO templates.^[332] With graphene as the cathode, porous TiNb_2O_7 //graphene hybrid capacitors reached a maximum energy density of $\approx 74 \text{ Wh kg}^{-1}$, which was much higher than that of TiNb_2O_7 fibers//AC ($\approx 43 \text{ Wh kg}^{-1}$).^[333] Intertwined CNT/ V_2O_5 nanowire networks with controlled porosities also demonstrated good intercalation pseudocapacitive behavior.^[51,319] The ensemble of these results demonstrates that hybrid LICs can achieve fast charge/discharge while maintaining their energy density.

Pseudocapacitive energy storage based on Li^+ or Na^+ ions intercalation offers the promise of new LICs and sodium ion capacitors (SICs) as well.^[308,309,334–337] Nanomaterials, especially porous 1D nanomaterials which exhibit enhanced intercalation pseudocapacitance, are designed to combine the advantages of both batteries and supercapacitors; that is, high energy density with high power density.

5. Summary and Outlook

The development of porous 1D nanomaterials with designed properties and architectures has led to significant advances in electrochemical energy storage. Here, we have highlighted the state-of-the-art on porous 1D nanostructures, from methodologies for rational and controllable synthesis (Table 1), to their successful application in different types of energy storage devices (Table 2 and Table 3). We suggest that porous 1D nanostructures, as described in this review, will overcome the limitations of many electrode materials, so that high capacity, fast charge and discharge, and long cycle life can be realized.

In alkali ion batteries (LIBs and SIBs), porous 1D nanostructures with much shorter bi-continuous ion and electron transport pathways benefit high rate applications. Concurrently, the development of a robust porous structure offers the advantages of accommodating large volume changes which prevent structure collapse and improve cycle life. Outstanding electrochemical performance has been reported using a variety of different porous 1D nanomaterials as they can overcome certain limitations: (1) the poor ionic and electronic conductivity of electrode materials; (2) the interfacial impedance between electrode and electrolyte which arise from SEI layers forming on the interface of active materials; and (3) low volumetric energy density. The rational design of porosity and architecture leads to materials

with properties that enable fast ion diffusion and rapid electron transport, reduce the exposure of active materials to the electrolyte and use assembly methods to increase volumetric energy density.

Advanced lithium batteries (Li-S and Li-O₂ systems) that offer higher energy density than LIBs can also benefit from using porous 1D nanostructures. Through nanocasting, sulfur can be embedded in porous nanofibers, establish strong adsorption properties and thereby inhibit the “shuttle effect” in polysulfide systems. A gradient macro/meso/micro-porous structure with increased sulfur loading is able to significantly enhance the energy density of Li-S batteries. In Li-O₂ batteries, porous nanowires provide large surface area, continuous O₂ and electrolyte diffusion channels, as well as good electron transport. Nanowires also provide numerous deposition/decomposition sites for reaction products enabling improved electrochemical performance.

The electrochemical performance of supercapacitors that store charge by double layer or redox processes has been improved by using porous 1D nanostructures. Carbon-based EDLC materials with heteroatom-doping are able to create more redox sites to increase the energy density. In addition, well-constructed porous nanowires enable intrinsic and extrinsic pseudocapacitor materials to achieve improved performance by implementing short diffusion paths, large ion adsorption and fast electrolyte access to redox-active sites. Constructing electrodes with porous 1D nanostructures that enable bi-continuous transport of electrons and ions will be beneficial for fabricating high energy density hybrid supercapacitors whose cathodes and anodes effectively combine the advantages of pseudocapacitive materials, especially for intercalation pseudocapacitance.

We have discussed the rational design and controllable porosity of 1D nanomaterials in this review. More systematic studies, both theoretical and experimental, are needed to optimize the design of these nanostructures for specific applications. For large scale and low cost production, the required synthesis procedures, which are relatively complex, must be simplified and engineered. We believe that high-performance energy storage devices based on advanced porous 1D nanomaterials will be an important direction for the future.

Acknowledgements

This work was supported by the National Key Research and Development Program of China (2016YFA0202603), the National Basic Research Program of China (2013CB934103), the Program of Introducing Talents of Discipline to Universities (B17034), the National Science Fund for Distinguished Young Scholars (51425204), the National Natural Science Foundation of China (51521001), and Fundamental Research Funds for the Central Universities (WUT: 22016111001), the International Postdoctoral Exchange Fellowship Program (20160025). Additional funding from the Office of Naval Research (B.D. and E.L.) is acknowledged. The authors are deeply thankful to Professor Charles M. Lieber of Harvard University, Professor Dongyuan Zhao of Fudan University, and Professor Jun Liu of Pacific Northwest National Laboratory for their stimulating discussions and kind help.

Received: April 30, 2016

Revised: November 14, 2016

Published online:

- [1] D. Larcher, J. M. Tarascon, *Nature Chem.* **2015**, *7*, 19.
- [2] S. Chu, A. Majumdar, *Nature* **2012**, *488*, 294.
- [3] L. Mai, X. Tian, X. Xu, L. Chang, L. Xu, *Chem. Rev.* **2014**, *114*, 11828.
- [4] D. Kundu, E. Talaie, V. Duffort, L. F. Nazar, *Angew. Chem. Int. Ed.* **2015**, *54*, 3431.
- [5] B. Dunn, H. Kamath, J. M. Tarascon, *Science* **2011**, *334*, 928.
- [6] M. S. Whittingham, *Chem. Rev.* **2014**, *114*, 11414.
- [7] J.-M. Tarascon, M. Armand, *Nature* **2001**, *414*, 359.
- [8] M. Armand, J.-M. Tarascon, *Nature* **2008**, *451*, 652.
- [9] Y.-K. Sun, Z. Chen, H.-J. Noh, D.-J. Lee, H.-G. Jung, Y. Ren, S. Wang, C. S. Yoon, S.-T. Myung, K. Amine, *Nature Mater.* **2012**, *11*, 942.
- [10] P. G. Bruce, B. Scrosati, J. M. Tarascon, *Angew. Chem. Int. Ed.* **2008**, *47*, 2930.
- [11] Y. Gogotsi, *ACS Nano* **2014**, *8*, 5369.
- [12] Q. Zhang, E. Uchaker, S. L. Candelaria, G. Cao, *Chem. Soc. Rev.* **2013**, *42*, 3127.
- [13] H.-G. Wang, S. Yuan, D.-L. Ma, X.-B. Zhang, J.-M. Yan, *Energy Environ. Sci.* **2015**, *8*, 1660.
- [14] H. Pan, Y.-S. Hu, L. Chen, *Energy Environ. Sci.* **2013**, *6*, 2338.
- [15] Y. Shao, M. Gu, X. Li, Z. Nie, P. Zuo, G. Li, T. Liu, J. Xiao, Y. Cheng, C. Wang, *Nano Lett.* **2013**, *14*, 255.
- [16] M.-C. Lin, M. Gong, B. Lu, Y. Wu, D.-Y. Wang, M. Guan, M. Angell, C. Chen, J. Yang, B.-J. Hwang, H. Dai, *Nature* **2015**, *520*, 324.
- [17] L. Geng, G. Lv, X. Xing, J. Guo, *Chem. Mater.* **2015**, *27*, 4926.
- [18] H. Wang, Y. Bai, S. Chen, X. Luo, C. Wu, F. Wu, J. Lu, K. Amine, *ACS Appl. Mater. Inter.* **2014**, *7*, 80.
- [19] L.-F. Cui, R. Ruffo, C. K. Chan, H. Peng, Y. Cui, *Nano Lett.* **2008**, *9*, 491.
- [20] H. Wu, G. Chan, J. W. Choi, Y. Yao, M. T. McDowell, S. W. Lee, A. Jackson, Y. Yang, L. Hu, Y. Cui, *Nature Nanotechnol.* **2012**, *7*, 310.
- [21] M. Ge, J. Rong, X. Fang, C. Zhou, *Nano Lett.* **2012**, *12*, 2318.
- [22] C. K. Chan, H. Peng, G. Liu, K. Mcllwraith, X. F. Zhang, R. A. Huggins, Y. Cui, *Nature Nanotechnol.* **2008**, *3*, 31.
- [23] T. Song, H. Cheng, H. Choi, J.-H. Lee, H. Han, D. H. Lee, D. S. Yoo, M.-S. Kwon, J.-M. Choi, S. G. Doo, *ACS Nano* **2011**, *6*, 303.
- [24] K. H. Seng, M. H. Park, Z. P. Guo, H. K. Liu, J. Cho, *Angew. Chem. Int. Ed.* **2012**, *124*, 5755.
- [25] M. H. Park, Y. Cho, K. Kim, J. Kim, M. Liu, J. Cho, *Angew. Chem. Int. Ed.* **2011**, *123*, 9821.
- [26] Y. Xu, Y. Zhu, Y. Liu, C. Wang, *Adv. Energy Mater.* **2013**, *3*, 128.
- [27] H. Zhu, Z. Jia, Y. Chen, N. Weadock, J. Wan, O. Vaaland, X. Han, T. Li, L. Hu, *Nano Lett.* **2013**, *13*, 3093.
- [28] T. Kennedy, E. Mullane, H. Geaney, M. Osiak, C. O'Dwyer, K. M. Ryan, *Nano Lett.* **2014**, *14*, 716.
- [29] X. Li, A. Dhanabalan, L. Gu, C. Wang, *Adv. Energy Mater.* **2012**, *2*, 238.
- [30] K. Zhao, L. Zhang, R. Xia, Y. Dong, W. Xu, C. Niu, L. He, M. Yan, L. Qu, L. Mai, *Small* **2015**, *12*, 588.
- [31] C. K. Chan, X. F. Zhang, Y. Cui, *Nano Lett.* **2008**, *8*, 307.
- [32] L. Zhang, K. Zhao, W. Xu, Y. Dong, R. Xia, F. Liu, L. He, Q. Wei, M. Yan, L. Mai, *Phys. Chem. Chem. Phys.* **2015**, *17*, 7619.
- [33] W. Xu, K. Zhao, C. Niu, L. Zhang, Z. Cai, C. Han, L. He, T. Shen, M. Yan, L. Qu, *Nano Energy* **2014**, *8*, 196.
- [34] M. Obrovac, V. Chevrier, *Chem. Rev.* **2014**, *114*, 11444.
- [35] M. T. McDowell, S. W. Lee, W. D. Nix, Y. Cui, *Adv. Mater.* **2013**, *25*, 4966.
- [36] L. Huang, Q. Wei, R. Sun, L. Mai, *Frontiers Energy Res.* **2014**, *2*, 43.
- [37] V. Augustyn, P. Simon, B. Dunn, *Energy Environ. Sci.* **2014**, *7*, 1597.
- [38] Y. Yang, G. Zheng, Y. Cui, *Chem. Soc. Rev.* **2013**, *42*, 3018.
- [39] Y. Tang, Y. Zhang, W. Li, B. Ma, X. Chen, *Chem. Soc. Rev.* **2015**, *44*, 5926.

- [40] Z. Yang, J. Ren, Z. Zhang, X. Chen, G. Guan, L. Qiu, Y. Zhang, H. Peng, *Chem. Rev.* **2015**, *115*, 5159.
- [41] N. P. Dasgupta, J. Sun, C. Liu, S. Brittman, S. C. Andrews, J. Lim, H. Gao, R. Yan, P. Yang, *Adv. Mater.* **2014**, *26*, 2137.
- [42] T. J. Kempa, R. W. Day, S.-K. Kim, H.-G. Park, C. M. Lieber, *Energy Environ. Sci.* **2013**, *6*, 719.
- [43] B. Tian, T. J. Kempa, C. M. Lieber, *Chem. Soc. Rev.* **2009**, *38*, 16.
- [44] A. I. Hochbaum, P. Yang, *Chem. Rev.* **2009**, *110*, 527.
- [45] Y. S. Bae, R. Q. Snurr, *Angew. Chem. Int. Ed.* **2011**, *50*, 11586.
- [46] A. Vu, Y. Qian, A. Stein, *Adv. Energy Mater.* **2012**, *2*, 1056.
- [47] C. Perego, R. Millini, *Chem. Soc. Rev.* **2013**, *42*, 3956.
- [48] C. M. Parlett, K. Wilson, A. F. Lee, *Chem. Soc. Rev.* **2013**, *42*, 3876.
- [49] B. Kong, C. Selomulya, G. Zheng, D. Zhao, *Chem. Soc. Rev.* **2015**, *44*, 7997.
- [50] D. Li, C. Lv, L. Liu, Y. Xia, X. She, S. Guo, D. Yang, *ACS Cent. Sci.* **2015**, *1*, 261.
- [51] Z. Chen, V. Augustyn, X. Jia, Q. Xiao, B. Dunn, Y. Lu, *ACS Nano* **2012**, *6*, 4319.
- [52] J. S. Cho, Y. J. Hong, Y. C. Kang, *ACS Nano* **2015**, *9*, 4026.
- [53] K. Qin, J. Kang, J. Li, C. Shi, Y. Li, Z. Qiao, N. Zhao, *ACS Nano* **2015**, *9*, 481.
- [54] L. Ji, M. Gu, Y. Shao, X. Li, M. H. Engelhard, B. W. Arey, W. Wang, Z. Nie, J. Xiao, C. Wang, J. G. Zhang, J. Liu, *Adv. Mater.* **2014**, *26*, 2901.
- [55] V. Aravindan, Y.-S. Lee, S. Madhavi, *Adv. Energy Mater.* **2015**, *5*, 1402225.
- [56] Y. Wang, T. Zhou, K. Jiang, P. Da, Z. Peng, J. Tang, B. Kong, W.-B. Cai, Z. Yang, G. Zheng, *Adv. Energy Mater.* **2014**, *4*, 1400696.
- [57] X.-Y. Yu, L. Yu, X. W. Lou, *Adv. Energy Mater.* **2015**, 1501333.
- [58] Y. Wang, H. C. Zeng, J. Y. Lee, *Adv. Mater.* **2006**, *18*, 645.
- [59] L. Zhang, G. Zhang, H. B. Wu, L. Yu, X. W. D. Lou, *Adv. Mater.* **2013**, *25*, 2589.
- [60] Y. Zhao, W. Wu, J. Li, Z. Xu, L. Guan, *Adv. Mater.* **2014**, *26*, 5113.
- [61] D. Gu, W. Li, F. Wang, H. Bongard, B. Spliethoff, W. Schmidt, C. Weidenthaler, Y. Xia, D. Zhao, F. Schüth, *Angew. Chem. Int. Ed.* **2015**, *54*, 7060.
- [62] Z. Li, J. Zhang, X. W. Lou, *Angew. Chem. Int. Ed.* **2015**, *54*, 12886.
- [63] Q. Wei, Q. An, D. Chen, L. Mai, S. Chen, Y. Zhao, K. M. Hercule, L. Xu, A. Minhas-Khan, Q. Zhang, *Nano Lett.* **2014**, *14*, 1042.
- [64] Q. An, F. Lv, Q. Liu, C. Han, K. Zhao, J. Sheng, Q. Wei, M. Yan, L. Mai, *Nano Lett.* **2014**, *14*, 6250.
- [65] Q. Li, Z.-L. Wang, G.-R. Li, R. Guo, L.-X. Ding, Y.-X. Tong, *Nano Lett.* **2012**, *12*, 3803.
- [66] C. Niu, J. Meng, X. Wang, C. Han, M. Yan, K. Zhao, X. Xu, W. Ren, Y. Zhao, L. Xu, Q. Zhang, D. Zhao, L. Mai, *Nature Commun.* **2015**, *6*, 7402.
- [67] Z. Li, J. T. Zhang, Y. M. Chen, J. Li, X. W. D. Lou, *Nature Commun.* **2015**, *6*, 8850.
- [68] Y. Zhao, L. Xu, L. Mai, C. Han, Q. An, X. Xu, X. Liu, Q. Zhang, *P Natl Acad Sci USA* **2012**, *109*, 19569.
- [69] L. Mai, L. Xu, C. Han, X. Xu, Y. Luo, S. Zhao, Y. Zhao, *Nano Lett.* **2010**, *10*, 4750.
- [70] W. Ren, Z. Zheng, Y. Luo, W. Chen, C. Niu, K. Zhao, M. Yan, L. Zhang, J. Meng, L. Mai, *J. Mater. Chem. A* **2015**, *3*, 19850.
- [71] D. Li, Y. Xia, *Adv. Mater.* **2004**, *16*, 1151.
- [72] Y. J. Hong, J. W. Yoon, J. H. Lee, Y. C. Kang, *Chem. Eur. J.* **2015**, *21*, 371.
- [73] Q. Wali, A. Fakhruddin, I. Ahmed, M. H. Ab Rahim, J. Ismail, R. Jose, *J. Mater. Chem. A* **2014**, *2*, 17427.
- [74] S. Peng, L. Li, Y. Hu, M. Srinivasan, F. Cheng, J. Chen, S. Ramakrishna, *ACS Nano* **2015**, *9*, 1945.
- [75] L. Li, S. Peng, J. Wang, Y. L. Cheah, P. Teh, Y. Ko, C. Wong, M. Srinivasan, *ACS Appl. Mater. Inter.* **2012**, *4*, 6005.
- [76] J.-S. Lee, Y.-I. Lee, H. Song, D.-H. Jang, Y.-H. Choa, *Curr. Appl. Phys.* **2011**, *11*, S210.
- [77] L. Li, S. Peng, Y. Cheah, P. Teh, J. Wang, G. Wee, Y. Ko, C. Wong, M. Srinivasan, *Chem. Eur. J.* **2013**, *19*, 5892.
- [78] a) Y. Chen, Z. Lu, L. Zhou, Y.-W. Mai, H. Huang, *Energy Environ. Sci.* **2012**, *5*, 7898; b) Y. Chen, Z. Lu, L. Zhou, Y.-W. Mai, H. Huang, *Nanoscale* **2012**, *4*, 6800.
- [79] J. S. Cho, Y. C. Kang, *Small* **2015**, *11*, 4673.
- [80] Y. Sun, R. B. Sills, X. Hu, Z. W. Seh, X. Xiao, H. Xu, W. Luo, H. Jin, Y. Xin, T. Li, *Nano Lett.* **2015**, *15*, 3899.
- [81] L. Qiao, X. Wang, X. Sun, X. Li, Y. Zheng, D. He, *Nanoscale* **2013**, *5*, 3037.
- [82] H. Y. Wang, Y. Yang, X. Li, L. J. Li, C. Wang, *Chinese Chem. Lett.* **2010**, *21*, 1119.
- [83] D. Lei, B. Qu, H.-T. Lin, T. Wang, *Ceram. Int.* **2015**, *41*, 10308.
- [84] Y. Zhao, X. He, J. Li, X. Gao, J. Jia, *Sens. Actuators B* **2012**, *165*, 82.
- [85] Y. Gao, S. Chen, D. Cao, G. Wang, J. Yin, *J. Power Sources* **2010**, *195*, 1757.
- [86] F. Zhang, C. Yuan, X. Lu, L. Zhang, Q. Che, X. Zhang, *J. Power Sources* **2012**, *203*, 250.
- [87] W. Mei, J. Huang, L. Zhu, Z. Ye, Y. Mai, J. Tu, *J. Mater. Chem.* **2012**, *22*, 9315.
- [88] Y. Li, B. Tan, Y. Wu, *J. Am. Chem. Soc.* **2006**, *128*, 14258.
- [89] Q. Li, D. Sun, H. Kim, *Mater. Res. Bull.* **2011**, *46*, 2094.
- [90] Y. Li, B. Tan, Y. Wu, *Nano Lett.* **2008**, *8*, 265.
- [91] J. Jiang, J. Liu, R. Ding, X. Ji, Y. Hu, X. Li, A. Hu, F. Wu, Z. Zhu, X. Huang, *J. Phys. Chem. C* **2009**, *114*, 929.
- [92] B. Liu, J. Zhang, X. Wang, G. Chen, D. Chen, C. Zhou, G. Shen, *Nano Lett.* **2012**, *12*, 3005.
- [93] R. B. Rakhi, W. Chen, D. Cha, H. N. Alshareef, *Nano Lett.* **2012**, *12*, 2559.
- [94] L. Zhang, K. Zhao, W. Xu, J. Meng, L. He, Q. An, X. Xu, Y. Luo, T. Zhao, L. Mai, *RSC Adv.* **2014**, *4*, 33332.
- [95] Y. Cai, S. Liu, X. Yin, Q. Hao, M. Zhang, T. Wang, *Phys. E* **2010**, *43*, 70.
- [96] D. Su, H. S. Kim, W. S. Kim, G. Wang, *Chem.* **2012**, *18*, 8224.
- [97] X. Jiang, Y. Wang, T. Herricks, Y. Xia, *J. Mater. Chem.* **2004**, *14*, 695.
- [98] Y. Han, X. Wu, Y. Ma, L. Gong, F. Qu, H. Fan, *CrystEngComm* **2011**, *13*, 3506.
- [99] H. Liu, D. Wexler, G. Wang, *J. Alloys Compd.* **2009**, *487*, L24.
- [100] X. Lu, M. Yu, T. Zhai, G. Wang, S. Xie, T. Liu, C. Liang, Y. Tong, Y. Li, *Nano Lett.* **2013**, *13*, 2628.
- [101] C. Wu, J. Maier, Y. Yu, *Adv. Mater.* **2016**, *28*, 174.
- [102] H. Xia, Y. Wan, W. Assenmacher, W. Mader, G. Yuan, L. Lu, *NPG Asia Mater.* **2014**, *6*, e126.
- [103] L. Q. Mai, B. Hu, W. Chen, Y. Y. Qi, C. S. Lao, R. S. Yang, Y. Dai, Z. L. Wang, *Adv. Mater.* **2007**, *19*, 3712.
- [104] C. Yuan, X. Zhang, L. Hou, L. Shen, D. Li, F. Zhang, C. Fan, J. Li, *ster. Chem.* **2010**, *20*, 10809.
- [105] Z. Pei, X. Zhang, X. Gao, *J. Alloys Compd.* **2013**, *546*, 92.
- [106] S. Zhang, L. M. Peng, Q. Chen, G. H. Du, G. Dawson, W. Z. Zhou, *Phys. Rev. Lett.* **2003**, *91*, 256103.
- [107] Y. Tang, Y. Zhang, J. Deng, J. Wei, H. L. Tam, B. K. Chandran, Z. Dong, Z. Chen, X. Chen, *Adv. Mater.* **2014**, *26*, 6111.
- [108] S. A. Corr, M. Grossman, J. D. Furman, B. C. Melot, A. K. Cheetham, K. R. Heier, R. Seshadri, *Chem. Mater.* **2008**, *20*, 6396.
- [109] Y. Kobayashi, H. Hata, M. Salama, T. E. Mallouk, *Nano Lett.* **2007**, *7*, 2142.
- [110] H. W. Shim, D. K. Lee, I. S. Cho, K. S. Hong, D. W. Kim, *Nanotechnol.* **2010**, *21*, 255706.
- [111] Z. Jin, F.-L. Meng, Y. Jia, T. Luo, J.-Y. Liu, B. Sun, J. Wang, J.-H. Liu, X.-J. Huang, *Micropor. Mesopor. Mater.* **2013**, *181*, 146.
- [112] J. Liu, J. Jiang, C. Cheng, H. Li, J. Zhang, H. Gong, H. J. Fan, *Adv. Mater.* **2011**, *23*, 2076.
- [113] X. Xia, J. Tu, Y. Zhang, X. Wang, C. Gu, X.-b. Zhao, H. J. Fan, *ACS Nano* **2012**, *6*, 5531.

- [114] L. Yu, G. Zhang, C. Yuan, X. W. Lou, *Chem. Commun.* **2013**, 49, 137.
- [115] K. Xu, W. Li, Q. Liu, B. Li, X. Liu, L. An, Z. Chen, R. Zou, J. Hu, *J. Mater. Chem. A* **2014**, 2, 4795.
- [116] J. B. Wu, Z. G. Li, X. H. Huang, Y. Lin, *J. Power Sources* **2013**, 224, 1.
- [117] X. Xia, J. Tu, Y. Zhang, J. Chen, X. Wang, C. Gu, C. Guan, J. Luo, H. J. Fan, *Chem. Mater.* **2012**, 24, 3793.
- [118] H. Jiang, L. Yang, C. Li, C. Yan, P. S. Lee, J. Ma, *Energy Environ. Sci.* **2011**, 4, 1813.
- [119] J.-Y. Liao, A. Manthiram, *Adv. Energy Mater.* **2014**, 4, 1400403.
- [120] Z. Cai, L. Xu, M. Yan, C. Han, L. He, K. M. Hercule, C. Niu, Z. Yuan, W. Xu, L. Qu, K. Zhao, L. Mai, *Nano Lett.* **2015**, 15, 738.
- [121] H. Jiang, Y. Hu, S. Guo, C. Yan, P. S. Lee, C. Li, *ACS Nano* **2014**, 8, 6038.
- [122] A. K. Ganguli, A. Ganguly, S. Vaidya, *Chem. Soc. Rev.* **2010**, 39, 474.
- [123] R. Xu, J. Wang, Q. Li, G. Sun, E. Wang, S. Li, J. Gu, M. Ju, *J. Solid State Chem.* **2009**, 182, 3177.
- [124] N. Du, Y. Xu, H. Zhang, J. Yu, C. Zhai, D. Yang, *Inorg. Chem.* **2011**, 50, 3320.
- [125] C. An, Y. Wang, Y. Huang, Y. Xu, L. Jiao, H. Yuan, *Nano Energy* **2014**, 10, 125.
- [126] G. G. Yadav, A. David, T. Favaloro, H. Yang, A. Shakouri, J. Caruthers, Y. Wu, *J. Mater. Chem. A* **2013**, 1, 11901.
- [127] G. G. Yadav, A. David, H. Zhu, J. Caruthers, Y. Wu, *Nanoscale* **2014**, 6, 860.
- [128] X. Zhang, F. Cheng, J. Yang, J. Chen, *Nano Lett.* **2013**, 13, 2822.
- [129] J. Yang, F. Cheng, X. Zhang, H. Gao, Z. Tao, J. Chen, *J. Mater. Chem. A* **2014**, 2, 1636.
- [130] G. Bai, H. Dai, J. Deng, Y. Liu, W. Qiu, Z. Zhao, X. Li, H. Yang, *Chem. Eng. J.* **2013**, 219, 200.
- [131] L. Liu, E. Pippel, R. Scholz, U. Gösele, *Nano Lett.* **2009**, 9, 4352.
- [132] C.-H. Cui, H.-H. Li, S.-H. Yu, *Chem. Commun.* **2010**, 46, 940.
- [133] X. Zhang, D. Li, L. Bourgeois, H. Wang, P. A. Webley, *ChemPhysChem* **2009**, 10, 436.
- [134] K. Cai, Z. Lv, K. Chen, L. Huang, J. Wang, F. Shao, Y. Wang, H. Han, *Chem. Commun.* **2013**, 49, 6024.
- [135] C.-H. Cui, H.-H. Li, S.-H. Yu, *Chem. Sci.* **2011**, 2, 1611.
- [136] C. Du, M. Chen, W. Wang, G. Yin, *ACS Appl. Mater. Inter.* **2010**, 3, 105.
- [137] L. Liu, R. Scholz, E. Pippel, U. Gösele, *J. Mater. Chem.* **2010**, 20, 5621.
- [138] Z. Wei, Z. X. Feng, L. X. Ze, J. N. Er, *J. Porous Mater.* **2010**, 17, 253.
- [139] G. Zheng, Y. Yang, J. J. Cha, S. S. Hong, Y. Cui, *Nano Lett.* **2011**, 11, 4462.
- [140] Y. Shi, Y. Wan, R. Zhang, D. Zhao, *Adv. Funct. Mater.* **2008**, 18, 2436.
- [141] H. Li, H. Lin, S. Xie, W. Dai, M. Qiao, Y. Lu, H. Li, *Chem. Mater.* **2008**, 20, 3936.
- [142] A. Pendashteh, S. E. Moosavifard, M. S. Rahmanifar, Y. Wang, M. F. El-Kady, R. B. Kaner, M. F. Mousavi, *Chem. Mater.* **2015**, 27, 3919.
- [143] H. Kim, J. Cho, *Nano Lett.* **2008**, 8, 3688.
- [144] H.-J. Liu, X.-M. Wang, W.-J. Cui, Y.-Q. Dou, D.-Y. Zhao, Y.-Y. Xia, *J. Mater. Chem.* **2010**, 20, 4223.
- [145] F. Li, J. He, W. L. Zhou, J. B. Wiley, *J. Am. Chem. Soc.* **2003**, 125, 16166.
- [146] M. Bechelany, A. A. Chaaya, F. Frances, O. Akdim, D. Cot, U. B. Demirci, P. Miele, *J. Mater. Chem. A* **2013**, 1, 2133.
- [147] T. Zhu, H. B. Wu, Y. Wang, R. Xu, X. W. D. Lou, *Adv. Energy Mater.* **2012**, 2, 1497.
- [148] N. Du, H. Zhang, B. Chen, J. Wu, X. Ma, Z. Liu, Y. Zhang, D. Yang, X. Huang, J. Tu, *Adv. Mater.* **2007**, 19, 4505.
- [149] N. D. Hoa, N. Van Quy, H. Jung, D. Kim, H. Kim, S.-K. Hong, *Sens. Actuators B* **2010**, 146, 266.
- [150] N. Du, H. Zhang, B. Chen, X. Ma, X. Huang, J. Tu, D. Yang, *Mater. Res. Bull.* **2009**, 44, 211.
- [151] Y. Jia, L. He, Z. Guo, X. Chen, F. Meng, T. Luo, M. Li, J. Liu, *J. Phys. Chem. C* **2009**, 113, 9581.
- [152] X. Qian, Y. Lv, W. Li, Y. Xia, D. Zhao, *J. Mater. Chem.* **2011**, 21, 13025.
- [153] W. Tang, Y. Hou, F. Wang, L. Liu, Y. Wu, K. Zhu, *Nano Lett.* **2013**, 13, 2036.
- [154] H. Li, Q. Zhou, Y. Gao, X. Gui, L. Yang, M. Du, E. Shi, J. Shi, A. Cao, Y. Fang, *Nano Res.* **2015**, 8, 900.
- [155] N. Du, H. Zhang, B. Chen, X. Ma, Z. Liu, J. Wu, D. Yang, *Adv. Mater.* **2007**, 19, 1641.
- [156] H.-W. Liang, J.-W. Liu, H.-S. Qian, S.-H. Yu, *Accounts Chem. Res.* **2013**, 46, 1450.
- [157] G. Zhang, L. Yu, H. E. Hoster, X. W. Lou, *Nanoscale* **2013**, 5, 877.
- [158] G. Zhang, H. B. Wu, H. E. Hoster, X. W. D. Lou, *Energy Environ. Sci.* **2014**, 7, 302.
- [159] F. Zhou, S. Xin, H. W. Liang, L. T. Song, S. H. Yu, *Angew. Chem. Int. Ed.* **2014**, 53, 11552.
- [160] L. Li, S. Peng, H. B. Wu, L. Yu, S. Madhavi, X. W. D. Lou, *Adv. Energy Mater.* **2015**, 5, 1401172.
- [161] L.-X. Ding, A.-L. Wang, G.-R. Li, Z.-Q. Liu, W.-X. Zhao, C.-Y. Su, Y.-X. Tong, *J. Am. Chem. Soc.* **2012**, 134, 5730.
- [162] L. X. Ding, G. R. Li, Z. L. Wang, Z. Q. Liu, H. Liu, Y. X. Tong, *Chem. Eur. J.* **2012**, 18, 8386.
- [163] Y.-X. Yin, S. Xin, Y.-G. Guo, L.-J. Wan, *Angew. Chem. Int. Ed.* **2013**, 52, 13186.
- [164] F. Cao, G. Pan, X. Xia, P. Tang, H. Chen, *J. Power Sources* **2014**, 264, 161.
- [165] H. Liu, L.-H. Jin, P. He, C. Wang, Y. Xia, *Chem. Commun.* **2009**, 6813.
- [166] H. T. Tan, X. Rui, H. Yu, W. Liu, C. Xu, Z. Xu, H. H. Hng, Q. Yan, *ACS Nano* **2014**, 8, 4004.
- [167] H. Hu, L. Yu, X. Gao, Z. Lin, X. W. D. Lou, *Energy Environ. Sci.* **2015**, 8, 1480.
- [168] C. Shan, Z. Liu, C. Ng, S. Hark, *Appl. Phys. Lett.* **2005**, 86, 213106.
- [169] C. Shan, Z. Liu, Z. Zhang, D. Shen, S. Hark, *J. Phys. Chem. B* **2006**, 110, 11176.
- [170] S. Y. Bae, H. W. Seo, J. Park, H. Yang, B. Kim, *Chem. Phys. Lett.* **2003**, 376, 445.
- [171] G. D. Sulka, A. Brzózka, L. Liu, *Electrochim. Acta* **2011**, 56, 4972.
- [172] J. Duay, S. A. Sherrill, Z. Gui, E. Gillette, S. B. Lee, *ACS Nano* **2013**, 7, 1200.
- [173] R. Laocharoensuk, S. Sattayasamitsathit, J. Burdick, P. Kanatharana, P. Thavarungkul, J. Wang, *ACS Nano* **2007**, 1, 403.
- [174] D. Yang, L. F. Fonseca, *Nano Lett.* **2013**, 13, 5642.
- [175] D. Yang, J. Carpena-Núñez, L. F. Fonseca, A. Biaggi-Labiosa, G. W. Hunter, *Sci. Rep.* **2014**, 4, 3773.
- [176] C. Marichy, M. Bechelany, N. Pinna, *Adv. Mater.* **2012**, 24, 1017.
- [177] X. Meng, X. Q. Yang, X. Sun, *Adv. Mater.* **2012**, 24, 3589.
- [178] X. Chen, M. Knez, A. Berger, K. Nielsch, U. Gösele, M. Steinhart, *Angew. Chem. Int. Ed.* **2007**, 46, 6829.
- [179] Y. Qin, Y. Kim, L. Zhang, S. M. Lee, R. B. Yang, A. Pan, K. Mathwig, M. Alexe, U. Gösele, M. Knez, *Small* **2010**, 6, 910.
- [180] Y. Qin, S.-M. Lee, A. Pan, U. Gösele, M. Knez, *Nano Lett.* **2008**, 8, 114.
- [181] C. Guan, X. Wang, Q. Zhang, Z. Fan, H. Zhang, H. J. Fan, *Nano Lett.* **2014**, 14, 4852.
- [182] D. Gu, H. Baumgart, T. M. Abdel-Fattah, G. Namkoong, *ACS Nano* **2010**, 4, 753.
- [183] D. Gu, H. Baumgart, K. Tapily, P. Shrestha, G. Namkoong, X. Ao, F. Müller, *Nano Res.* **2011**, 4, 164.
- [184] J.-S. Na, B. Gong, G. Scarel, G. N. Parsons, *ACS Nano* **2009**, 3, 3191.

- [185] Z. Huang, N. Geyer, P. Werner, J. de Boor, U. Gosele, *Adv. Mater.* **2011**, *23*, 285.
- [186] A. Cullis, L. Canham, P. Calcott, *J. Appl. Phys.* **1997**, *82*, 909.
- [187] R. Archer, *J. Phys. Chem. Solids* **1960**, *14*, 104.
- [188] K.-Q. Peng, Y.-J. Yan, S.-P. Gao, J. Zhu, *Adv. Mater.* **2002**, *14*, 1164.
- [189] A. I. Hochbaum, D. Gargas, Y. J. Hwang, P. Yang, *Nano Lett.* **2009**, *9*, 3550.
- [190] M.-L. Zhang, K.-Q. Peng, X. Fan, J.-S. Jie, R.-Q. Zhang, S.-T. Lee, N.-B. Wong, *J. Phys. Chem. C* **2008**, *112*, 4444.
- [191] K. Peng, Y. Xu, Y. Wu, Y. Yan, S. T. Lee, J. Zhu, *Small* **2005**, *1*, 1062.
- [192] K. Peng, J. Zhu, *J. Electroanal. Chem.* **2003**, *558*, 35.
- [193] K. Peng, J. Hu, Y. Yan, Y. Wu, H. Fang, Y. Xu, S. Lee, J. Zhu, *Adv. Funct. Mater.* **2006**, *16*, 387.
- [194] Y. Qu, L. Liao, Y. Li, H. Zhang, Y. Huang, X. Duan, *Nano Lett.* **2009**, *9*, 4539.
- [195] H. Chen, R. Zou, H. Chen, N. Wang, Y. Sun, Q. Tian, J. Wu, Z. Chen, J. Hu, *J. Mater. Chem.* **2011**, *21*, 801.
- [196] X. L. Wang, W. Q. Han, *ACS Appl. Mater. Inter.* **2010**, *2*, 3709.
- [197] K.-Q. Peng, X. Wang, S.-T. Lee, *Appl. Phys. Lett.* **2009**, *95*, 243112.
- [198] X. Zhong, Y. Qu, Y. C. Lin, L. Liao, X. Duan, *ACS Appl. Mater. Inter.* **2011**, *3*, 261.
- [199] C. Chiappini, X. Liu, J. R. Fakhoury, M. Ferrari, *Adv Funct Mater* **2010**, *20*, 2231.
- [200] J. Kim, H. Han, Y. H. Kim, S.-H. Choi, J.-C. Kim, W. Lee, *ACS Nano* **2011**, *5*, 3222.
- [201] K. Balasundaram, J. S. Sadhu, J. C. Shin, B. Azeredo, D. Chanda, M. Malik, K. Hsu, J. A. Rogers, P. Ferreira, S. Sinha, *Nanotechnol.* **2012**, *23*, 305304.
- [202] J. M. Weisse, C. H. Lee, D. R. Kim, X. Zheng, *Nano Lett.* **2012**, *12*, 3339.
- [203] X. Li, C. Yan, J. Wang, A. Graff, S. L. Schweizer, A. Sprafke, O. G. Schmidt, R. B. Wehrspohn, *Adv. Energy Mater.* **2015**, *5*, 1401556.
- [204] Y. Chen, L. Liu, J. Xiong, T. Yang, Y. Qin, C. Yan, *Adv. Funct. Mater.* **2015**, *25*, 6701.
- [205] A. Van der Ven, J. Bhattacharya, A. A. Belak, *Accounts Chem. Res.* **2013**, *46*, 1216.
- [206] X. Li, F. Cheng, B. Guo, J. Chen, *J. Phys. Chem. B* **2005**, *109*, 14017.
- [207] Y.-L. Ding, J. Xie, G.-S. Cao, T.-J. Zhu, H.-M. Yu, X.-B. Zhao, *Adv. Funct. Mater.* **2011**, *21*, 348.
- [208] C. Zhu, Y. Yu, L. Gu, K. Weichert, J. Maier, *Angew. Chem. Int. Ed.* **2011**, *50*, 6278.
- [209] H. Wang, Y. Yang, Y. Liang, L.-F. Cui, H. Sanchez Casalongue, Y. Li, G. Hong, Y. Cui, H. Dai, *Angew. Chem. Int. Ed.* **2011**, *123*, 7502.
- [210] X. Su, Q. Wu, J. Li, X. Xiao, A. Lott, W. Lu, B. W. Sheldon, J. Wu, *Adv. Energy Mater.* **2014**, *4*, 1300882.
- [211] D. J. Lee, H. Lee, M. H. Ryou, G. B. Han, J. N. Lee, J. Song, J. Choi, K. Y. Cho, Y. M. Lee, J. K. Park, *ACS Appl. Mater. Inter.* **2013**, *5*, 12005.
- [212] M.-H. Park, M. G. Kim, J. Joo, K. Kim, J. Kim, S. Ahn, Y. Cui, J. Cho, *Nano Lett.* **2009**, *9*, 3844.
- [213] H. B. Wu, G. Zhang, L. Yu, X. W. Lou, *Nanoscale Horiz.* **2016**, *1*, 27.
- [214] C. Yuan, H. B. Wu, Y. Xie, X. W. D. Lou, *Angew. Chem. Int. Ed.* **2014**, *53*, 1488.
- [215] J. Wang, Q. Zhang, X. Li, B. Zhang, L. Mai, K. Zhang, *Nano Energy* **2015**, *12*, 437.
- [216] N. Yabuuchi, K. Kubota, M. Dahbi, S. Komaba, *Chem. Rev.* **2014**, *114*, 11636.
- [217] J. Liu, K. Tang, K. Song, P. A. van Aken, Y. Yu, J. Maier, *Nanoscale* **2014**, *6*, 5081.
- [218] S. Li, Y. Dong, L. Xu, X. Xu, L. He, L. Mai, *Adv. Mater.* **2014**, *26*, 3545.
- [219] Y. Jiang, Z. Yang, W. Li, L. Zeng, F. Pan, M. Wang, X. Wei, G. Hu, L. Gu, Y. Yu, *Adv. Energy Mater.* **2015**, *5*, 1402104.
- [220] N. Yabuuchi, M. Kajiyama, J. Iwatate, H. Nishikawa, S. Hitomi, R. Okuyama, R. Usui, Y. Yamada, S. Komaba, *Nature Mater.* **2012**, *11*, 512.
- [221] W. K. Pang, S. Kalluri, V. K. Peterson, N. Sharma, J. Kimpton, B. Johannessen, H. K. Liu, S. X. Dou, Z. Guo, *Chem. Mater.* **2015**, *27*, 3150.
- [222] L. Fu, K. Tang, K. Song, P. A. van Aken, Y. Yu, J. Maier, *Nanoscale* **2014**, *6*, 1384.
- [223] S. Komaba, W. Murata, T. Ishikawa, N. Yabuuchi, T. Ozeki, T. Nakayama, A. Ogata, K. Gotoh, K. Fujiwara, *Adv. Funct. Mater.* **2011**, *21*, 3859.
- [224] R. Alcántara, J. M. Jiménez-Mateos, P. Lavela, J. L. Tirado, *Electrochem. Commun.* **2001**, *3*, 639.
- [225] K. Tang, L. Fu, R. J. White, L. Yu, M.-M. Titirici, M. Antonietti, J. Maier, *Adv. Energy Mater.* **2012**, *2*, 873.
- [226] Y. Cao, L. Xiao, M. L. Sushko, W. Wang, B. Schwenzer, J. Xiao, Z. Nie, L. V. Saraf, Z. Yang, J. Liu, *Nano Lett.* **2012**, *12*, 3783.
- [227] H. Xiong, M. D. Slater, M. Balasubramanian, C. S. Johnson, T. Rajh, *J. Phys. Chem. Lett.* **2011**, *2*, 2560.
- [228] W. Wang, C. Yu, Z. Lin, J. Hou, H. Zhu, S. Jiao, *Nanoscale* **2013**, *5*, 594.
- [229] H. Li, H. Fei, X. Liu, J. Yang, M. Wei, *Chem. Commun.* **2015**, *51*, 9298.
- [230] F. Xie, Y. Deng, Y. Xie, H. Xu, G. Chen, *Chem. Commun.* **2015**, *51*, 3545.
- [231] J.-Y. Liao, A. Manthiram, *Nano Energy* **2015**, *18*, 20.
- [232] Y. Zhang, L. Guo, S. Yang, *Chem. Commun.* **2014**, *50*, 14029.
- [233] Y. Mo, Q. Ru, J. Chen, X. Song, L. Guo, S. Hu, S. Peng, *J. Mater. Chem. A* **2015**, *3*, 19765.
- [234] L. Wu, X. Hu, J. Qian, F. Pei, F. Wu, R. Mao, X. Ai, H. Yang, Y. Cao, *Energy Environ. Sci.* **2014**, *7*, 323.
- [235] L. Wang, K. Zhang, Z. Hu, W. Duan, F. Cheng, J. Chen, *Nano Res.* **2013**, *7*, 199.
- [236] X. Xiong, W. Luo, X. Hu, C. Chen, L. Qie, D. Hou, Y. Huang, *Sci. Rep.* **2015**, *5*, 9254.
- [237] W. H. Ryu, J. W. Jung, K. Park, S. J. Kim, I. D. Kim, *Nanoscale* **2014**, *6*, 10975.
- [238] X. Ji, K. T. Lee, L. F. Nazar, *Nature Mater.* **2009**, *8*, 500.
- [239] X. Ji, L. F. Nazar, *J. Mater. Chem.* **2010**, *20*, 9821.
- [240] A. Manthiram, Y. Fu, S.-H. Chung, C. Zu, Y.-S. Su, *Chem. Rev.* **2014**, *114*, 11751.
- [241] P. G. Bruce, S. A. Freunberger, L. J. Hardwick, J.-M. Tarascon, *Nature Mater.* **2012**, *11*, 19.
- [242] A. Manthiram, Y. Fu, Y.-S. Su, *Accounts Chem. Res.* **2013**, *46*, 1125.
- [243] M. Wild, L. O'Neill, T. Zhang, R. Purkayastha, G. Minton, M. Marinescu, G. J. Offer, *Energy Environ. Sci.* **2015**, *8*, 3477.
- [244] X. Fang, H. Peng, *Small* **2015**, *11*, 1488.
- [245] L. Zeng, F. Pan, W. Li, Y. Jiang, X. Zhong, Y. Yu, *Nanoscale* **2014**, *6*, 9579.
- [246] S. Xin, L. Gu, N.-H. Zhao, Y.-X. Yin, L.-J. Zhou, Y.-G. Guo, L.-J. Wan, *J. Am. Chem. Soc.* **2012**, *134*, 18510.
- [247] H. Ye, Y.-X. Yin, S. Xin, Y.-G. Guo, *J. Mater. Chem. A* **2013**, *1*, 6602.
- [248] Z. Li, L. Yuan, Z. Yi, Y. Sun, Y. Liu, Y. Jiang, Y. Shen, Y. Xin, Z. Zhang, Y. Huang, *Adv. Energy Mater.* **2014**, *4*, 1301473.
- [249] J. Guo, Y. Xu, C. Wang, *Nano Lett.* **2011**, *11*, 4288.
- [250] G. Zheng, Q. Zhang, J. J. Cha, Y. Yang, W. Li, Z. W. Seh, Y. Cui, *Nano Lett.* **2013**, *13*, 1265.
- [251] S. Chen, X. Huang, H. Liu, B. Sun, W. Yeoh, K. Li, J. Zhang, G. Wang, *Adv. Energy Mater.* **2014**, *4*, 1301761.
- [252] F. Wu, J. Chen, L. Li, T. Zhao, R. Chen, *J. Phys. Chem. C* **2011**, *115*, 24411.
- [253] L. Xiao, Y. Cao, J. Xiao, B. Schwenzer, M. H. Engelhard, L. V. Saraf, Z. Nie, G. J. Exarhos, J. Liu, *Adv. Mater.* **2012**, *24*, 1176.
- [254] C. Wang, W. Wan, J.-T. Chen, H.-H. Zhou, X.-X. Zhang, L.-X. Yuan, Y.-H. Huang, *J. Mater. Chem. A* **2013**, *1*, 1716.

- [255] Y. Chen, X. Li, K.-S. Park, J. Hong, J. Song, L. Zhou, Y.-W. Mai, H. Huang, J. B. Goodenough, *J. Mater. Chem. A* **2014**, *2*, 10126.
- [256] L. Zeng, Y. Jiang, J. Xu, M. Wang, W. Li, Y. Yu, *Nanoscale* **2015**, *7*, 10940.
- [257] H.-J. Peng, Q. Zhang, *Angew. Chem. Int. Ed.* **2015**, *54*, 11018.
- [258] Q. Pang, D. Kundu, M. Cuisinier, L. F. Nazar, *Nature Commun.* **2014**, *5*, 4759.
- [259] X. Tao, J. Wang, Z. Ying, Q. Cai, G. Zheng, Y. Gan, H. Huang, Y. Xia, C. Liang, W. Zhang, Y. Cui, *Nano Lett.* **2014**, *14*, 5288.
- [260] J. Lu, L. Li, J.-B. Park, Y.-K. Sun, F. Wu, K. Amine, *Chem. Rev.* **2014**, *114*, 5611.
- [261] A. C. Luntz, B. D. McCloskey, *Chem. Rev.* **2014**, *114*, 11721.
- [262] F. Cheng, J. Chen, *Chem. Soc. Rev.* **2012**, *41*, 2172.
- [263] Y. Shao, F. Ding, J. Xiao, J. Zhang, W. Xu, S. Park, J.-G. Zhang, Y. Wang, J. Liu, *Adv. Funct. Mater.* **2013**, *23*, 987.
- [264] J. Yuan, J.-S. Yu, B. Sundén, *J. Power Sources* **2015**, *278*, 352.
- [265] Z. Wen, C. Shen, Y. Lu, *ChemPlusChem* **2015**, *80*, 270.
- [266] G. Girishkumar, B. McCloskey, A. C. Luntz, S. Swanson, W. Wilcke, *J. Phys. Chem. Lett.* **2010**, *1*, 2193.
- [267] Z.-L. Wang, D. Xu, J.-J. Xu, X.-B. Zhang, *Chem. Soc. Rev.* **2014**, *43*, 7746.
- [268] W.-B. Luo, X.-W. Gao, S.-L. Chou, J.-Z. Wang, H.-K. Liu, *Adv. Mater.* **2015**, *27*, 6862.
- [269] A. Débart, A. J. Paterson, J. Bao, P. G. Bruce, *Angew. Chem. Int. Ed.* **2008**, *120*, 4597.
- [270] P. Zhang, D. Sun, M. He, J. Lang, S. Xu, X. Yan, *ChemSusChem* **2015**, *8*, 1972.
- [271] Q. Liu, Y. Jiang, J. Xu, D. Xu, Z. Chang, Y. Yin, W. Liu, X. Zhang, *Nano Res.* **2014**, *8*, 576.
- [272] B. Wu, H. Zhang, W. Zhou, M. Wang, X. Li, H. Zhang, *ACS Appl. Mater. Inter.* **2015**, *7*, 23182.
- [273] L. Li, L. Shen, P. Nie, G. Pang, J. Wang, H. Li, S. Dong, X. Zhang, *J. Mater. Chem. A* **2015**, *3*, 24309.
- [274] J. Suntivich, H. A. Gasteiger, N. Yabuuchi, H. Nakanishi, J. B. Goodenough, Y. Shao-Horn, *Nature Chem.* **2011**, *3*, 546.
- [275] J. Suntivich, K. J. May, H. A. Gasteiger, J. B. Goodenough, Y. Shao-Horn, *Science* **2011**, *334*, 1383.
- [276] J.-J. Xu, D. Xu, Z.-L. Wang, H.-G. Wang, L.-L. Zhang, X.-B. Zhang, *Angew. Chem. Int. Ed.* **2013**, *52*, 3887.
- [277] N.-S. Choi, Z. Chen, S. A. Freunberger, X. Ji, Y.-K. Sun, K. Amine, G. Yushin, L. F. Nazar, J. Cho, P. G. Bruce, *Angew. Chem. Int. Ed.* **2012**, *51*, 9994.
- [278] P. Simon, Y. Gogotsi, B. Dunn, *Science* **2014**, *343*, 1210.
- [279] A. Vlad, N. Singh, C. Galande, P. M. Ajayan, *Adv. Energy Mater.* **2015**, *5*, 1402115.
- [280] Y. Zhai, Y. Dou, D. Zhao, P. F. Fulvio, R. T. Mayes, S. Dai, *Adv. Mater.* **2011**, *23*, 4828.
- [281] B. Xu, F. Wu, Y. Su, G. Cao, S. Chen, Z. Zhou, Y. Yang, *Electrochim. Acta* **2008**, *53*, 7730.
- [282] X. Y. Tao, X. B. Zhang, L. Zhang, J. P. Cheng, F. Liu, J. H. Luo, Z. Q. Luo, H. J. Geise, *Carbon* **2006**, *44*, 1425.
- [283] Y. Zeng, X. Li, S. Jiang, S. He, H. Fang, H. Hou, *Mater. Lett.* **2015**, *161*, 587.
- [284] Y. Lu, K. Fu, S. Zhang, Y. Li, C. Chen, J. Zhu, M. Yanilmaz, M. Dirican, X. Zhang, *J. Power Sources* **2015**, *273*, 502.
- [285] D. Lee, J.-Y. Jung, M.-J. Jung, Y.-S. Lee, *Chem. Eng. J.* **2015**, *263*, 62.
- [286] K. Huang, M. Li, Z. Chen, Y. Yao, X. Yang, *Electrochim. Acta* **2015**, *158*, 306.
- [287] Y. Liu, J. Zhou, L. Chen, P. Zhang, W. Fu, H. Zhao, Y. Ma, X. Pan, Z. Zhang, W. Han, E. Xie, *ACS Appl. Mater. Inter.* **2015**, *7*, 23515.
- [288] P. Simon, Y. Gogotsi, *Nature Mater.* **2008**, *7*, 845.
- [289] L.-F. Chen, X.-D. Zhang, H.-W. Liang, M. Kong, Q.-F. Guan, P. Chen, Z.-Y. Wu, S.-H. Yu, *ACS Nano* **2012**, *6*, 7092.
- [290] L.-F. Chen, Z.-H. Huang, H.-W. Liang, H.-L. Gao, S.-H. Yu, *Adv. Funct. Mater.* **2014**, *24*, 5104.
- [291] T. Lin, I.-W. Chen, F. Liu, C. Yang, H. Bi, F. Xu, F. Huang, *Science* **2015**, *350*, 1508.
- [292] J. Zhang, J. Ma, L. L. Zhang, P. Guo, J. Jiang, X. S. Zhao, *J. Phys. Chem. C* **2010**, *114*, 13608.
- [293] C.-C. Hu, K.-H. Chang, M.-C. Lin, Y.-T. Wu, *Nano Lett.* **2006**, *6*, 2690–2695.
- [294] H. Xia, J. Feng, H. Wang, M. O. Lai, L. Lu, *J. Power Sources* **2010**, *195*, 4410.
- [295] M. Huang, Y. Zhang, F. Li, L. Zhang, R. S. Ruoff, Z. Wen, Q. Liu, *Sci. Rep.* **2014**, *4*, 3878.
- [296] G. A. Snook, P. Kao, A. S. Best, *J. Power Sources* **2011**, *196*, 1.
- [297] K. Wang, H. Wu, Y. Meng, Z. Wei, *Small* **2014**, *10*, 14.
- [298] X. Tian, B. Xiao, X. Xu, L. Xu, Z. Liu, Z. Wang, M. Yan, Q. Wei, L. Mai, *Nano Res.* **2016**, *1*.
- [299] L. Ran, C. Seung Il, L. Sang Bok, *Nanotechnol.* **2008**, *19*, 215710.
- [300] M. Dirican, M. Yanilmaz, X. Zhang, *RSC Adv.* **2014**, *4*, 59427.
- [301] T. Xue, X. Wang, J.-M. Lee, *J. Power Sources* **2012**, *201*, 382.
- [302] S. Xiong, C. Yuan, X. Zhang, Y. Qian, *CrystEngComm* **2011**, *13*, 626.
- [303] H. Jiang, J. Ma, C. Li, *Chem. Commun.* **2012**, *48*, 4465.
- [304] L. Shen, Q. Che, H. Li, X. Zhang, *Adv. Funct. Mater.* **2014**, *24*, 2630.
- [305] L. Qu, Y. Zhao, A. M. Khan, C. Han, K. M. Hercule, M. Yan, X. Liu, W. Chen, D. Wang, Z. Cai, W. Xu, K. Zhao, X. Zheng, L. Mai, *Nano Lett.* **2015**, *15*, 2037.
- [306] K. M. Hercule, Q. Wei, O. K. Asare, L. Qu, A. M. Khan, M. Yan, C. Du, W. Chen, L. Mai, *Adv. Energy Mater.* **2015**, *5*, 1500060.
- [307] C. Zhou, Y. Zhang, Y. Li, J. Liu, *Nano Lett.* **2013**, *13*, 2078.
- [308] T. Brezesinski, J. Wang, S. H. Tolbert, B. Dunn, *Nature Mater.* **2010**, *9*, 146.
- [309] V. Augustyn, J. Come, M. A. Lowe, J. W. Kim, P.-L. Taberna, S. H. Tolbert, H. D. Abruña, P. Simon, B. Dunn, *Nat Mater* **2013**, *12*, 518.
- [310] G. A. Muller, J. B. Cook, H.-S. Kim, S. H. Tolbert, B. Dunn, *Nano Lett.* **2015**, *15*, 1911.
- [311] J. W. Kim, V. Augustyn, B. Dunn, *Adv. Energy Mater.* **2012**, *2*, 141.
- [312] J. Come, V. Augustyn, J. W. Kim, P. Rozier, P.-L. Taberna, P. Gogotsi, J. W. Long, B. Dunn, P. Simon, *J. Electrochem. Soc.* **2014**, *161*, A718.
- [313] A. A. Lubimtsev, P. R. C. Kent, B. G. Sumpter, P. Ganesh, *J. Mater. Chem. A* **2013**, *1*, 14951.
- [314] X. Wang, G. Li, Z. Chen, V. Augustyn, X. Ma, G. Wang, B. Dunn, Y. Lu, *Adv. Energy Mater.* **2011**, *1*, 1089.
- [315] M. Zúkalová, M. Kalbáč, L. Kavan, I. Exnar, M. Graetzel, *Chem. Mater.* **2005**, *17*, 1248.
- [316] J. Li, Z. Tang, Z. Zhang, *Chem. Phys. Lett.* **2006**, *418*, 506.
- [317] Y. Wang, Z. Hong, M. Wei, Y. Xia, *Adv. Funct. Mater.* **2012**, *22*, 5185.
- [318] J. Li, Z. Tang, Z. Zhang, *Chem. Mater.* **2005**, *17*, 5848.
- [319] Z. Chen, V. Augustyn, J. Wen, Y. W. Zhang, M. Q. Shen, B. Dunn, Y. F. Lu, *Adv Mater* **2011**, *23*, 791.
- [320] I. E. Rauda, V. Augustyn, L. C. Saldarriaga-Lopez, X. Chen, L. T. Schelhas, G. W. Rubloff, B. Dunn, S. H. Tolbert, *Adv. Funct. Mater.* **2014**, *24*, 6717.
- [321] M. Okubo, E. Hosono, J. Kim, M. Enomoto, N. Kojima, T. Kudo, H. Zhou, I. Honma, *J. Am. Chem. Soc.* **2007**, *129*, 7444.
- [322] J. Wang, J. Polleux, J. Lim, B. Dunn, *J. Phys. Chem. C* **2007**, *111*, 14925.
- [323] V. Augustyn, E. R. White, J. Ko, G. Gruner, B. C. Regan, B. Dunn, *Mater. Horiz.* **2014**, *1*, 219.
- [324] T. Brezesinski, J. Wang, J. Polleux, B. Dunn, S. H. Tolbert, *J. Am. Chem. Soc.* **2009**, *131*, 1802.
- [325] Y. Cai, H.-E. Wang, S. Zhuan Huang, J. Jin, C. Wang, Y. Yu, Y. Li, B.-L. Su, *Sci. Rep.* **2015**, *5*, 11557.
- [326] J. Qu, J. E. Cloud, Y. Yang, J. Ding, N. Yuan, *ACS Appl. Mater. Inter.* **2014**, *6*, 22199.
- [327] H. Hu, L. Yu, X. Gao, Z. Lin, X. W. Lou, *Energy Environ. Sci.* **2015**, *8*, 1480.

- [328] J. Yang, L. Lian, P. Xiong, M. Wei, *Chem. Commun.* **2014**, 50, 5973.
- [329] H. Zhang, X. P. Gao, G. R. Li, T. Y. Yan, H. Y. Zhu, *Electrochim. Acta* **2008**, 53, 7061.
- [330] S. R. Sivakkumar, A. G. Pandolfo, *J. Appl. Electrochem.* **2014**, 44, 105.
- [331] X. Wang, G. Shen, *Nano Energy* **2015**, 15, 104.
- [332] H. Li, L. Shen, J. Wang, S. Fang, Y. Zhang, H. Dou, X. Zhang, *J. Mater. Chem. A* **2015**, 3, 16785.
- [333] V. Aravindan, J. Sundaramurthy, A. Jain, P. S. Kumar, W. C. Ling, S. Ramakrishna, M. P. Srinivasan, S. Madhavi, *ChemSusChem* **2014**, 7, 1858.
- [334] Y. Wang, Y. Xia, *Adv. Mater.* **2013**, 25, 5336.
- [335] V. Aravindan, J. Gnanaraj, Y.-S. Lee, S. Madhavi, *Chem. Rev.* **2014**, 114, 11619.
- [336] M. Ghidui, M. R. Lukatskaya, M.-Q. Zhao, Y. Gogotsi, M. W. Barsoum, *Nature* **2014**, 516, 78.
- [337] M. R. Lukatskaya, O. Mashtalir, C. E. Ren, Y. Dall'Agnese, P. Rozier, P. L. Taberna, M. Naguib, P. Simon, M. W. Barsoum, Y. Gogotsi, *Science* **2013**, 341, 1502.
- [338] R. Wang, J. Lang, P. Zhang, Z. Lin, X. Yan, *Adv. Funct. Mater.* **2015**, 25, 2270.
- [339] W. Li, F. Zhang, Y. Dou, Z. Wu, H. Liu, X. Qian, D. Gu, Y. Xia, B. Tu, D. Zhao, *Adv. Energy Mater.* **2011**, 1, 382.
- [340] X. Ren, Z. Lun, *Mater. Lett.* **2012**, 68, 228.
- [341] B. Yao, D. Fleming, M. A. Morris, S. E. Lawrence, *Chem. Mater.* **2004**, 16, 4851.
- [342] S. Baber, M. Zhou, Q. Lin, M. Naalla, Q. Jia, Y. Lu, H. Luo, *Nanotechnol.* **2010**, 21, 165603.
- [343] H. Xiang, Y. Long, X. Yu, X. Zhang, N. Zhao, J. Xu, *CrystEngComm* **2011**, 13, 4856.
- [344] C. Ji, P. C. Searson, *Appl. Phys. Lett.* **2002**, 81, 4437.
- [345] L. Liu, W. Lee, Z. Huang, R. Scholz, U. Gösele, *Nanotechnol.* **2008**, 19, 335604.
- [346] H.-M. Bok, K. L. Shuford, S. Kim, S. K. Kim, S. Park, *Nano Lett.* **2008**, 8, 2265.
- [347] X. Zhang, W. Lu, J. Da, H. Wang, D. Zhao, P. A. Webley, *Chem. Commun.* **2009**, 195.
- [348] C. Ji, P. C. Searson, *J. Phys. Chem. B* **2003**, 107, 4494.
- [349] A. Serrà, E. Gómez, E. Vallés, *Int. J. Hydrogen Energy* **2015**, 40, 8062.
- [350] A. Serrà, M. Montiel, E. Gómez, E. Vallés, *Nanomaterials* **2014**, 4, 189.
- [351] R. B. Khomane, *J. Colloid Interf. Sci.* **2011**, 356, 369.
- [352] H. g. Wang, D. Ma, Y. Huang, X. b. Zhang, *Chem. Eur. J.* **2012**, 18, 8987.
- [353] C. Xu, Y. Zhao, G. Yang, F. Li, H. Li, *Chem. Commun.* **2009**, 7575.
- [354] H. Li, R. Xu, Y. Wang, B. Qian, H. Wang, L. Chen, H. Jiang, Y. Yang, Y. Xu, *RSC Adv.* **2014**, 4, 51960.
- [355] H. Huang, W. Zhu, X. Tao, Y. Xia, Z. Yu, J. Fang, Y. Gan, W. Zhang, *ACS Appl. Mater. Inter.* **2012**, 4, 5974.
- [356] L. Yao, K. Kan, Y. Lin, J. Song, J. Wang, J. Gao, P. Shen, L. Li, K. Shi, *RSC Adv.* **2015**, 5, 15515.
- [357] Y. Xiao, L. Li, Y. Li, M. Fang, L. Zhang, *Nanotechnol.* **2005**, 16, 671.
- [358] L. Xu, B. Dong, Y. Wang, X. Bai, Q. Liu, H. Song, *Sens. Actuators B* **2010**, 147, 531.
- [359] Y. Zhang, J. Li, G. An, X. He, *Sens. Actuators B* **2010**, 144, 43.
- [360] X. Xia, X. Dong, Q. Wei, Y. Cai, K. Lu, *Express Polym. Lett.* **2012**, 6, 169.
- [361] L. Li, X. Yin, S. Liu, Y. Wang, L. Chen, T. Wang, *Electrochem. Commun.* **2010**, 12, 1383.
- [362] A. Yang, X. Tao, G. K. H. Pang, K. G. G. Siu, *J. Am. Ceram. Soc.* **2008**, 91, 257.
- [363] Z. Xiao, L. Zhang, X. Tian, X. Fang, *Nanotechnol.* **2005**, 16, 2647.
- [364] T. Xue, J.-M. Lee, *J. Power Sources* **2014**, 245, 194.
- [365] M.-S. Wu, J.-F. Wu, *J. Power Sources* **2013**, 240, 397.
- [366] W. Luo, X. Hu, Y. Sun, Y. Huang, *J. Mater. Chem.* **2012**, 22, 8916.
- [367] Q. Peng, X.-Y. Sun, J. C. Spagnola, C. Saquing, S. A. Khan, R. J. Spontak, G. N. Parsons, *ACS Nano* **2009**, 3, 546.
- [368] G. Huang, F. Zhang, X. Du, J. Wang, D. Yin, L. Wang, *Chemistry* **2014**, 20, 11214.
- [369] H. W. Park, D. U. Lee, P. Zamani, M. H. Seo, L. F. Nazar, Z. Chen, *Nano Energy* **2014**, 10, 192.
- [370] D. Yan, C. Yu, Y. Bai, W. Zhang, T. Chen, B. Hu, Z. Sun, L. Pan, *Chem. Commun.* **2015**, 51, 8261.
- [371] S. Yuan, X. L. Huang, D. L. Ma, H. G. Wang, F. Z. Meng, X. B. Zhang, *Adv. Mater.* **2014**, 26, 2273.
- [372] B. Wang, T. Zhu, H. B. Wu, R. Xu, J. S. Chen, X. W. Lou, *Nanoscale* **2012**, 4, 2145.
- [373] X. Lu, G. Wang, T. Zhai, M. Yu, J. Gan, Y. Tong, Y. Li, *Nano Lett.* **2012**, 12, 1690.
- [374] L. Li, Z. A. Hu, N. An, Y. Y. Yang, Z. M. Li, H. Y. Wu, *J. Phys. Chem. C* **2014**, 118, 22865.